Design and Performance Optimization of Heart Assist Devices: iHeart VAD and iATVA

By

İbrahim Başar Aka

A Dissertation Submitted to the
Graduate School of Sciences and Engineering
in Partial Fulfillment of the Requirements for
the Degree of

Doctor of Philosophy

in

Bio-Medical Sciences and Engineering

July 27 2018

Design and Performance Optimization of Heart Assist Devices: iHeart VAD and iATVA

Koç University

Graduate School of Sciences and Engineering

This is to certify that I have examined this copy of a doctoral thesis by

İbrahim Başar Aka

and have found that it is complete and satisfactory in all respects,
and that any and all revisions required by the final
examining committee have been made.

Committee Members:

_____

Prof. Dr. İsmail Lazoğlu

_____

Prof. Dr. Deniz Süha Küçükaksu

_____

Prof. Dr. Metin Muradoğlu

_____

Assoc. Prof. Dr. Kerem Pekkan

_____

Assist. Prof. Dr. Fethi Okyar

Date: _____

I dedicate this thesis to my father, Hasan.

ABSTRACT

Heart failure, some congenital heart defects, and some circulatory disorders are diseases which are treated or alleviated with mechanical circulatory support devices. Even though the ideal therapy for heart failure is a cardiac transplant, due to the donor shortage, Left Ventricular Assist Devices has emerged. As a mechanical pump, an LVAD pumps the blood from the left ventricle to the aorta for supporting the heart. Similarly, for the treatment of Fontan patients with a univentricular heart, some experimental mechanical circulatory support devices have been proposed in the literature. These devices are called Fontan Ventricle Assist Device (FVAD).

This work comprised the design, development, and experiments of İstanbul Heart VAD (iHeart VAD) and integrated Aortic-Turbine Venous-Assist (iATVA) which are a novel centrifugal LVAD and a novel FVAD (a centrifugal turbine-pump couple), respectively. Both devices were designed following the turbomachinery theory. For the iHeart VAD, this work includes computer simulations, hydraulics tests, blood tests and acute animal tests. For the iATVA, this work focuses on hydraulic tests and cardiovascular mock-loop tests. For both devices, chronical animal tests are planned for the near future.

ÖZET

Kalp yetersizliği, bazı konjenital kalp hastalıkları ve bazı dolaşım bozuklukları, yapay dolaşım destek cihazlarıyla tedavi edilmeye veya hafifletilmeye çalışılmaktadır. Kalp yetersizliğinin ideal tedavisi nakil olsa da donör sayısının azlığı Sol Ventriküler Destek Cihazlarının (SVDC) geliştirilmesine yol açmıştır. Mekanik bir pompa olan SVDC sol karıncıktan aldığı kanı aorta pompalayarak kalbe yardımcı olur. Benzer şekilde, tek karıncıkla doğan hastaların tedavisi için gerçekleştirilen Fontan operasyonu sonucu gerçekleşen yüksek pulmoner tansiyonun dengelenmesi için de literatürde bazı deneysel mekanik dolaşım destek cihazları önerilmiştir. Bu pompalara Fontan Ventrikül Destek Cihazı (FVDC) denilmektedir.

Bu çalışma özgün bir santrifüj akışlı SVDC olan İstanbul Heart VAD (iHeartVAD) ve santrifüj akışlı tribün-pompa çiftinden oluşan özgün biir FVDC olan integrated Aortic-Turbine Venous-Assist (iATVA)'nın tasarım, geliştirme ve test süreçlerini anlatmaktadır. Her iki cihaz da turbomakine teorisine göre tasarlanmıştır. Bu tez iHeart VAD hakkında; bilgisayar simülasyonları, hidrolik testler, kan testleri ve akut hayvan testlerini kapsamaktadır. iATVA hakkında; hidrolik testler ve fiziki kalp simülasyonu devresi testlerini kapsamaktadır. Her iki çalışma için de gelecekte kronik hayvan testleri yapılması planlatılmaktadır.

ACKNOWLEDGMENTS

This thesis developed during my time as a research assistant in the Manufacturing and Automation Research Center (MARC) of Koç University - İstanbul. I am very grateful to Prof. Dr. İsmail Lazoğlu for giving me the opportunity to join this world-class research group. His vision and advice made iHeart VAD successful. Moreover, Assoc. Prof. Kerem Pekkan's advice was greatly appreciated through the design of iATVA. Also, Prof. Dr. Deniz Süha Küçükaksu helped this work with his support, guidance, and clinical expertise.

Furthermore, I would like to thank Muzaffer Bütün for his support and cooperativeness throughout the manufacturing process of iHeart VAD models. Many warm thanks go to all my colleagues from MARC for creating an always friendly and productive atmosphere. I owe gratitude to Dr. Ehsan Layegh, Dr. Adnan Hassan, İsmail Enes Yiğit, Talha Irfan Khan who helped me through this journey. Special thanks go to Dr. Çağlar Öztürk, my research partner, and brother for many years. I owe gratitude to Erhan Ermek and Pekkan Biofluid Mechanics Laboratory members for their great hospitality and helpfulness during the experimental studies of iATVA. I also thank Prof. Dr. Metin Muradoğlu, who answered my CFD related questions patiently.

Further thanks I want to express to my former advisor Prof. Dr. Kamuran Kadıpaşaoğlu, who introduced this research field to me. I have learned a great deal of knowledge from his experiences.

Last but not least, I deeply appreciate the support of my family, my mother Ayşe and my brother Umur. Exclusively, my father Hasan without whom I would have never dared to follow this path. He encouraged me for seeking engineering degrees to the Ph.D. level. I also thank my girlfriend Deniz Erol for her patience and caring support during the development process of this thesis.

TABLE OF CONTENTS

LIST OF TABLES

LIST OF FIGURES

NOMENCLATURE

β = Blade Angle
θ = Volute Angle
M = Dynamic Viscosity (Pa·s)
v = Kinematic Viscosity (m^2/S)
ρ = Density (Kg/m^3)
σ = Average Stress (Pa)
T = Shear Stress (N/m^2)
Ω = Angular Velocity(Rad/s)
D = Diameter(m)
G = Gravitational Acceleration (m/s^2)
H = Pressure Head (Pa)
N = Rotational Speed (Rpm)
Ns = Specific Speed
Q = Flow (m^3/s)
R = Radius (m)
T = Torque (N·m)
U = Peripheral Velocity Of Impeller (m/s)
U = Velocity (m/s)
C_w = Velocity Of Flow, Relative To The Blade (m/s)
MRF = Multiple Reference Frame
SM = Sliding Mesh
HTx = Heart Transplant
CO = Total Cardiac Output
LVAD = Left Ventricular Assist Device
FVAD = Fontan Ventricular Assist Device
SSS = Scalar Shear Stress
CPAD = Cavopulmonary Assist Device
iATVA = Integrated Aortic-Turbine Venous-Assist System
IVC = Inferior Vena Cava
LPM = Liters Per Minute
DI = Damage Index
PA = Pulmonary Artery
SVC = Superior Vena Cava
SVP = Systemic Venous Pressure
TCPC = Total Cavopulmonary Connection
HF = Heart Failure
MI = Myocardial Infarction
ΔP = Net Pressure Difference

INTRODUCTION

Cardiovascular diseases are the one of the leading cause of death worldwide[1]. Heart failure (HF) is one of the most significant diseases among them. Advanced CHF treatment can be in three ways as, drug therapy, surgery and cardiac transplantation[2]. However, the only option left for a last-stage HF patient is heart replacement. Due to the lack of treatment options and a shortage of donor pool, researchers have been investigating the mechanical circulatory supports (MSC) devices[3]. In the last several decades, there has been a significant development in the field of MCS devices. These devices have appeared as a bridge to transplant option to increase the survival chance of the patients until a donor organ is found. Later these devices become an alternative to the heart transplant which is called a destination therapy. Left Ventricular Assist Devices (LVADs) are the utmost implanted version of blood pumps. LVADs operate by pumping blood from the left ventricle to aorta, energized by external batteries. One of the two circulatory support system designs proposed in this thesis is the İstanbul Heart (iHeart) VAD, a centrifugal heart pump.

Single Ventricle Defects are also another fatal disease which can be treated with heart transplantation or with surgery. In 1971, Fontan and Baudet proposed a surgical method for palliation of the tricuspid atresia[4]. Subsequently, this surgical procedure has been applied to treat most kinds of single ventricles diseases[5]. Theoretically, the systemic and pulmonary venous returns are disconnected to

recover the drawbacks of long-term hypoxemia. Moreover, this method reduces the thromboembolic events and extends the survival of patients with single-ventricle physiology. On the other hand, some opposing results of the Fontan procedure have also discovered. As the patient ages, this contradictory or unnatural circulation progressively fails due to high venous pressure levels. Mechanical assist devices can deliver an extra subpulmonic power for solving the Fontan paradox[6]. Therefore, the second device proposed in this thesis is intended with the objective of evaluating the hemodynamic performance of a totally implantable integrated aortic-turbine venous-assist (iATVA) system, which uses the power of aortic flow and does not need an external power source and preserves low venous pressure, for the Fontan circulation.

1.1 Motivation

Cardiovascular diseases are the primary cause of death in the developed world and a global health priority. 17 to 45% of patients admitted to healthcare facilities with HF dies within 5 years. Currently, 26 million patients are living with HF (Figure 1) [7]. Likewise, more than 5 million patients in the USA have HF[8]. Heart diseases are responsible for the deaths of nearly 600,000 patients annually in the United States. Similarly, around 5 million Europeans coronary artery diseases[9]. Almost half of the patients who develop heart failure die in 5 years of diagnosis. The heart failure-related economic burden is estimated as $32 billion annually in the US[10]. Presently, more than 6 million new cases of CVD exist in the EU and more than 11 million in European countries in total, per year. With nearly 49 million people

survive with the disease in the EU. Cost of CVDs to the EU economies is high at €210 billion per year [11]. Strategic Plan of the Turkish Ministry of Health estimates that by 2015, 20 million people will die annually due to cardiovascular diseases[12].

In most of the European countries, Cardio Vascular Diseases (CVD) is still the foremost cause of mortality with more than 2 million deaths annually and therefore are a significant threat economically and socially[13].

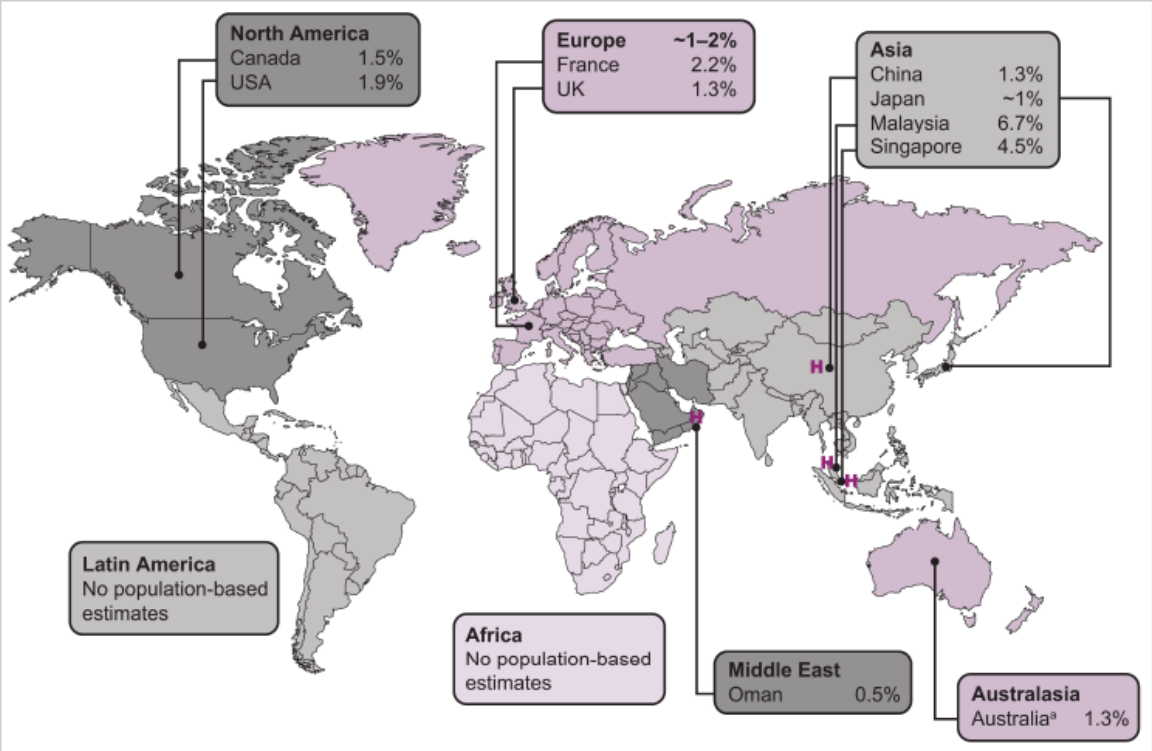

Figure 1: Worldwide HF data [7].

CVD related deaths, the prevalence of the disease rates is lower in the European Union (EU) than outside of the EU. Positively, CVD mortality is now

lessening in almost all of Europe according to the statistical reports. This improvement is in accordance with the decreasing trends in smoking and alcohol consumption.

Statistics show that HF is pandemic in Turkey as well. About a million people have HF, and nearly %20 of these patients develops into last stage HF annually. Every year, roughly 3000 patients need immediate heart replacement, but coarsely 60 transplantations have been performed due to short donor pool. Thus, more than 95% of the required transplants are delayed up until an organ is found. Unfortunately, half of these patients die annually, and most of them expire in 24 months[12].

As defined beforehand, less than 5% of the HF patients receive heart replacement in Turkey. Remaining HF patients need mechanically circulatory support systems (MCSS), typically LVADs to live. Companies manufacture the majority of the LVADs are from the US, Germany or Japan. Therefore, the rest of the world has to import LVADs for their needs. On the other hand, LVADs and maintenance costs bring substantial financial burden. Moreover, due to the limited research on LVAD development and patient care, these devices cannot be skillfully implanted on patients, as these devices must be used and maintained by knowledgeable healthcare personnel. Consequently, training technicians and healthcare professionals through physical and clinical testing will sustain patients for longer.

Congenital Heart Disease (CHD) is another critical heart disease[14] which can be described as a congenital cardiac disability. The PAN study[15] logged a general CHD prevalence of 1.08 % in Germany and CDC records [16,17] gives an incidence of 0.4 to 0.8% in the USA. Global prevalence of CHD is about 1% [18]. The estimations of prevalence published during the last several decades are around 12 – 14 / 1000 live births [15]. The actual history for these patients is quite poor[19]. Likewise, single ventricle defects are affecting millions of neonatal globally every year. Single ventricle defect is a rare, but complex cardiac illness. It embodies 7.7% of total congenital heart diseases [14]. Even after a palliative surgery, the most hopeful historical 3-year survival rate reported is 75%. The most conclusive surgical technique existing for these patients is the Fontan operation [19]. Recent modifications of the procedure have resulted in more extended survival rates. Multiple centers have reported greater than 80% survival rates at more than 5 years after Fontan. A recent report shows that a health center has achieved a 10-year survival rate of 87%[19]. However, Fontan circulation is unnatural and remains a paradox. Fontan circulation causes a risk of chronic high venous pressure, congestion of the systemic veins, and reduced cardiac output. Cavopulmonary assist devices can be a solution to this problem. There are some studies to address this need yet none of these devices are approved for clinical use as of today [20,21].

In Turkey, the only our research group in Manufacturing and Automation Research Center in Koç University has completed a centrifugal pump prototype, conducted in-vitro blood tests and acute in-vivo tests by 2017 [22,23]. Another

research group has started hydraulic tests [24,25]. There are two different domestic efforts to develop LVADs. However, there are many steps to follow yet for completing a prototype, such as physical performance testing and later in-vivo testing (animal and human tests).

1.2 Aim and Scope

This thesis aims to investigate the design methodology of centrifugal blood contacting turbomachinery in the emphasis of two different circulatory support devices. Design and optimization procedures for radial flow blood pumps are examined from turbomachinery calculations to the physical tests. Turbomachinery approach is explained based on the physiologic conditions and needs. CFD methods are studied and illustrated for creating a realistic simulation of radial blood pumps considering the requirements urged from the human circulation. iHeart VAD, a novel centrifugal left ventricular pump has been designed and tested as a part of this thesis. Additionally, an innovative blood turbine has been developed for the first time in literature for the use of natural cardiac flow for energy harvesting as a part of the second cardiac assist device iATVA, proposed in this thesis. In-silico, in-vitro and in-vivo validations of the iHeart VAD is presented. For iATVA, the scope of this thesis covers the in-vitro validations.

LITERATURE REVIEW

Dr. John Gibbon designed a heart-lung machine after observing a patient's death caused by pulmonary embolism in 1930. In 1939, Gibbon successfully experimented with a rotating cylinder film oxygenator on cats perfusion while their pulmonary artery was gradually occluded. [26,27]. A higher capacity oxygenator was designed in collaboration with the IBM Corporation, during the late 1940s and early 1950s. Gibbon-IBM heart-lung machine was successfully applied to an atrial septal defect surgery in an 18-year-old girl in 1953 [28]. The original mechanical circulatory assist device is the intra-aortic balloon pump (IABP). As of today, IABP has become the most commonly used type of MCSS, assisting over 100,000 patients every year. The IABP was presented in 1962 by Moulopoulos et al. who used a latex balloon pump located in the descending aorta that was inflated during diastole and deflated during systole[29]. In June 1967, Dr. Adrian Kantrowitz et al. used a new intra-aortic balloon pump (IABP)—to save a patient in cardiogenic shock [30]. Liotta et al. proposed the initial use of a novel implantable artificial ventricle after an aortic valve replacement surgery where the patient was in cardiogenic shock following in 1963. The patient was supported for 4 days with this artificial ventricle [31]. NIH initiated an incentive to develop a mechanical heart assist device with the founding of the Artificial Heart Program in 1964. Also, NIH created the National Heart, Lung, and Blood Institute (NHLBI) in 1970 that supported a program to design an LVAD [32]. Efforts on developing

LVADs sustained with DeBakey whom successful supported and discharged 2 postcardiotomy patients with extracorporeal reciprocating (first generation) LVADs [33].

A total artificial heart (TAH) was tested in a patient by William DeVries, Willem S. Kolff, and Robert K. Jarvik and colleagues as destination therapy, in 1984 [34]. It was a pneumatically actuated reciprocating pump. After these efforts, researchers started trying to develop more dependable, durable and biocompatible systems for long-term or in other words destination therapy. Since the rise of continuous flow rotary blood pumps, the field of MCSS has progressed swiftly. Some of the clinically approved adult VADS are presented in the chapter 2.2 Mechanical Circulatory Support Systems.

2.1 Anatomy and Physiology of the heart

The cardiovascular system comprises the heart and the blood vessels with arteries, veins, and capillaries (Figure 2). The cardiovascular system carries oxygen and delivers nutrients to all cells in the body. Likewise, it carries waste materials to the organs responsible for exclusion. There are two coupled circulatory loops in humans (Figure 2): The systemic circulation delivers oxygenated and nutrients to the body cells while waste materials are also removed. The pulmonary circulation carries deoxygenated blood to the lungs to bring carbon dioxide and acquire oxygen [35].

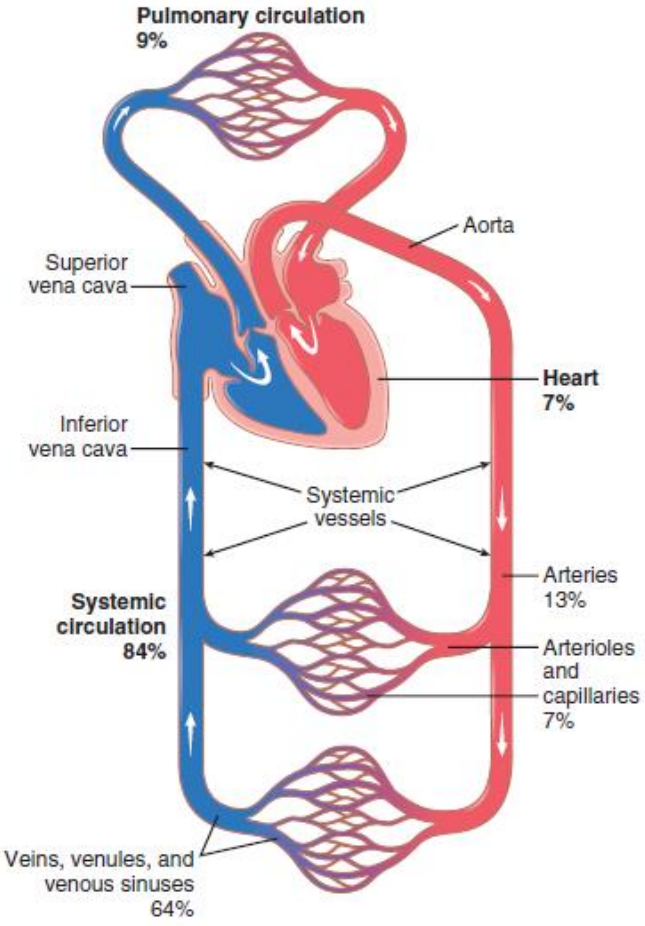

Figure 2: Distribution of blood (in the percentage of total blood) in the different parts of the circulatory system [35].

2.1.1 The Human Heart

The heart is the main component in the cardiovascular system and one of the most critical organs in the human body. The heart beats typically between 60 to 100 times/minute, equivalent to nearly 30 million beats annually[35].

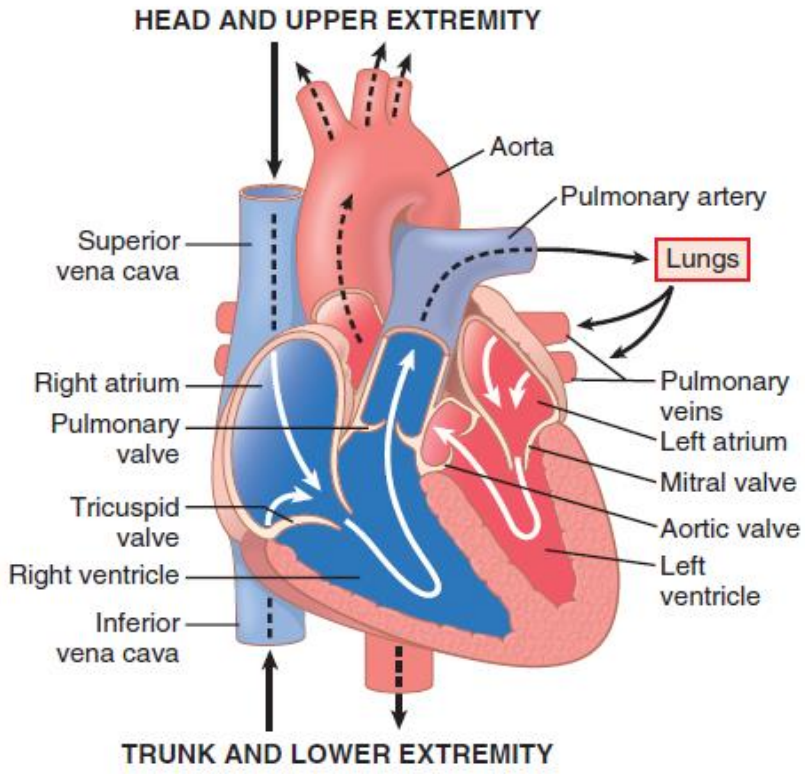

Figure 3: Structure of the human heart [35].

The heart is residing between two lungs. It consists of four chambers; the upper chambers called atrium, and the lower chambers called the ventricle (Figure 3). It performs as a synchronized two pumps for pulmonary (right) and systemic (left) circulations. The atria pump returning deoxygenated blood into the right, and oxygenated blood into the left ventricles and the ventricles pump blood to the lungs or body, outward the heart. The right atrium takes de-oxygenated blood from the systemic return and transfers it into the right ventricle. Subsequently, the right ventricle pumps it through the pulmonary artery into the lungs where the blood gets

oxygenated. Afterward, the oxygenated blood is guided to the left ventricle by passing through the mitral valve[35].

The pulsatile nature of the reciprocating action of the heart results with a periodic flow characteristic. The cardiac cycle categorized in two stages of diastole (relaxation) and systole (contraction) while the heart pumps blood. Each of these stages can be evaluated in two separate phases. Each phase is considered by the motion of the heart valves. Typically, a period of a cardiac cycle is ranging between 0.8 - 1.0 second (60 - 80 bpm) where relaxation (diastole) takes a relatively long time. The heart rate (HR) is also adjusted in harmony to physiological demands forced by the autonomic nerves.

2.1.1 Heart Failure

Congestive heart failure (CHF) is a result of abnormal cardiac function where the heart is incapable of providing sufficient blood flow to meet the metabolic demands. End-stage of this progressive heart disease dramatically shortens survival[36]. Even though the early stages can be treated with drug therapy, end-stage HF can be treated only with cardiac replacement (Figure 4). The number of patients needing a heart transplant has doubled last 1.5 decades while the donor pool has dropped to 30%. 2804 hearts transplants were achieved in the United States while 4134 patients were yet on the waiting list as of 2015 [3].

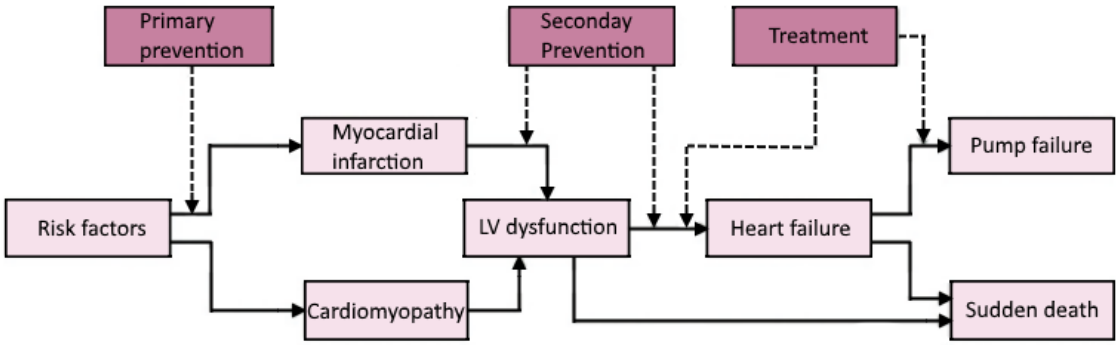

Figure 4: Stages of the HF[36].

CHF arises as a result of an irregularity in cardiac function, anatomy, or pace. Ventricular dysfunction (systolic or diastolic) is the primary reason for most CHF cases in the developed world and results from myocardial, hypertension or both. Other essential causes can be listed as idiopathic or alcoholic cardiomyopathy and degenerative valve. Heart failure frequently arises in elderly patients who have numerous chronical conditions like diabetes, and chronic lung disease [14]. Coronary heart disease replaced hypertension as the leading cause of CHF In Europe, North America and Australasia [37].

Nearly 18 million people live with chronic coronary artery disease (CAD) in the United States, and about 10 million of these patients suffers angina (chest pain), and almost 8 million have suffered a myocardial infarction (MI)[8]. CHF patients are susceptible to pulmonary health problems like sleep apnea and pulmonary edema [14].

2.1.2 Single Ventricle Defects

Contrary to normal physiology, a single ventricle or Fontan physiology contains only a single functional ventricle to both pump and draw blood through both systemic and pulmonary circulations[38]. In order to achieve the Fontan physiology, single ventricle patients must endure 3 or more open-heart surgeries[38]. These staged open-heart procedures are named the Norwood procedure, the Glenn (or Hemi-Fontan), and finally the Fontan completion.

Fontan and Bordeaux originally proposed surgical treatment of the patient with a univentricular heart, separating the systemic and the pulmonary circulation in 1971 [4]. Conceptually, the 'Fontan circulation' generates a circulation such as the systemic venous return is linked to the pulmonary circuit in the absence of the right ventricle. This linking virtually eliminates the chronic volume overload. However, this surgical separation of the circulations results in a risk of chronic venous hypertension, therefore, congestion of the systemic veins, and subsequently decreased cardiac output [39]. From 1971 until today, numerous variations have occurred in the Fontan procedure. The routine approach of a bidirectional cavopulmonary anastomosis previous to the Fontan operation takes place on first six months after birth. The final stage of the Fontan takes place several years later to that. [40]. The Norwood procedure happens at two weeks of age, where an artery-to-pulmonary-artery shunt achieves blood flow to the lungs. The Glenn procedure is applied at six weeks of age, with a linking between the superior vena cava and the pulmonary arteries while eliminating the previously placed Norwood shunt[41].

The final stage of the Fontan procedure is performed between 3 and 5 years of age, which links the inferior vena cava to the pulmonary arteries[42]. The new vessel configuration in the final Fontan physiology is named the total cavopulmonary connection (TCPC) (Figure 5), where the inferior and superior vena cava are linked straight to the pulmonary arteries[43].

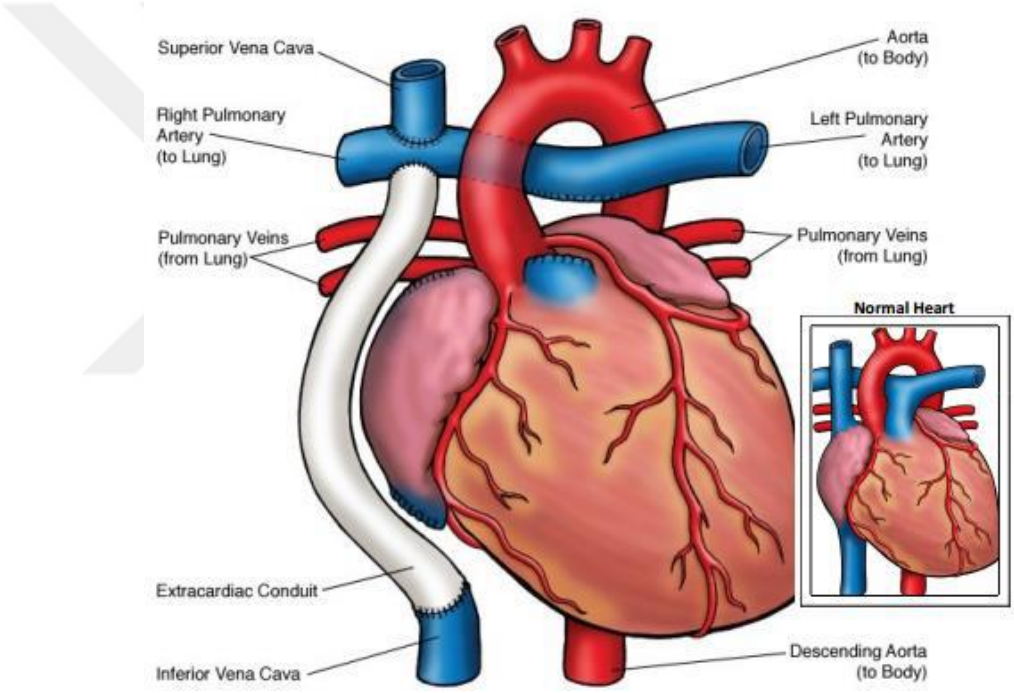

Figure 5: Fontan correction [44,45].

The TCPC configuration has circulatory advantages. It reduces the load on the single functioning ventricle by reducing the excess volume on it. The Energy of the capillaries is also utilized to draw the blood through the lungs[38]. Other supplementary surgical developments have improved the blood flow [46]. In

general, the Fontan circulation extends the life expectancy of the patients. On the other hand, there are some long-standing costs of this man-made physiology, and there are few surgical options or therapeutic treatments, following the early staged surgical procedures.

2.2 Mechanical Circulatory Support Systems

MCSS are mechanical pumps which assist the reducing cardiac output of failing heart. These artificial pumps are considered in four different main types namely, Left ventricular assist devices (LVAD), right ventricular assist devices (RVAD), extracorporeal membrane oxygenators (ECMO), biventricular assist devices (BiVAD) and total artificial hearts (TAH). For patients with single ventricle defects and Fontan circulation, several other pumps (Cavopulmonary Assist Devices) have been proposed in the literature. Cardiac assist devices are subjected to governmental regulations, CE marking in Europe and FDA approval in the US. The primary focus of this thesis is radial flow LVADs and radial flow Cavopulmonary Assist Devices (CAD). For a literature review, mainly the devices which are approved in Europe (Figure 6)Figure 6: Clinically approved heart pumps in Europe as of 2018 [47] is mentioned in this chapter.

Long-term devices	
Continuous flow	Berlin Heart INCOR CircuLite SYNERGY HeartAssist 5 HeartWare HVAD Jarvik 2000 MicroMed DeBakey Thoratec HeartMate II Thoratec HeartMate 3
Pulsatile extracorporeal	Berlin Heart EXCOR Thoratec PVAD Abiomed AB5000
Total artificial heart	SynCardia Cardiowest
Short-term devices	Medos DeltaStream Levitronix CentriMag Maquet CARDIOHELP

Figure 6: Clinically approved heart pumps in Europe as of 2018 [47].

In addition to these approved devices, numerous other devices have been applying for clinical approval in EU and US. Recent reports show that the use of pulsatile flow VADs has significantly reduced in the last decade[48]. Moreover, continuous flow centrifugal pumps have recently been approved, and the implantation of these devices have steadily increased in the last several years (Figure 8). Figure 7 depicts the US statistics between 2006 and 2016, showing 22866 LVAD/RVAD implants where 3845 patients received heart transplants and 17634 patients were still on LVAD support as of 2016. Usage of pulsatile flow LVADs were less than thousand in the US. A single usage of RVADs is also limited. Only 34 patients received an RVAD without LVAD support. TAH implants were less than

400 in this report. These statistics prove that LVAD is the most needed MCSS and centrifugal LVADs have become more frequently used during the last years of this decade (Figure 7).

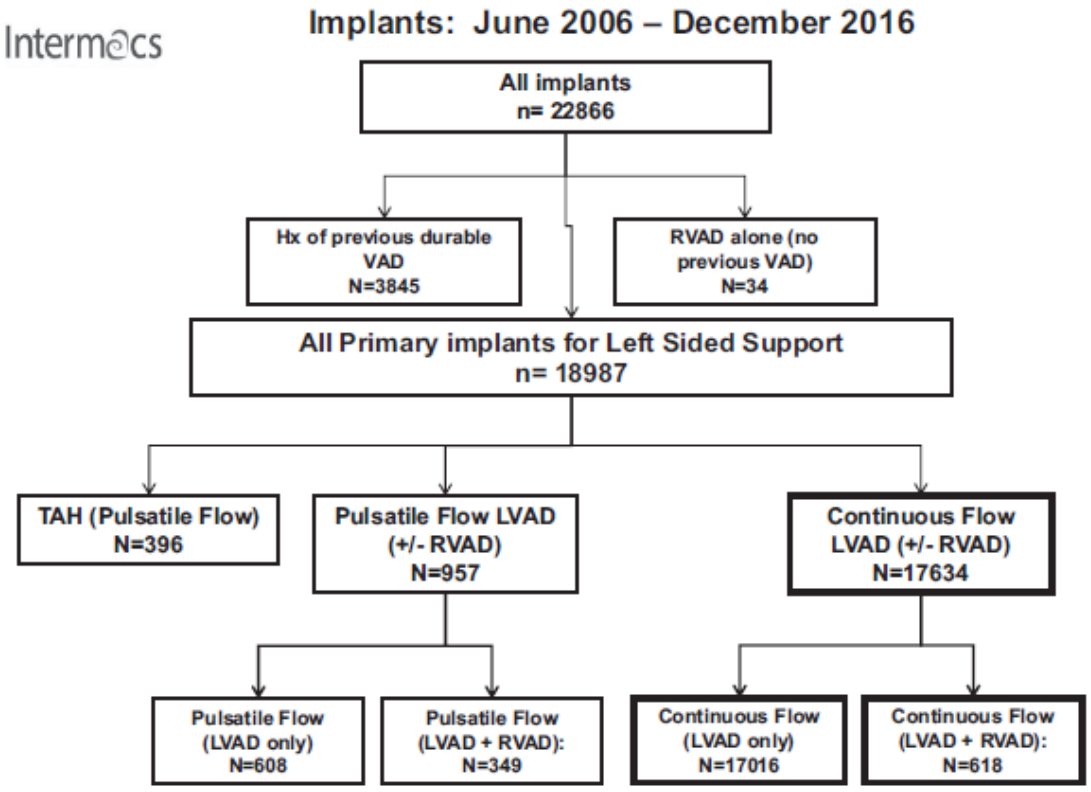

Figure 7: LVAD/RVAD/TAH statistics in US[49].

Reciprocating pumps are not durable for long-term use due to the diaphragm fatigue. Therefore, rotary pumps became the standard for LVADs. According to the pump design theory, centrifugal pumps are capable of producing higher pressures at lower flows. On the other hand, axial flow pumps provide higher flow rates at lower pressure gains (Figure 11). Moreover, axial flow pumps much more compact

in size compared to the centrifugal pumps. Thanks to their smaller size and cylindrical shape, implanting axial pumps require less time and decrease invasiveness of the operation [46]. However, the use of centrifugal pumps increases significantly during the last decade (Figure 8).

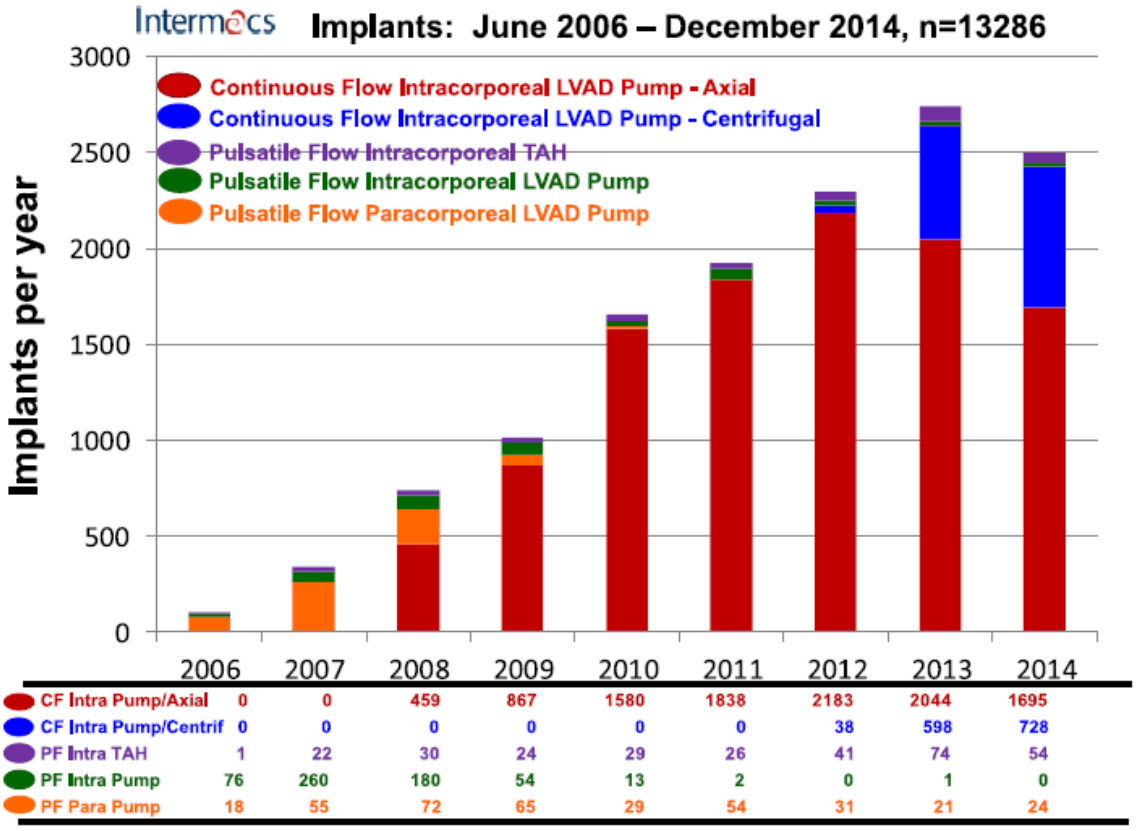

Figure 8: Amount of heart assist devices implanted between 2006-20014[48].

2.2.1 Left Ventricular Assist Devices

Over the last fifty years, countless heart pumps were developed with the aim of lessening the effects of HF by supporting blood flow[50]. VADs are categorized into three generations according to the chosen bearing or suspension technologies and in two groups considering flow types (pulsatile or continuous flow) [51]. Moreover, continuous flow VADs are categorized in two groups considering the flow types as axial or centrifugal (Figure 9). There has been a radical evolution from pulsatile pumps to continuous flow rotary pumps after FDA approval of new continuous pumps[52]. Percentage of centrifugal flow pumps among LVADs increased considerably since 2012[48]. Continuous-flow left-ventricular assist devices offer specific improvements over the older pulsatile-flow devices like less invasive implantation, compact size, quiet operation, and lengthier endurance. By 2011, nearly all of LVAD implants are continuous-flow devices[53].

Figure 10 shows a list of approved devices as of 2012.

Flow Type:

- Reciprocating-Pulsatile Pumps
- Continuous Flow Rotary Pumps
- Axial Flow
- Centrifugal (Radial) Flow
- Mixed (Diagonal) Flow

Device Generations:

1st generation: Volume-displacement (reciprocating) pumps,

2nd generation: Rotary pumps with conventional bearings,

3rd generation: Rotary pumps with active/passive-magnetic levitation or hydro-dynamic/static suspension

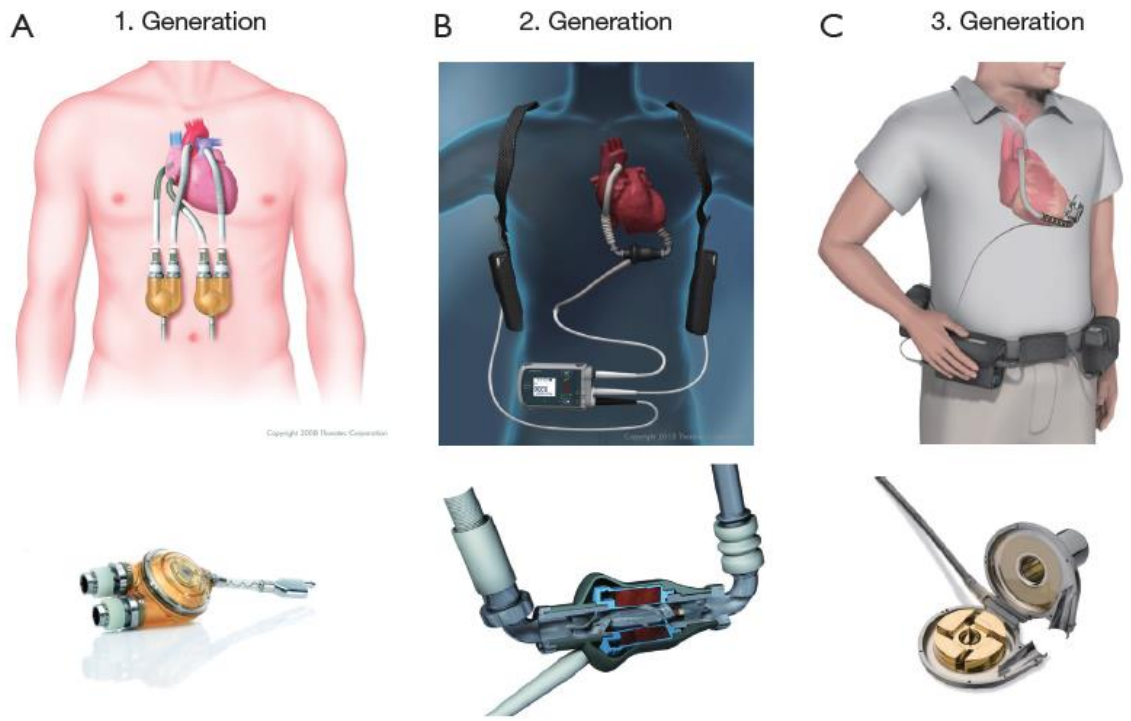

Figure 9: LVAD Types, (A) Thoratec PVAD, (B) Thoratec HeartMate II, (C) Heartware HVAD [52].

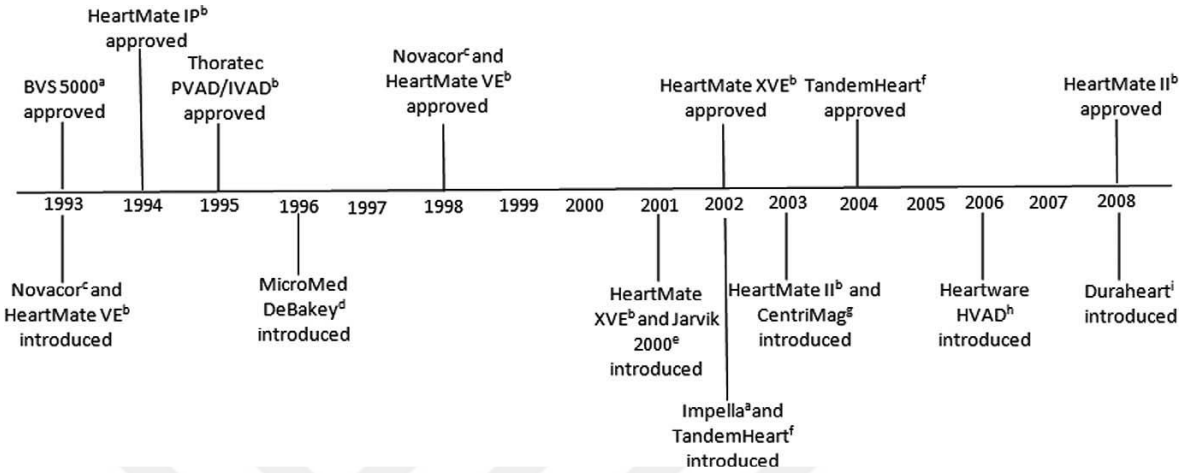

Figure 10: The list of approved devices as of 2012 [54].

1st generation pumps (reciprocating-pulsatile) increase pressure in a closed chamber to create blood flow via a pneumatically driven membrane piston mechanism. Increased pressure inside the chamber delivers unidirectional blood flow through the outlet valve (similar to aortic valve) of closed volume by overcoming afterload inside the aorta. The first-generation pumps supply pulsatile blood flows as imitating the pumping action of a heart. The annual survival rate of average end-stage HF patients on first generation pumps was 52% in contrast to drug therapy with 25%. This technology was not initially broadly recognized by the medical doctors due to the bulky dimensions, the short endurance of the membrane due to repetitive flexion, and sizeable percutaneous driveline carrying the pneumatic drive flow [50].

Recent generations (2nd and 3rd) are non-pulsatile, turbomachines that deliver continuous blood flow by exerting kinetic energy to blood by an impeller. The

impeller is the only moving component which agrees on a significant size reduction and fewer mechanical wear. Recent devices also allow controlling impeller speed to create an artificial pulse[55]. 2nd generation pumps with mechanical bearings are mostly axial flow, and 3rd generations are primarily centrifugal devices. The main difference of these two flow types is pressure head, and flow rate shows a strong inverse linear relationship in axial devices, a contrast to fairly flat pressure head curve of centrifugal pumps as seen in Figure 11 [56].

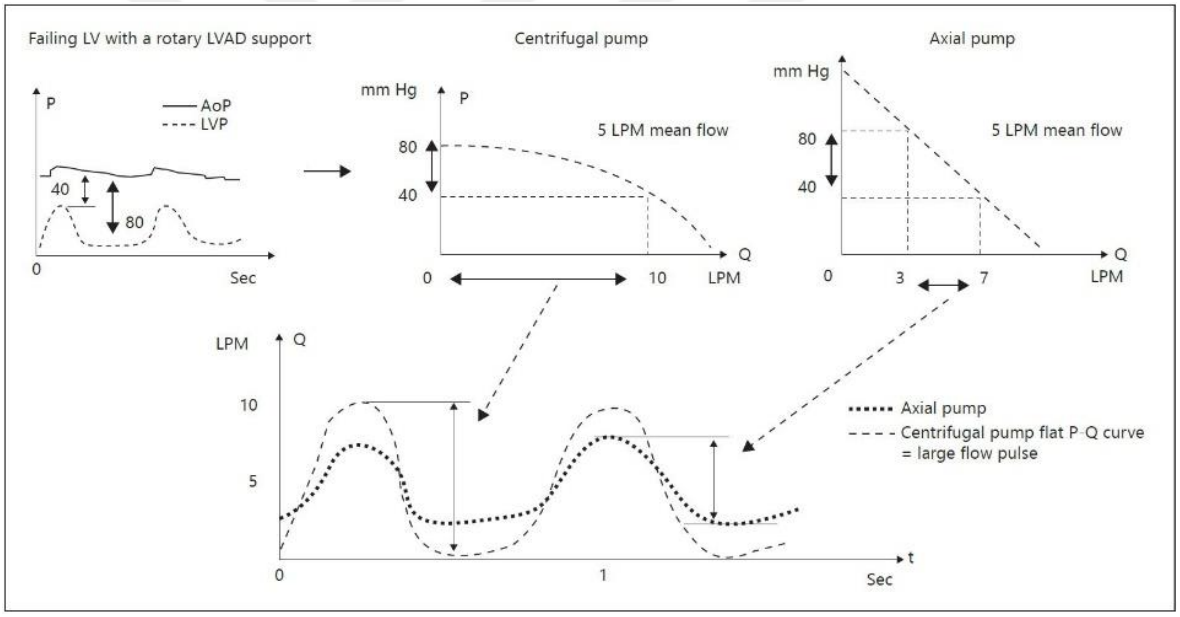

Figure 11: Pressure vs. flow rate characteristics of axial and centrifugal pumps [56]

2.2.2 Axial flow MCSS

In this type of pumps, the blood flow passes parallel to the rotary axis of the impeller. The main advantage of the axial pump is the compact size and tube-shaped body making it convenient for an anatomical fit. The main drawback of this pump is the comparatively high rotation speed. Axial flow (rotary) pumps consists of a rotating impeller with helical blades that curve around the shaft. A percutaneous driveline supplies power to a motor that actuates the rotation of the impeller by a radial flux electromagnetic induction.

2.2.2 Centrifugal (Radial) flow MCSS

Centrifugal flow pumps have an ejection direction vertical to the axis of rotation of the impeller. The advantage of these type of pump is the relatively low rotation speed. The main disadvantage of this type is large size compared to axial flow devices. Similar to the axial devices, a percutaneous driveline supplies power to a motor that actuates the rotation of the impeller by axial flux electromagnetic induction. The focus of this thesis is centrifugal machines. Therefore, the third chapter focuses on centrifugal pump and turbine design and numerical performance estimation methods.

2.2.3 First Generation VADs

The first generation of LVADs is either pneumatically or electrically actuated reciprocating pump. Some of the clinically approved first generation pumps are discussed in this chapter.

The Heartmate IP and XVE LVADs were developed by Thoratec Corporation is a reciprocating pump utilizing a pusher plate placed under a flexible plastic membrane to induce a piston-like action (Figure 12). The inlet is installed to the apex of the left ventricle, and the outlet is attached to the aorta. This device was further divided into two types. Initially, HeartMate IP was pneumatically powered and was replaced by Heartmate XVE which was electrically driven. The diameter of Heartmate XVE is Ø110 with a height of 40 mm weighing 1.2 kg [54]. The device is capable of a flow rate of 10 L/min at 120 beats per minute. Due to high reliability, this device was approved by the Food and Drug Authority as destination therapy in 2003 [54]. Heartmate XVE has been implanted in almost 5000 patients making it one the most frequently implanted VAD globally.

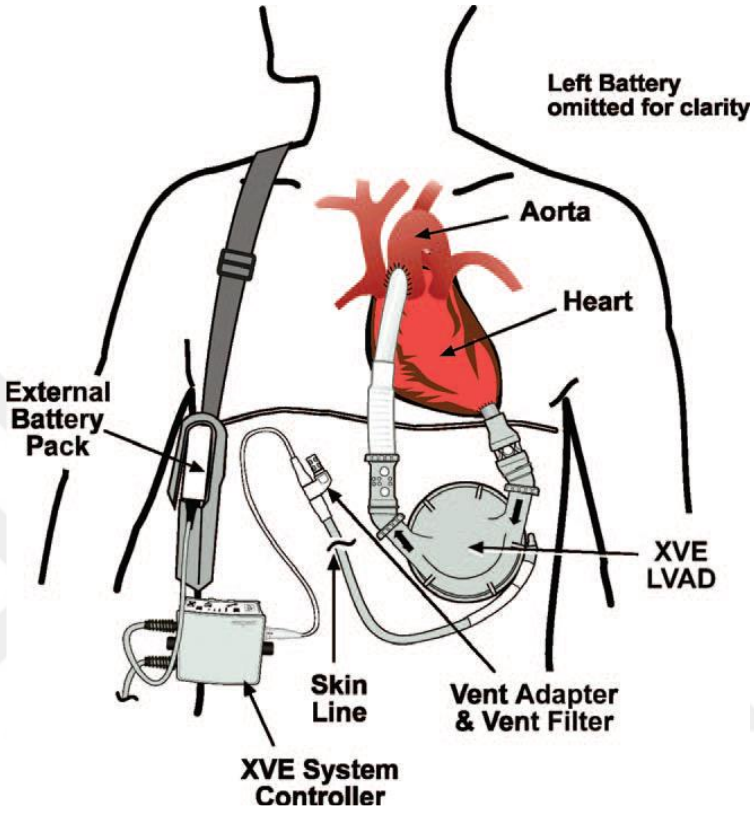

Figure 12: Heartmate XVE [54].

Berlin Heart EXCOR is a first-generation device which provides circulatory support extracorporeally (placed out of the body). The pump consisted of a polyurethane chamber and coated with heparin for avoiding thrombogenic events. This pneumatically actuated device is designed in various sizes like 50, 60 and 80 ml for adults and 10, 20 and 35 ml for pediatric use (Figure 13). The most massive pump (80 ml) can deliver a flow rate of 10 L/min at 150 bpm[57]. The devices were approved by FDA in 2008 and thus far more than 2000 devices have been implanted globally.

Figure 13: Berlin EXCOR[57].

The Abiomed AB5000 is a first generation pneumatically powered VAD. It is extracorporeal and functions by actuating the polyurethane diaphragm (Figure 14). The pump is 230 grams and can be utilized as LVAD, RVAD, and BiVAD. FDA approved this device in 2003 however the device is less popular than other first-generation devices [58].

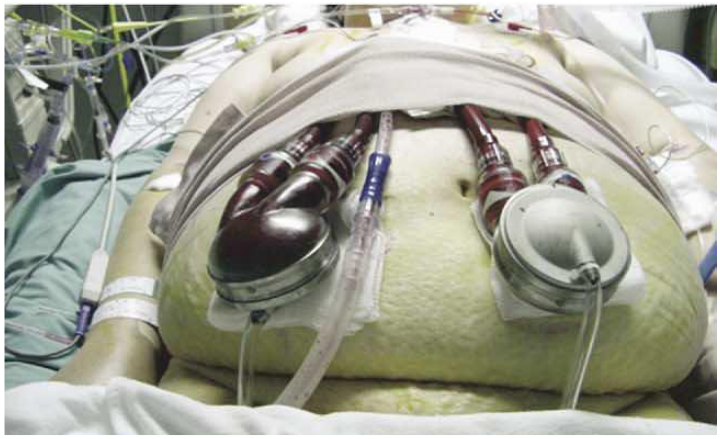

Figure 14: Abiomed 5000 as BiVAD support use [58].

The Thoratec PVAD and IVAD are pneumatically driven first generation devices. The PVAD is an extracorporeal device which was approved by in 1995. The IVAD is the incorporeal version of the same device and was approved in 2004. Both have the same internal flow path and able to supply a flow rate of around 7 L/min at 100 bpm (Figure 15). IVAD has a compact size and weight (125 mm×80 mm×50 mm weighing 339 g) as compared to the PVAD (125 mm × 80 mm×60 mm and 417 g). The number of patients which are supported by PVAD and IVAD is more than 5000[59].

Figure 15 Thoratec PVAD (plastic housing) -IVAD (titanium housing) [59].

2.2.4 Second Generation VADs

Secondary generation pump is rotary blood pumps with mechanical pivot bearing. Some of the clinically approved second generation pumps are discussed in this chapter.

DeBakey-HeartAssist 5 is designed in 1988 by the renown cardiac surgeon DeBakey and NASA engineers. The initial design was a joint effort of Drs. Michael E. DeBakey and George P. Noon [60]. MicroMed Technology was established in 1996 to develop and test the device. The device was later named HeartAssist 5. The final device was made of titanium with an rpm ranged from 7,500 to 12,500 capable of providing 10 L/min flow rate (Figure 16). A flow meter was merged inside the pump for continuous real-time flow measurements[61].

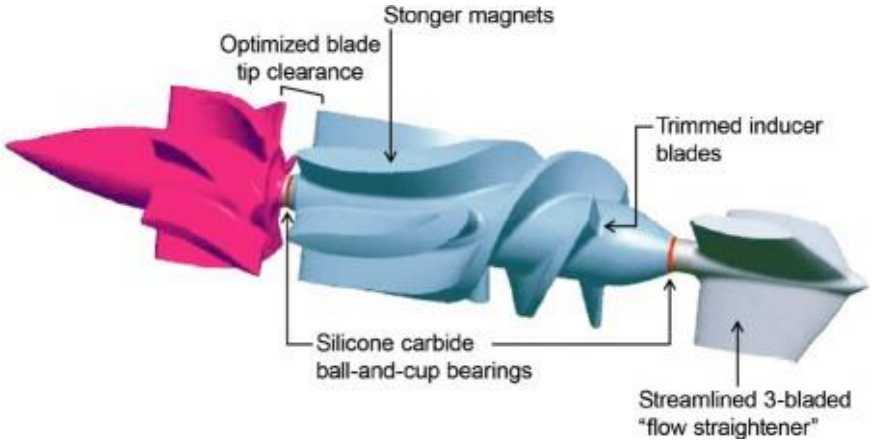

Figure 16: Debakey-HeartAssist 5[61].

The Heartmate II is another second-generation pump with the axial flow (Figure 17). The operation speed of this device ranges from 6000 to 15000 rpm with a maximum flow rate of 10 L/min. The physiologic design criteria (5 L/min and 100 mmHg) is attained at 9000 rpm. The weight of the device is 375 g, and the size is Ø40×60 mm [62]. TheHeartMateII (Abbott Laboratories, previously Thoratec Corporation) was approved as bridge-to-transplant therapy in 2008 and for destination therapy(DT) in 2010 by FDA [49]. According to the Thoratec data summary released in April 2014, more than 18000 patients have been implanted with this device which makes the device most popular LVAD in history.

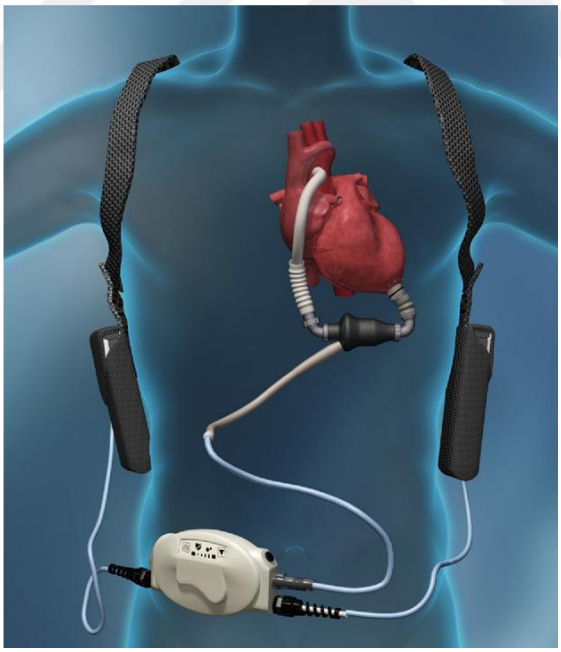

Figure 17: Heartmate II inside the body[62].

The Jarvik 2000 is a compact, incorporeal pump with the axial flow (Figure 18). It is able to provide the flow rates ranging from 3 to 7 L/min at the rotational speed between 8000 rpm to 12000 rpm. The device is tiny with the dimensions of Ø25×55 mm and weight of 75 g [63].

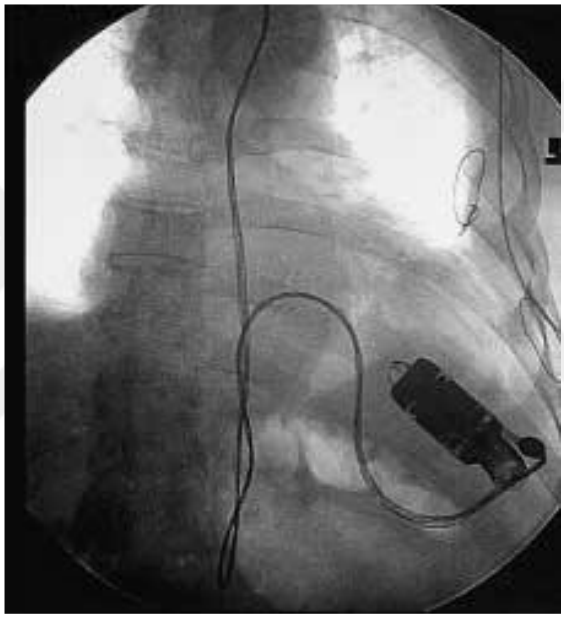

Figure 18: Jarvik 2000 inside the body [64].

2.2.5 Third Generation VADs

Third generation blood pump is the type of rotary blood pumps in which the rotating impeller is suspended with the magnetic or hydraulic forces without the support of a conventional bearing. Compared to the active magnetic system, passive magnets or hydrodynamic bearings are more efficient regarding power to levitate the rotor. These types of pumps have large flow passages due to the suspension

system, so the blood damage possibility is minimized. Some of the clinically approved third generation pumps are discussed in this chapter.

The Berlin heart InCOR is a third-generation axial flow pump. It is a long-term incorporeal device having a magnetically suspended rotor (Figure 19). The rotor of this device is suspended with active magnetic force while the radial balance is achieved using passive magnets. It is the most massive axial flow pump (Ø30×120 mm) and weights 200 g [55,65]. This device can achieve a maximum flow rate of 7 L/min at 10000 rpm. The first human clinical trial occurred in June 2002, and the device got CE mark approval in 2003.

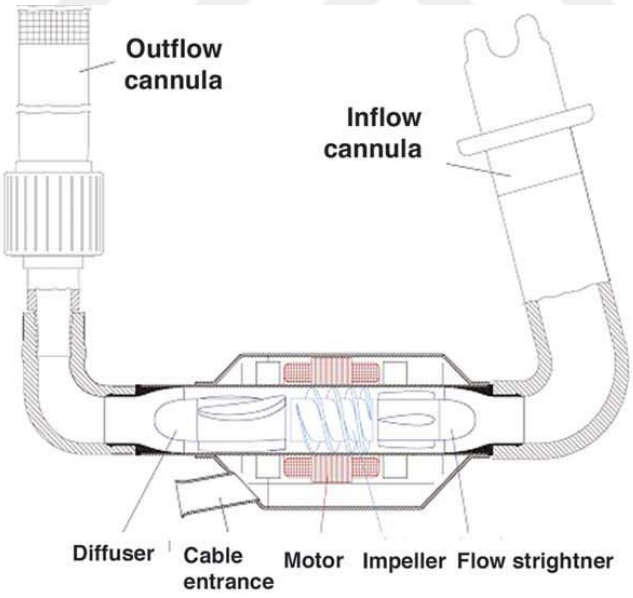

Figure 19: Berlin Heart Incor Design[65].

The DuraHeart LVAD is the world's first approved magnetically levitated continuous-flow centrifugal LVAD with the weight of 540 grams[66]. The pump rotor is levitated using a combination of hydrodynamic bearing designed as a spiral groove at the bottom of the rotor and a magnetic bearing system (Figure 20). The diameter of the device is Ø72, and the height is 45 mm[55]. The device is able to rotate at 2600 rpm providing a flow rate of 10 L/min. Conformité Européenne (CE) marking trials started in 2004, and in 2009 the device was approved in patients candidates to HTx (bridge to transplant therapy) [51].

Figure 20: DuraHeart VAD[66].

The HeartWare HVAD is an incorporeal generation centrifugal flow pump (Figure 21). The inlet of the HVAD is integrated into the apex of the heart. The rotary impeller is entirely levitated with both hydrodynamic forces and passive magnetic bearings. The device is the smallest in total volume and the lightest (Ø50 mm, 145 g) among the centrifugal flow pumps[67]. The impeller rotates at a particular speed of 2400 rpm, while speed can range between 1800 and 4000 rpm are, delivering up to 10 l/ min. Clinical trials of the HVAD device underway since 2008, with above 700 patients now received the device worldwide.

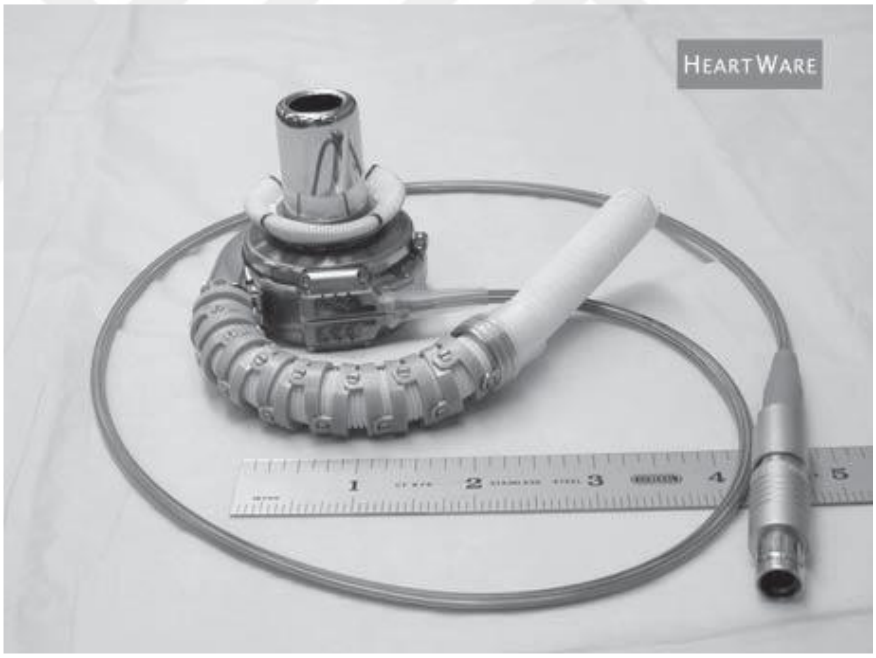

Figure 21: HVAD [67].

HeartMate III is intended for long-term (destination therapy) support in patients with end-stage heart failure. The LVAD has a compact design with a 6.9 cm diameter 30 mm in height weighing 500 g (Figure 22). The device has a

magnetically levitated impeller and has been developed in a joint effort between Thoratec Corporation and Levitronix GmbH. The use of an active magnetic bearing removes all friction wear [68]. In a study with 50 patients conducted between June and November 2014 , the device has a 6-month survival rate of 92%, exceeded the performance objective with complication rates for hemorrhage (14%), driveline related infections (10%), interior hemorrhage (8%) and stroke (8%)[52].

Figure 22: Heartmate 3[52].

2.3 Fontan (Cavopulmonary) Assist Devices

Fontan patients suffer relentless late health problems related to the digestive system, including feeding complaints, liver insufficiency, protein-losing enteropathy, plastic bronchitis, and following failed-Fontan states. Even though the reasons for these health problems are multifactorial, persistently high systemic venous pressure (SVP) is broadly recognized to be the essential challenging factor that causes gradual remodeling in the venous vascular and lymphatic systems[6]. Even though several methods exist to treat this disease (Figure 23), as the ultimate

remedy for high SVP, venous Fontan ventricular assist (FVAD) is required [69]. Mistakenly compared with traditional mechanical circulatory assistance, the first use of mechanical circulatory support for Fontan patients was introduced by de Leval [70] which creates low venous pressure and high flow rate to solve the ''Fontan paradox''.

In addition to the Fontan assist device development effort in our research group, numerous mechanical circulatory support systems have been implanted or proposed for supporting Fontan patients. Several research groups have designed novel devices aiming to support Fontan circulation for a patient with dysfunctional or failing single ventricle physiology [21]. The following chapter summarizes the novel devices/techniques for Fontan circulatory support.

As of today, there are no cavopulmonary assist devices (CPAD) approved for clinical use. However, several research labs are in the process of developing these devices or testing existing devices to serve as cavopulmonary support. A list of experimental treatment options for Fontan support is summarized in Figure 23.

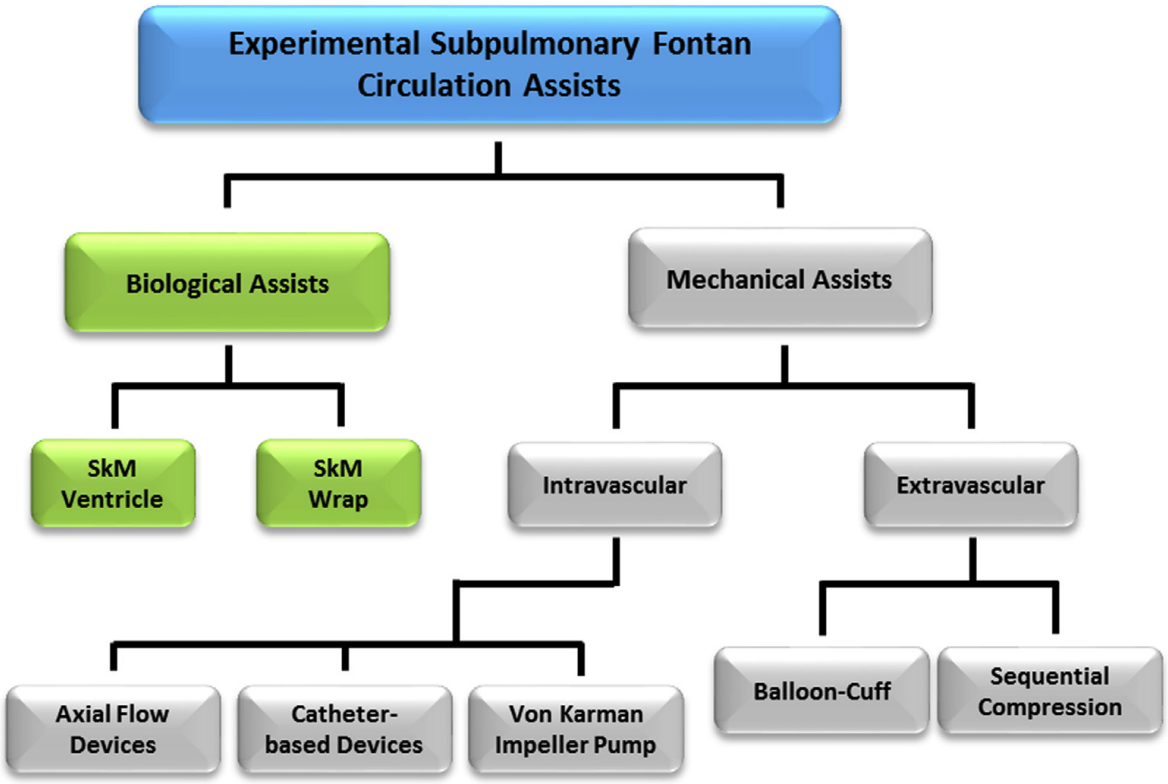

Figure 23: Cavopulmonary Assistance Strategies[21].

Lacour-Gayet et al. [71] proposed an artificial right ventricle (Figure 24). This novel design utilizes a channel connecting the SVC and IVC. The channel then forms a pathway (including an axial pump inside) to the LPA and RPA. Even though this technique improved the circulatory function in in-vitro studies, its fundamental weakness is the need for a complete reconstruction of the Fontan physiology.

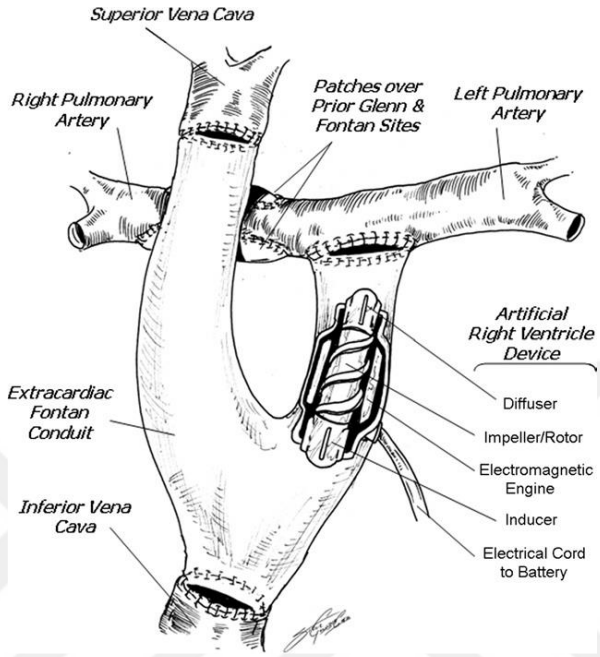

Figure 24: Artificial right ventricle of Lacour-Gayet[71].

Medvitz et al. [72] developed an extracardiac implant for complete circulatory assistance. This design includes a Tesla design pump which utilizes a set of firmly stacked parallel plates instead of a regular pump impeller (Figure 25). While this design proved an excellent hydrodynamic performance, the technique requires surgery, and the device is not designed explicitly for a Fontan physiology. The flow pathway of the device is also intensely obstructive and could cause sudden death in case of thrombus formation or device failure.

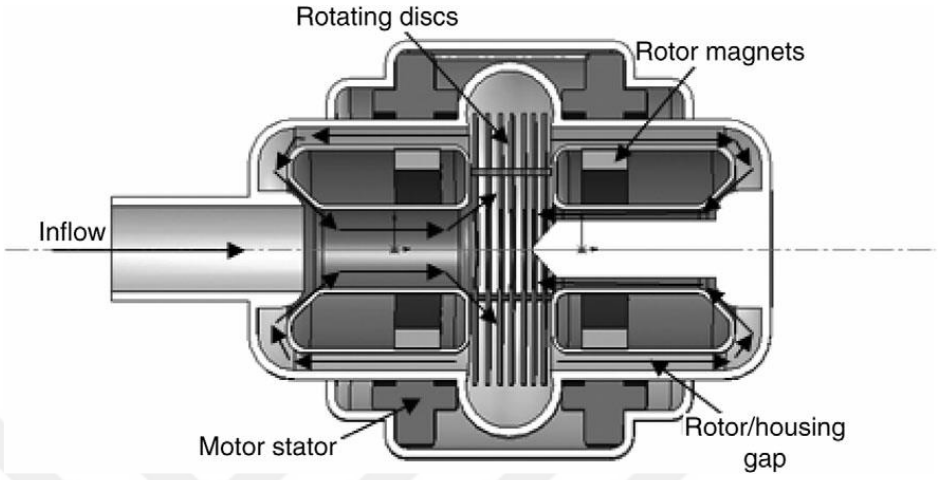

Figure 25: Medvitz Tesla pump[72].

Similarly, Wang et al. [73] conferred an extracorporeal concept, which combines their previously designed double lumen cannula (DLC) and a clinically approved Levitronix-CentriMag which is an extracorporeal blood pump, as a cavopulmonary assist system (Figure 26). The DLC draws blood from the systemic return and pumps the blood through a graft into the right pulmonary artery.

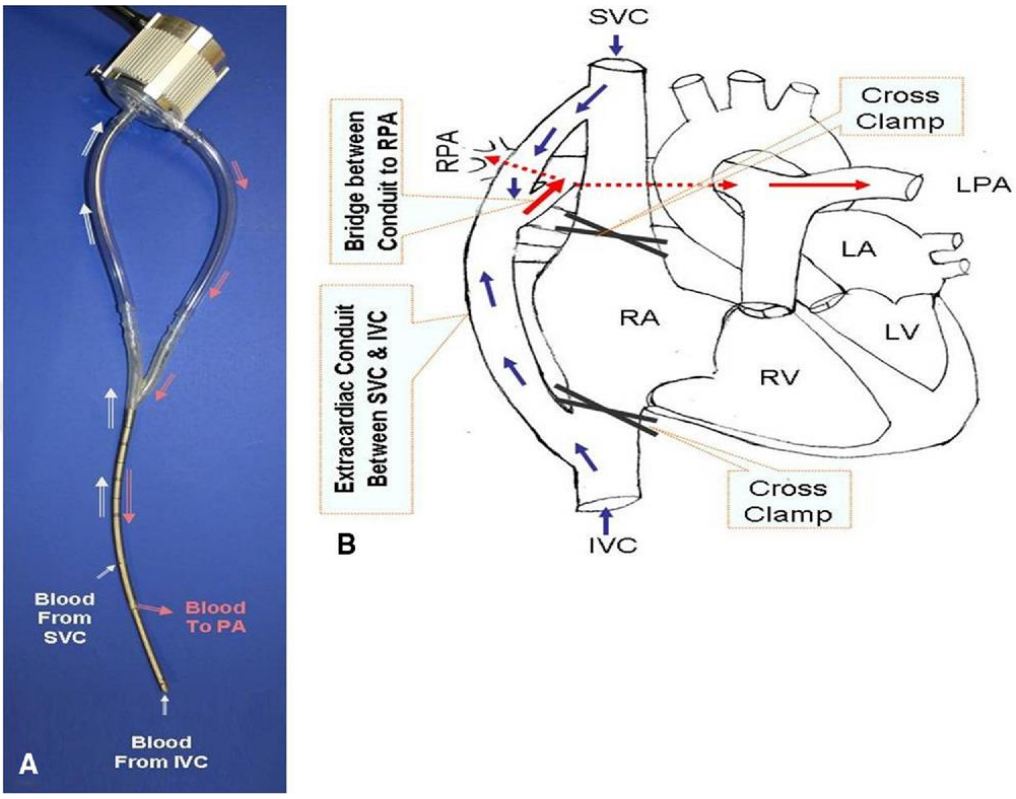

Figure 26: Wang et al. Fontan assist system[73].

Wang et al. [74] also developed a less invasive technique with a double lumen cannula (DLC) implanted in the TCPC with two folding membrane umbrellas and a pump in the SVC (Figure 27). While the pump assists the circulation, the umbrellas increase the efficiency of the pump by altering the diameter of the TCPC and preventing backflows by acting as a passive valve.

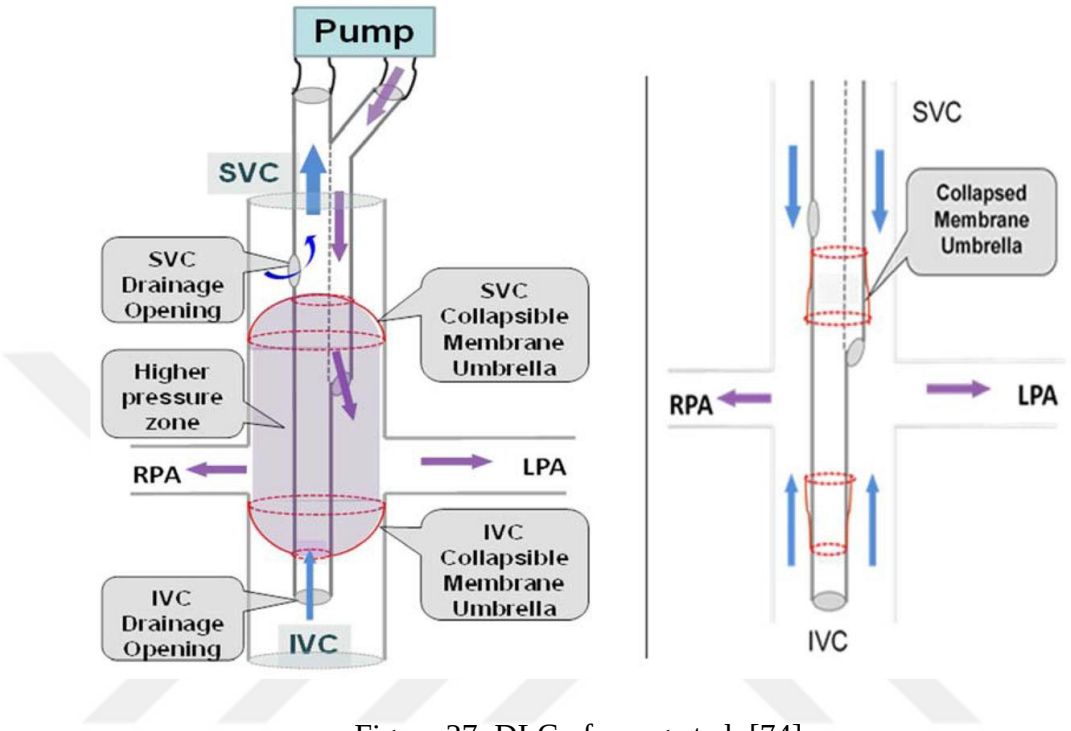

Figure 27: DLC of wang et al. [74].

Giridharan et al. proposed a short-term cavopulmonary assist device [75]. This system comprises an expandable viscous impeller pump (von Kármán viscous impeller pump) as seen in Figure 28. The pump is made of an inflatable nitinol cage and is placed in the center of TCPC. The pump is designed to be implanted percutaneously. The findings presented a 23% rise in cardiac output in in-vitro experiments with this method. Axial blood pumps are also being researched and have shown promising results as cavopulmonary support devices.

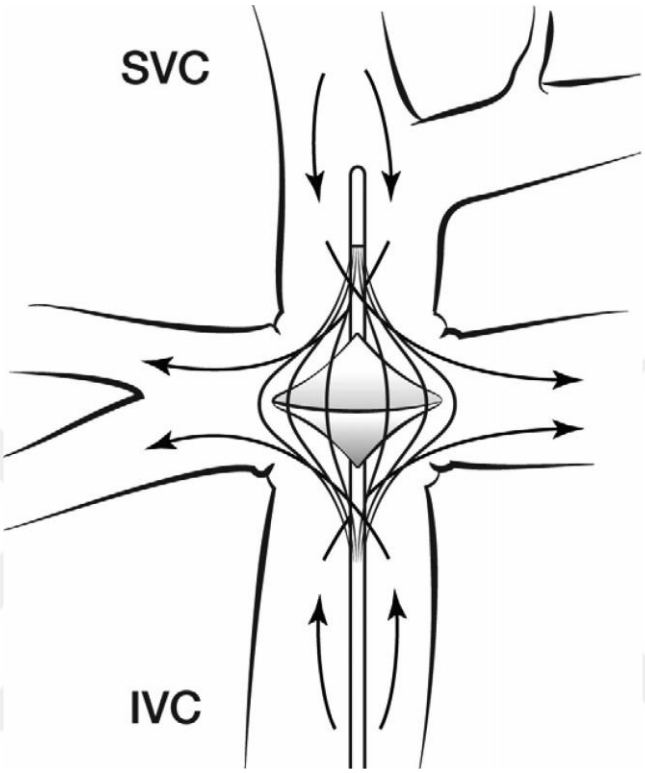

Figure 28: Giridharan pump[76].

Wang et al. [77] designed a microaxial pump to be implanted inside the IVC (Figure 29). The microaxial pump was successful in computational and in vitro studies. Likewise, Rodefeld et al. [78] implanted the axial flow Hemopump, in both vena cavae in a sheep model to create a total cavopulmonary alteration. This study confirmed the application of continuous axial flow pumps to provide circulatory assist in Fontan patients.

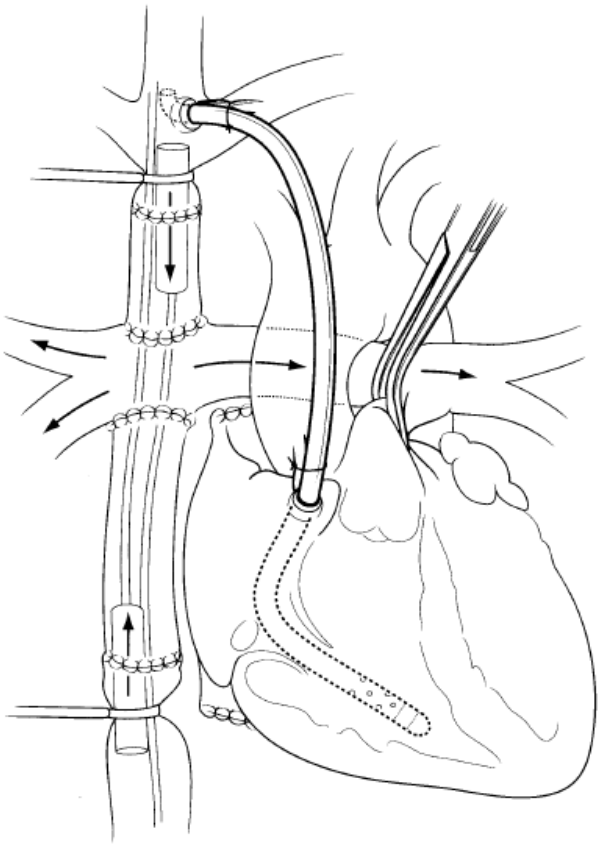

Figure 29: Passive Fontan Assist [78].

Throckmorton et al. [79] designed a percutaneously-implanted, folding axial flow blood pump to assist the cavopulmonary circulation in Fontan patients (Figure 30). The prototype comprises a 4-bladed impeller generated a pressure head of 2–30 mmHg under a flow rate of 0.5–4 L/min where the impeller spins at 3000 to 6000 RPM[79].

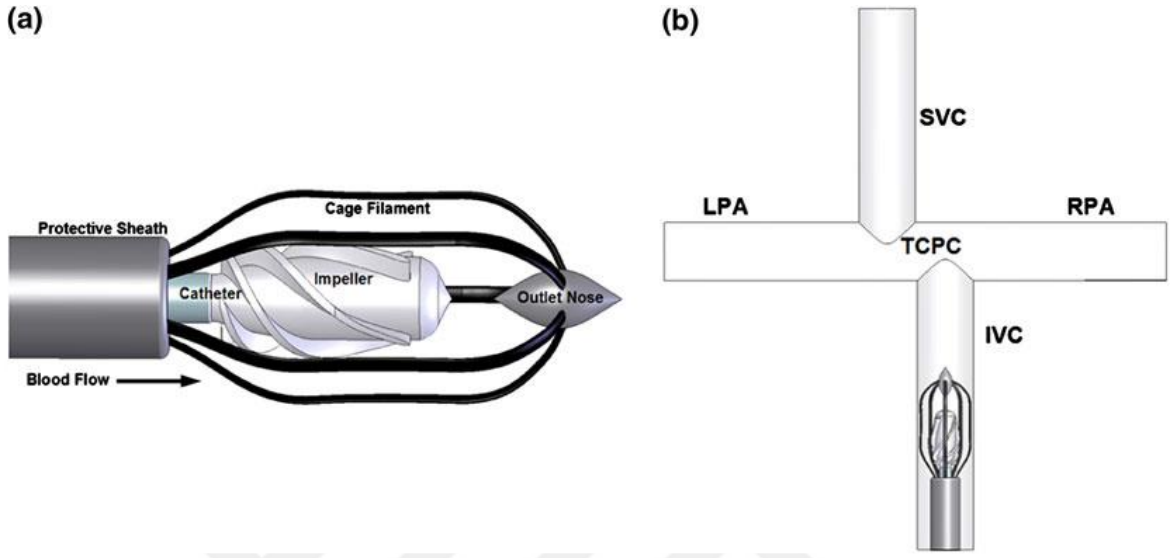

Figure 30: Micro-axial flow pump (a) Pump components, (b) Pump placement in TCPC shunt [79].

Table 1: Comparative analysis of current cavopulmonary assist devices[6].

Pump design	Venous pressure decrease, mmHg	Flow rate, lt/m	Rotation Speed, Rpm	Notes
Propeller[80]	5 to 50	0.5 to 3.5	5000 to 7000	Hydraulic in vitro
Axial[71]	5 to	2	1700 to 4500	Failing Fontan
Axial[78]	2.4	3.7	No information	
No impeller[75]	5 to 20	0 to 5	0 to 7000	Dual IVC/SVC support, Mock-up flow loop
Berlin heart[81]	No information	3.8	80 Strokes/min	Hypoplastic left heart
Centrifugal[82]	10	No information	No information	
Axial [83]	12	3.1 to 1.2	18,000 to 24,000	Piglet model
Axial [84]	7	4.6	10,000	Jarvik VAD

DESIGN OF CENTRIFUGAL BLOOD PUMPS

Based on the geometric structure and flow direction the pumps are divided into two types: reciprocating and rotary pumps. The rotary pumps the kinetic energy rise in fluid occurs as it is subjected to the rotation of the blades placed on the impeller. This transfer of kinetic energy rises the fluid velocity and therefore increases the dynamic pressure. This kinetic energy (velocity) of the fluid is converted into static energy (pressure) by passing through a diffuser or a volute. Before the fluid reaches to the impeller, there is a group of the stationary blades called inducer or flow straightener which regulates the off-angle velocity components at the inlet section for improving the performance.

Contrary to reciprocating pumps, rotary pumps operate by a pushing plate mechanism. Characteristically, these pumps are compact, have lower priming volume and longer endurance. The geometry of the flow clusters rotary blood pumps as axial, radial (centrifugal flow) or mixed (diagonal flow). Each of these flow types is efficient for a different specific speed coefficient, the radial pumps are better efficient at lower specific speeds, and as the specific speed increases, the more axial flow becomes efficient. A centrifugal pump is able to produce a higher pressure rise at a low flow rate while an axial pump provides a higher flow rate at a low-pressure rise. The design methodology of centrifugal pumps is further discussed in this chapter including the turbomachinery equations, velocity triangles, blade design and volute design.

All of these design criteria alter the hemolytic and hydrodynamic performance of the blood pumps (Figure 31). A better hydrodynamics performance means pumping the blood efficient regarding energy. Whereas, the hemolytic performance means a minimum mechanical induced hemolysis and fewer thromboembolic events during pump operation. The shear stress acting on the blood by the pump operation should be minimized by the geometric design. Likewise, the thrombosis formation is exterminated by achieving a regular flow pattern inside the pump. Therefore, recirculation and stagnation zones must be removed by design. Besides these criteria, a viable blood pump should be compact for improving the patient mobility. However, these design criteria may be contradictory. The conventional turbomachinery design method emphasizes only the hydraulic performance and does not focus on the hemolytic performance. Reducing the pump size creates a higher velocity gradient and therefore higher shear stress. These factors are investigated with CFD simulations which are discussed in the next chapter. In this chapter, the turbomachinery theory is explained. After all these design steps, the design might still fail. In case of a failure, the design must be re-considered for optimization by going back to the turbomachinery and geometry optimization stage. A design cycle is illustrated in Figure 32.

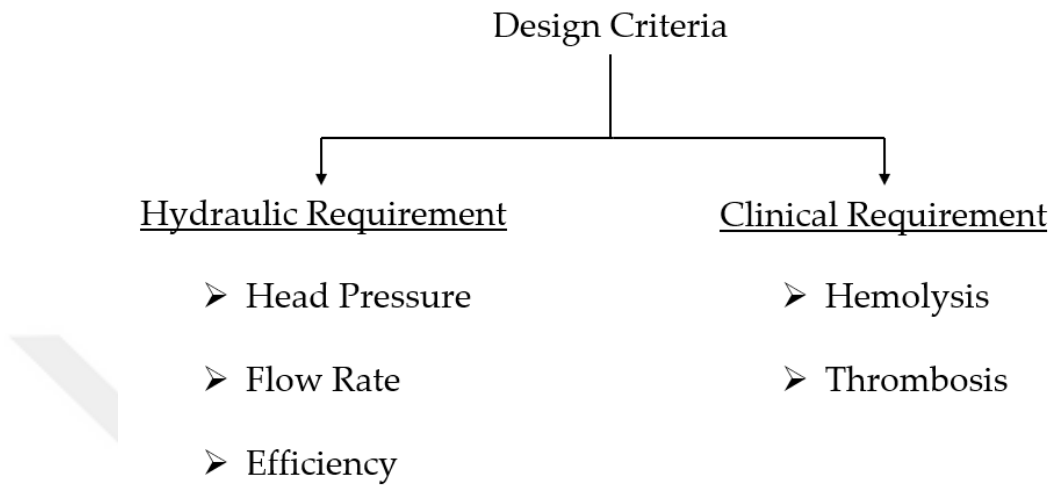

Figure 31: Blood pump design criteria.

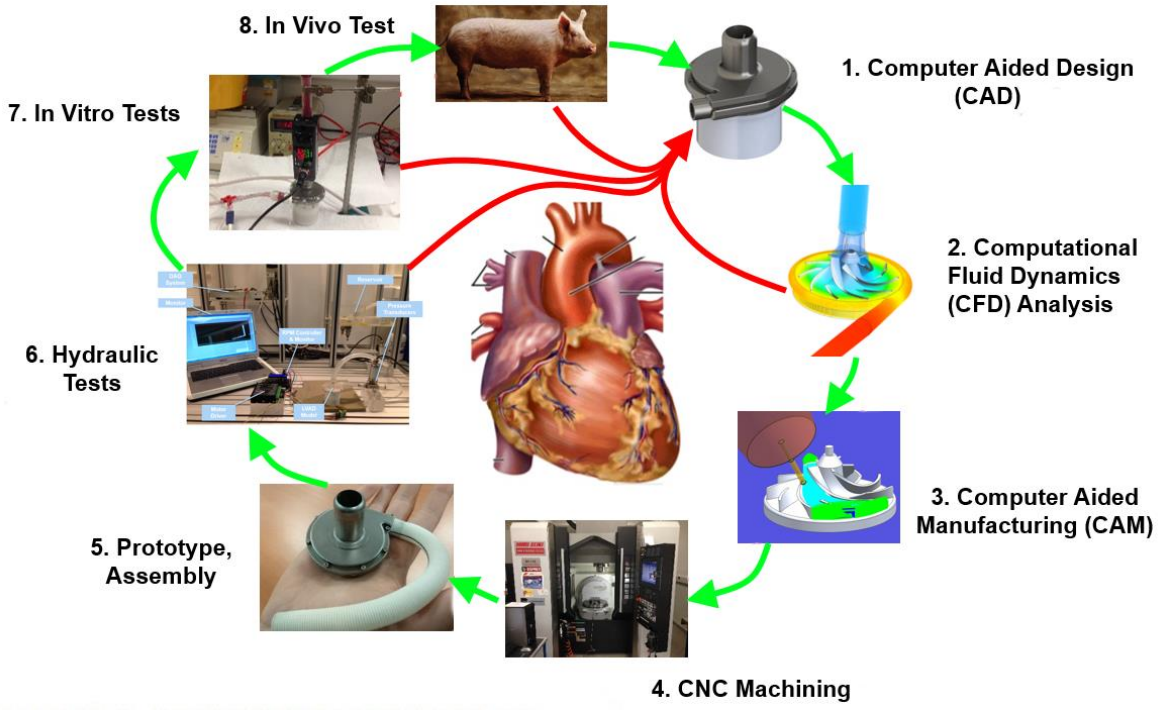

Figure 32: Design cycle of an LVAD.

3.1 Turbomachinery Theory

A turbomachine is a device which acts on or acts by the momentum of a fluid by the action of a rotary part [85-87]. This operation changes the pressure of the fluid flow. Mechanical energy transfer mostly occurs in a steady-state flow style. Turbomachines comprise all machines that generate energy, such as turbines, as well as those sorts that provide a pressure head, such as radial pumps and compressors. The turbomachine harvests energy from or exerts energy to a continuously moving stream of liquid or gas. Some examples of turbomachines are shown in Figure 33. However, in a positive displacement machine, it is reciprocating (same as the first-generation blood pumps). The turbomachine family includes an extensive variety of machines, such as gas, steam or hydraulic turbines, water wheels, centrifugal or axial flow pumps, radial and axial compressors, and hydraulic turbines[85]. In this work, the primary focus is **incompressible fluid using radial blood pumps and blood turbines** in the emphasis of a centrifugal LVAD (**iHeart VAD**) and an integrated centrifugal blood turbine-pump couple (**iATVA**).

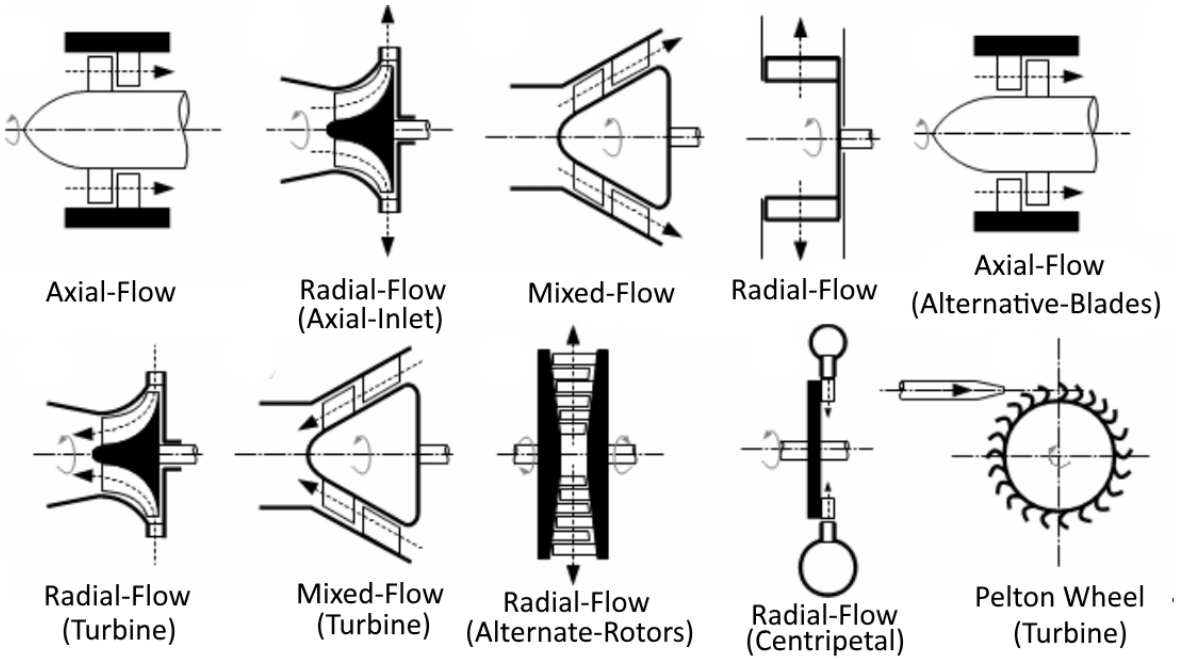

Figure 33: Types and shapes of some turbomachines[88].

3.1.1 Centrifugal Flow Pump

In an axial flow pump, the flow direction of the fluid is parallel to the rotation axis of the impeller. In contrast, a centrifugal pump has a vertical outlet flow to the rotation axis (Figure 34). The main advantage of the centrifugal (radial) design is efficient at relatively low specific speeds. Low rpm nature of centrifugal pump is also an advantage for creating relatively low shear stress inside the priming volume. The three vital parts of centrifugal pumps are the impeller, the volute casing, and the volute tongue.

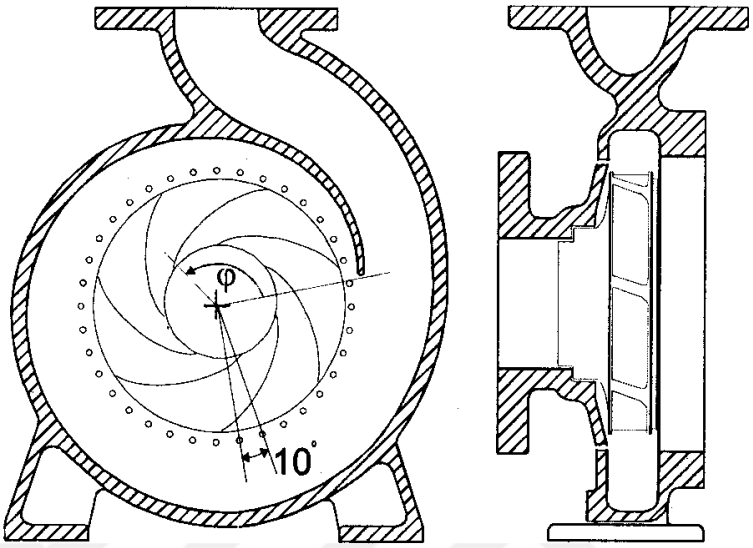

Figure 34: A centrifugal pump[89].

Denis Papin (1647-1710) invented the centrifugal pump in 1698 in France [86]. Leonardo da Vinci was also suggested to use centrifugal force for pumping action, however, could not achieve it due to the lack of adequately advanced machining options. Leonhard Euler (1707-1783) proposed a mathematical concept of the pump operation in 1751[90]. The industrial revolution has started in the same days, and the progress in manufacturing technologies made centrifugal pumps to be widely used by 1850s [86]. The first practical centrifugal pump, The Massachusetts pump was manufactured in 1818. W. D. Andrews enhanced its performance by in 1846 by introducing double-shrouding. At the same time engineers, John Appold (1800-1865) and Henry Bessemer (1813-1898) were investigating better designs [89,90]. Appold's pump ran at 788 rpm with 68% efficiency and provided 78 L/s flow rate at 5.9 m pressure head. Centrifugal pumps operate on the same physics as

compressors, but with liquids. Centrifugal pumps are used in countless agricultural, industrial and for household purposes.[85,86].

Despite all of the loss kinds, centrifugal pumps can be exceedingly efficient. A fine-designed centrifugal pump should have a hydromechanical efficiency of around 85%. Centrifugal pumps with rather rudimentary and crude geometries can even be 60% efficient[87]. These efficiency expectations are only valid for one "design" point for given volute and impeller geometries. Therefore, the hydraulic efficiency would decrease due to the losses at off-design conditions.

3.1.2 Radial Inflow Turbine

Radial (centrifugal) inflow turbines appear as auxiliary power turbines, natural-gas processing, harvesting the geothermal energy and in turboprop aircraft engines (Figure 35). However, the most renown application of radial inflow turbines is in car turbochargers [86,91,92]. In a turbocharger, exhaust gases from the engine are flowing into a radial inflow turbine, which actuates a centrifugal compressor on the same shaft and rotation axis. The compressor pressurizes the air intake to the engine. Therefore they are made low in inertia for allowing a rapid adjustment to the varying engine speeds. [92,93].

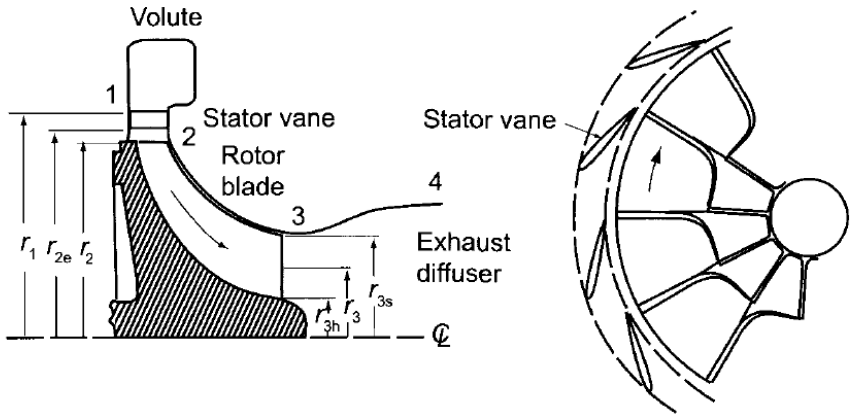

Figure 35: Radial inflow turbine[86].

Figure 35 is a side view of a radial inflow turbine. It looks like a centrifugal compressor with an inverted flow track. Hot gases enter through a volute and then into the impeller. For highest efficiency, the inflow angle must be negative by design.

3.1.3 Hydraulic Performance and Velocity Triangles

Basics of centrifugal pump/turbine design depend on the first rule of thermodynamics and standard Bernoulli equation. For a fully developed uniform flow in a pipe, the first law of thermodynamics converts into;

$$\dot{m}\left(u_1+p_1v_1+\frac{1}{2}V_1^2+gz_1\right)+Q=\dot{m}\left(u_2+p_2v_2+\frac{1}{2}V_2^2+gz_2\right)+\dot{W} \qquad 3.1$$

Incompressibility means that specific volume does not change with pressure, in other words, the density of the fluid remains constant under pressure change. For liquid water, substantial changes in pressure results in negligible changes in the density, thus, liquid water is almost incompressible. However, the specific volume of the water may change due to the temperature change.

For an adiabatic and reversible flow, the internal energy of the fluid remains constant. Also, Thermal energy terms are negligible for an LVAD like application. Then, the Bernoulli equation becomes;

$$\frac{p_1}{\rho} + \frac{1}{2}V_1^2 + gz_1 = \frac{p_2}{\rho} + \frac{1}{2}\dot{V}_2^2 + gz_2 \qquad 3.2$$

Therefore, when the flow is constant on a streamline, Bernoulli constant p_0 becomes;

$$p + \frac{1}{2}\rho V^2 + \rho g z = p_0 \qquad 3.3$$

It is the total pressure generated by the pump except the frictional loses. Bernoulli's equation is valid for steady-state flow conditions to calculate the pressure head. The net pressure head is accounting the inertial forces neglecting viscous effect in the flow as [56];

$$H = \left(\frac{p_2}{\rho g} + \frac{v_2^2}{2g} + z_2\right) - \left(\frac{p_1}{\rho g} + \frac{v_1^2}{2g} + z_1\right) \quad 3.4$$

Where subscript 1 is the inlet, and 2 is the outlet. Then, the shaft power is given by,

$$\dot{W}_0 = \frac{\rho Q g H}{\eta} \quad 3.5$$

The hydraulic or hydro-mechanical efficiency (η) of a rotary pump is the ratio of the mechanical power given to the pump versus the hydraulic power generated by it. In other words, hydraulic efficiency is a representation of the efficiency of a pump while converting the momentum (mechanical energy) of the impeller into the kinetic energy (dynamic pressure) of the fluid. Therefore, hydraulic efficiency can be represented as;

$$\eta = \frac{\Delta p Q}{\tau \omega} \quad 3.6$$

For the highest efficiency of a pump, the fluid should enter the impeller radially (inducer blades are introduced to ensure this). Employing the Euler's pump equation, the work applied to the fluid per unit mass per second [85];

$$E = \frac{W}{m} = (U_2 C_{w_2} - U_1 C_{w_1}) \quad 3.7$$

Where the absolute velocity in the tangential direction is denoted as C_w. E is the Euler head and represents the ideal or theoretical pressure rise developed by the impeller only (Figure 36). The flow rate is

$$Q = 2\pi r_1 C_1 b_1 \qquad 3.8$$

Where, the radial part of absolute velocity is Cr which is vertical to the tangent at the inlet and outlet. b is the width (or height) of the blade. It is assumed that the fluid enters and exits the vane tips in a parallel direction to the relative velocities at the tips[85].

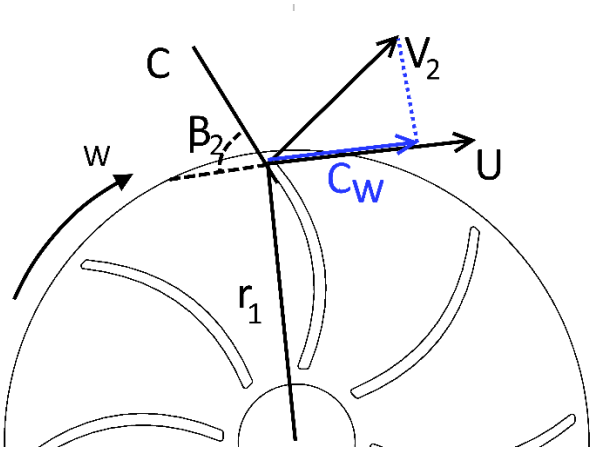

Figure 36: Velocity triangles for a centrifugal pump impeller outlet assuming a radial inlet.

Assuming the inlet is radial, the pressure head becomes;

$$H = \frac{1}{g} U_2 C_{w2} \qquad 3.9$$

Therefore, the outlet blade angle is represented as;

$$cot\beta_2 = \frac{U_2 - C_{w2}}{C_r} \qquad 3.10$$

Velocity triangles for radial turbines

Velocity triangles of radial turbines are similar to the previously described velocity triangles for the pump (Figure 37). The main difference is the direction of the velocity C which is the tangential part of the absolute velocity.

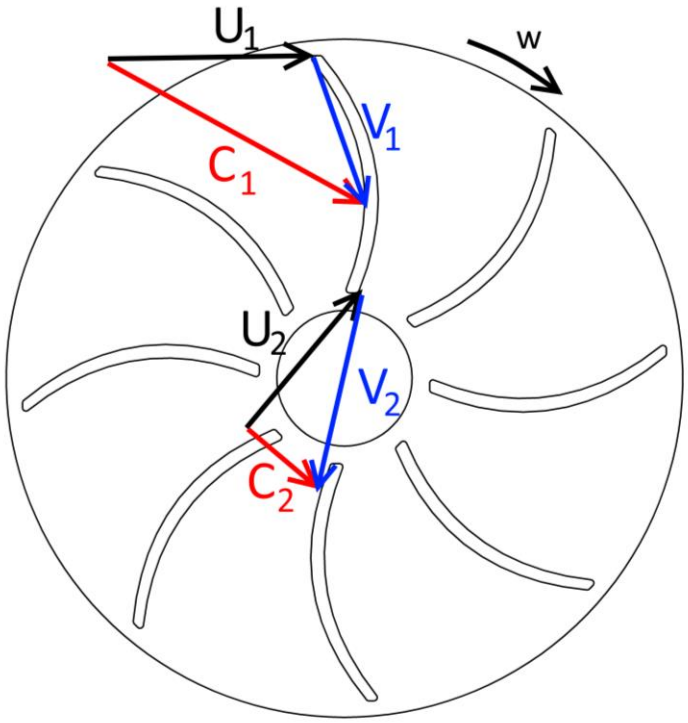

Figure 37: Velocity triangles for radial inflow turbines

$$\omega = \frac{1}{2}(V_1^2 - V_2^2) + \frac{1}{2}(U_1^2 - U_2^2) \qquad 3.11$$

This equation suggests that work and the inlet velocity V_2 are directly proportional. Therefore, a smaller V_2 increases the work. This is gained by guiding the relative velocity centrifugally inward at the inlet. Likewise, the exit velocity should be axial and as small as possible so the relative velocity W_3 is large. This can be achieved by increasing the flow angle of the relative velocity β_3. Lastly, a small U_3 and a large U_2 increase the work transported.

Some major blade shapes used in centrifugal pumps/turbine impellers are given in Figure 38. The blade shapes can be categorized as; Backward-curved blades (β_2<90°), Radial blades (β_2=90°) and, Forward-curved blades (β_2>90°)

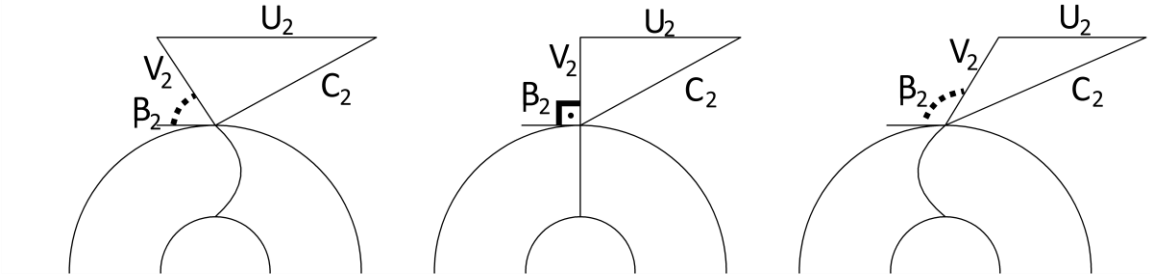

Figure 38: Centrifugal pump blade outlet angles[85]

The value of $C_{w_2}$is decreased for backward-curved vanes, and thus, these sorts of impellers provide a low energy transfer for a constant rotation speed, though forward-curved vanes have a higher value of energy transfer. Therefore,

high values of β_2(over 90°) is necessary. However, this also leads to a very high value of C_2. High velocity is rarely desired due to the difficulties of converting this kinetic energy to static pressure in a practical sized volute. Moreover, radial vanes (β_2=90°)) are advantageous for highspeed compressors where the highest pressure is desired. Besides, radial vanes are easy to manufacture.

3.1.4 Specific Speed

The specific speed is a unitless parameter which handles the power directly proportional to the rotational speed. Flow and work coefficients are combined in such a way that the diameter is eliminated as;

$$N_s = \frac{\omega Q^{\frac{1}{2}}}{(H)^{\frac{3}{4}}} \qquad 3.12$$

It demonstrates that turbomachines with low flow rates and high-pressure head have low specific speed. In radial turbomachines, the inlet area is relatively small, and the flow rate is relatively low for keeping the inlet velocity in a desirable place. Since centrifugal force can generate relatively high pressure, these machines have a low specific speed. In axial flow machines, the inlet diameter is relatively large and therefore a significant flow rate is possible. Therefore, the specific speed of axial machines is higher (Figure 39). There are different versions of the same equations which calculate the specific speed with a different unit and therefore, different orders of magnitude.

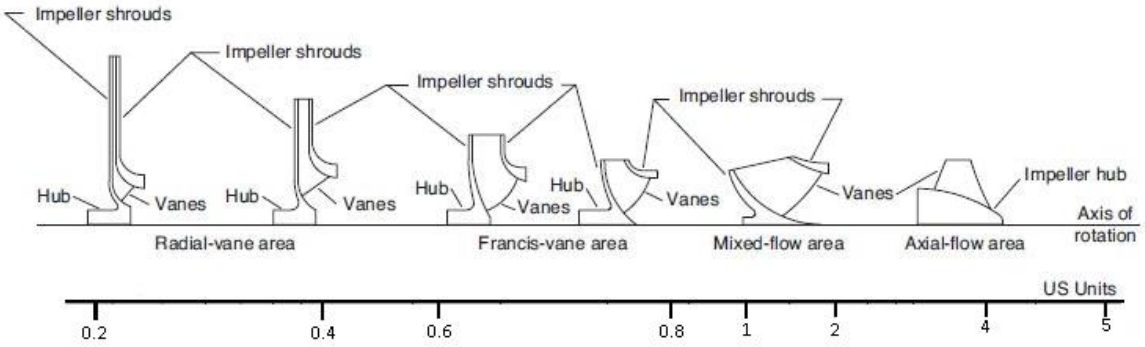

Figure 39: Pump shapes according to the specific speed [87].

3.1.5 Meridional Section

The design parameter wrap angle defines the blade camber line lengthwise on the meridional distance to feature on constant attack and trail angles, and thus the twirl of blade profile is defined with a single parameter (Figure 40).

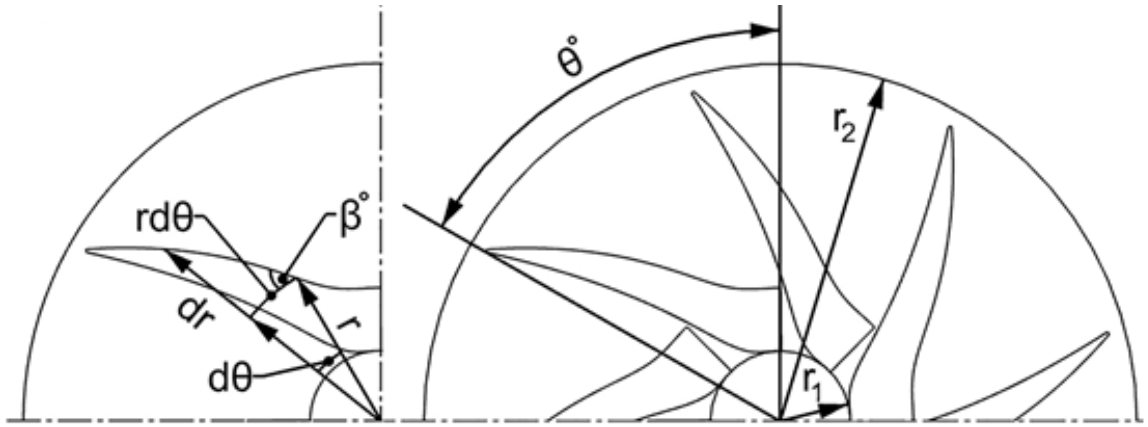

Figure 40: Wrap angle defined on the impeller [23].

Scheit et al.[71] describes the wrap angle by a geometric relation as;

$$\tan\big(\beta(r)\big) = \frac{dr}{r d\theta} \qquad 3.13$$

The wrap angle θ can be found by integrating the equation along the impeller radius if the meridional line has a constant wrap angle;

$$\theta = \int_{r_1}^{r_2} \frac{1}{r \tan\big(\beta(r)\big)} dr \qquad 3.14$$

Where the blade wrap angle is θ, the blade flow angle is β.

3.1.6 Volute Design

The volute design is critical in centrifugal pumps performance as it converts the kinetic energy (momentum) generated by the impeller to potential energy (static pressure). Logarithmic spiral is the typical geometric shape of a volute where the radius of the spiral grows with angular position. The volute structure is similarly vital with the impeller geometry for guaranteeing steady flow lines, an efficient kinetic to potential energy conversion [96]. Moreover, the regularity of the pressure distribution acting on the impeller is an essential constraint for radial forces which affects the bearing life. The spiral geometry of the volute creates a non-uniform pressure distribution on the impeller and therefore creating a radial force which needs to be balanced.

The volute tongue is one of the main parameters which is essential for bearing design and magnetic levitation applications. The outcome of the volute tongue shape has been extensively studied in for enhancing the pump endurance, reducing the noise, and overall for improving the hydraulic performance [97].

In Figure 41, the volute tongue angle is represented by the angular position. Radial gap (δ) between the impeller edge and volute tongue was shown as a percentage according to the standard of Stepanoff[98].

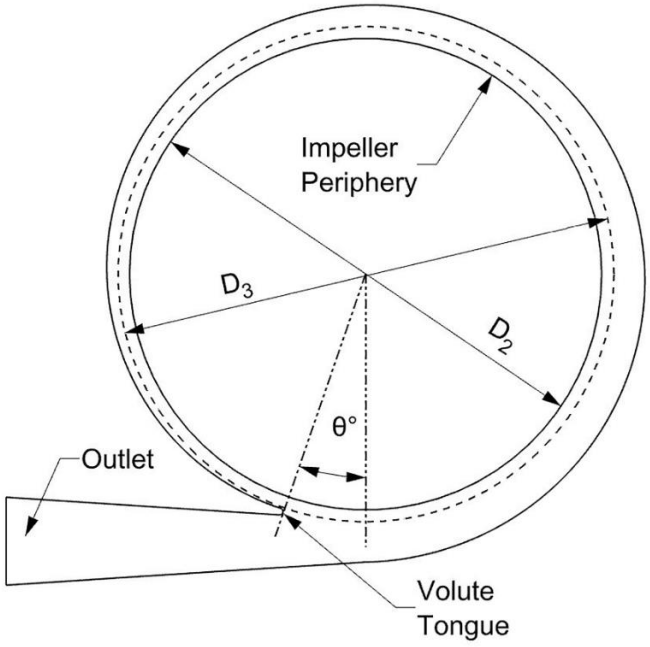

Figure 41: Definition of the volute tongue angle [96].

Diameter D3 considers the distance from the impeller eye (center) to the edge of the volute tongue. Impeller diameter is D2. Then, the ratio of D3/D2 is labeled as the base circle diameter[96].

$$\delta = \frac{D_3 - D_2}{D_2} \times 100\% \qquad 3.15$$

3.2 Computational Fluid Dynamics Analysis

Turbomachinery calculations are 2D estimations of the total performance of the pumps, and therefore they are not sufficient for understanding the real performance of a blood pump. Therefore, computational fluid dynamics analysis is required for understanding the flow characteristics inside the pump. Fluid dynamics calculation is based on Continuity, Momentum, Energy, and Reynolds Averaged Navier Stokes (RANS) equations [46,99–101]. Overall, CFD is a numerical approximation of a flow field based on these equations. Moreover, CFD is able to find dynamic results for further analysis of heat and shear stress transfer which is crucial for understanding the hemolytic performance of a blood pump. For achieving an accurate CFD analysis, boundary layer separation, turbulence theory, fluid modeling must be carefully implemented since these conditions are crucial for achieving a realistic simulation. Virtual performance of the complete 3D geometry of iHeart and iATVA is completed on ANSYS Fluent software and results are explained later in this work. However, CFD methodology is similar for both pumps and explained in this chapter. A list of possible applications of CFD is given in Figure 42.

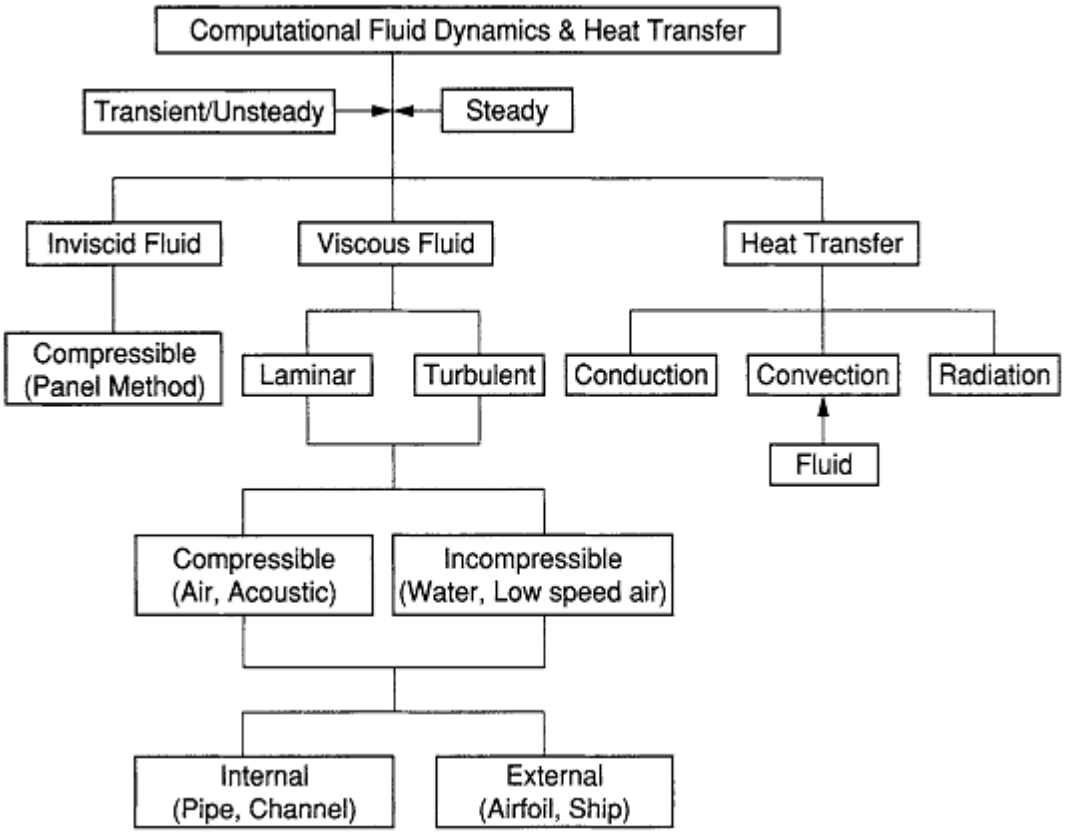

Figure 42: Types of computational fluid dynamics [102].

CFD software principally splits the fluid domain into small cells (voxels) and solves the fluid dynamics equations associated to the physical model at every cell. The grid structure of these small cells is named 'mesh.' Mesh size can be very fine according to the CFD model regarding the turbulence model which increases the calculation time. For the desired physical model, some boundary conditions are assumed in the software for identifying the physical environment in a virtual environment, as the wall motion, flow rate, pressure, etc.

After finding the solution of every cell inside the flow domain, previous results are taken as the input for the next iteration and the CFD software solves the same equations with these updated parameters for every cell recurrently. These iterations continue up until the difference of results between the two iterations become significantly small. This phenomenon is named as the numerical convergence of the solution.

3.2.1 Reynolds Number and Shear Rate

In fluid dynamics, the fluid flow regime can be categorized as laminar and turbulent based on the velocity distribution and the flow path of the fluid. Reynolds number purely is the ratio of the viscous forces to the inertial forces. When the inertial forces in a flow are smaller than the viscous forces, the Reynolds number of the flow is low. There, the viscous forces dissipate the energy imbalances in the flow. This flow is namely the laminar flow. The laminar flow is simple and regular. Therefore, the flow properties of such flow can be represented using only the continuity and momentum equations. However, larger inertial forces can result in an arbitrary and chaotic flow pattern namely, the turbulence. Turbulent type of flow is much more intricate because it comprises eddies or vortices which are random swirling flow patterns. In a turbomachine, the flow regime can be estimated as;

$$Re = \frac{\rho \omega D^2}{\mu} \qquad 3.16$$

Flow profile inside a rotary pump is assumed to be laminar for Re <105 [103]. The nature of an LVAD comprises a high-speed impeller thus turbulent flow is typical in such devices. However, low rpm devices may be mostly laminar. Reynolds numbers of iHeart and iATVA are further discussed in Chapters 4 and 6.

3.2.2 Fluid Modeling

For the CFD simulation, the solver can accurately calculate the flow behavior only when the accurate fluid properties are specified. The required properties of the fluid for a standard single phase CFD simulation are density, viscosity, and compressibility. Other properties like specific heat, conductivity vapor pressure are needed for the problems such as heat transfer. Consequently, the properties of human blood are required to be assumed reasonably for an accurate CFD simulation of a blood pump.

Human blood is a heterogeneous fluid containing 55% of liquid plasma which is mainly the fluid medium of blood [104]. Plasma consists of water, ions, proteins, and nutrients. Red blood cells (RBCs) namely the erythrocytes is the second fundamental element in blood that builts 45% of the blood volume. The rest are platelets and with the lowest percentage at less than 1%, are white blood cells or so-called leukocytes[104]. RBCs are biconcave disk-shaped cells which contain hemoglobin, the oxygen-carrying protein. The cell wall permits the cell to be significantly elastic so the RBCs can squeeze and get into various shapes required for passing through the narrow capillaries [105]. The amount of RBCs is commonly

called hematocrit which is a percentage of cells in total blood volume. The average hematocrit of men is 42% where for women it is 38%[35]. Due to the heterogeneous character of it, human blood is a compressible and shear-thinning non-Newtonian fluid. However, expresses Newtonian behavior when the exerted shear rate is above 100 s-1[101]. Since LVADs are required to deliver a high flow rate with a compact size, most of these devices create a shear rate of higher than 100 s-1 thus commonly blood is modeled as a single phase Newtonian fluid in the CFD simulations. The density and viscosity of blood are typically assumed as 1,040 – 1,060 kg/m3 and 0.0030 - 0.0036 Pa, respectively[101,106].

3.2.3 Navier Stokes equations

Claude-Louis Navier and George Gabriel Stokes created a set of equations that describe the motion of viscous fluid flow, namely the Navier-Stokes equations [107,108]. The conservation laws are the fundamentals of these equations. Explicitly, the conservation of mass, momentum, and energy are the equations to be solved for modeling a flow domain. The main equations are;

Conservation of mass

$$\frac{\delta \rho}{\delta t} + \nabla.(\rho U) = 0 \qquad 3.17$$

Conservation of momentum

$$\rho g - \nabla \rho + \nabla.\tau_{ij} = \rho \frac{dU}{dt} \qquad 3.18$$

Conservation of energy

$$\rho \frac{dh}{dt} = \frac{dp}{dt} + \nabla.(k\nabla \mathrm{T}) + \emptyset \qquad 3.19$$

The conversation of scalar quantities

$$\frac{\partial(\rho\emptyset)}{\partial t} + \nabla.(\rho\emptyset V) = \frac{dp}{dt} + \nabla.(k\nabla \mathrm{T}) + \emptyset \qquad 3.20$$

Other equations may also be needed for modeling further physical investigation like heat flux, phase change, etc.

3.2.4 k-epsilon Turbulence Model

There are several types of turbulence modeling equations exist for estimating the physics of turbulence occurring in a flow field [98–101]. Eddy viscosity model is one of the typical models for CFD applications. Eddy viscosity model accepts that turbulence consists of small eddies and the Reynolds stresses which are a proportional relation to the mean velocity gradients. This model also includes velocity gradients from the last iteration[112]. Consequently, the transport equations essentially integrate local molecular viscosity and flow history effects of the eddy viscosity μ_t, henceforth the turbulence kinetic energy (k), was chosen for the velocity scale of the energy equation [99,101]. The eddy viscosity is described as the addition of local and turbulent viscosities:

$$\mu_{eff} = \mu + \mu_t \qquad 3.21$$

The velocity-turbulence kinetic energy relationship is given as;

$$k = \frac{1}{2}(\overline{u'^2} + \overline{v'^2} + \overline{w'^2}) \qquad 3.22$$

To create the turbulence energy equation, the Boussinesq eddy viscosity assumption was used to approximate the momentum transfer caused by the turbulence eddy. This assumption states that the Reynolds (viscous) stress tensor, τ_{ij} , has a proportional relationship to the strain rate tensor σ_{ij}, as follows[110,112]:

$$\tau_{ij} = 2\mu_t\sigma_{ij} + \frac{2}{3}\,\delta_{ij}\rho k \qquad 3.23$$

Smearing averaged velocity components occurring due to flow fluctuations into the conservation of momentum and mass equations assuming an incompressible and constant flow field leads to the equation called a Reynolds averaged Navier-Stokes (RANS) equation such as[112];

$$\rho\frac{\partial \mathrm{U_i}}{\partial t} + \rho U_j\frac{\partial \mathrm{U_i}}{\partial x_j} = -\frac{\partial P}{\partial x_i} + \frac{\partial}{\partial x_i}\left(\tau_{ij} - \rho(\overline{u'^2} + \overline{v'^2} + \overline{w'^2})\right) \qquad 3.24$$

Where, τ_{ij} is the viscous stress. Assuming a for the compressible flow σ_{ij} becomes zero and τ_{ii}= -2k. Hence the RANS equation takes the following form an named the turbulence energy equation which is the basis of most turbulence energy models[113];

$$\frac{\partial \rho k}{\partial t} + U_j\frac{\partial \rho k}{\partial x_j} = \rho\tau_{ij}\frac{\partial U_i}{\partial x_j} - \rho\varepsilon + \frac{\partial}{\partial x_j}\left(\left(\mu + \frac{\mu_t}{\sigma_k}\right)\frac{\partial \kappa}{\partial x_j}\right) \qquad 3.25$$

σ_k is the closure coefficient and the turbulence eddy dissipation "ε" is the dissipation rate of the turbulent kinetic energy k. This relation is assumed to be proportional including a length scale of eddies (l) as;

$$\varepsilon \sim \frac{k^{3/2}}{l} \qquad 3.26$$

The standard k-epsilon is one of the most employed models which is based on one turbulence energy equation. It is a considerably simple model which tends to converge straightforwardly. Similar to the energy equation given above, the turbulence kinetic energy (κ) is obtained from[111]:

$$\frac{\partial \kappa}{\partial t} + U_j \frac{\partial(\kappa)}{\partial x_i} = -\overline{v_i' v_i'} \frac{\partial \overline{v_i}}{\partial x_j} - \rho\varepsilon + \frac{\partial}{\partial x_i}\left(\left(\mu + \frac{\mu_t}{\sigma_k}\right)\frac{\partial \kappa}{\partial x_i}\right) \qquad 3.27$$

Including the dissipation rate, transport equation becomes;

$$\frac{\partial \rho\kappa}{\partial t} + \frac{\partial(\rho\varepsilon \bar{V}_i)}{\partial x_i} = \frac{\partial}{\partial x_j}\left(\left(\mu + \frac{\mu_t}{\sigma_\varepsilon}\right)\frac{\partial \kappa}{\partial x_j}\right) + C_1 P_k \frac{\varepsilon}{\kappa} - C_2 \rho \frac{\varepsilon^2}{\kappa} \qquad 3.28$$

Therefore, the turbulent viscosity is characterized as a ratio of dissipation rate and the kinetic energy[111];

$$\mu_t = \rho C_\mu \frac{\kappa^2}{\varepsilon} \qquad 3.29$$

The coefficients, $\sigma_k, \sigma_\varepsilon, C_\mu, C_1, C_2$and are found with empirical methods and data analysis[112].

3.2.5 Meshing

Meshing (or grid generation) is a discretization of a continuous spatial domain (a flow field) of interest into a small array of elements, where some desired engineering parameters are obtained by numerical solutions. [101]. ANSYS Fluent is capable of creating structured meshes of triangular or quadrilateral cells in 2D, and tetrahedral, hexahedral, polyhedral, pyramid, or wedge cells in 3D (Figure 43) [111]. Ansys also is able to combine these different structures for required regions of a single CAD model. The mesh type is chosen regarding the application. Main concerns while selecting the mesh type are the meshing time, computational time, and numericaliffusion[114].

Many CFD problems including the blood pump involve complex geometries. The structured meshes (hexahedral or quadrilateral) are often very time consuming to generate. Therefore, unstructured meshes are frequently used (triangular or tetrahedral). Using block-type meshing also may lead to oversimplification of the geometry. Unstructured (quadrilateral or hexahedral) meshes offer many of the advantages of triangular and tetrahedral meshes for moderately-complex fluid bodies. However, triangular/tetrahedral meshes create fewer cells for a geometry with a significant complexity or broad range of length scales.

On the other hand, if a relatively simple geometry like standard rectangular shape is studied, using a mesh of high-aspect-ratio quadrilateral/hexahedral cells are desired. The mesh is most probable to have much fewer cells than triangular/tetrahedral cells are used. Also, triangular/tetrahedral cells have a larger aspect ratio, and therefore they have a skewness which is undesired for achieving a good convergence.

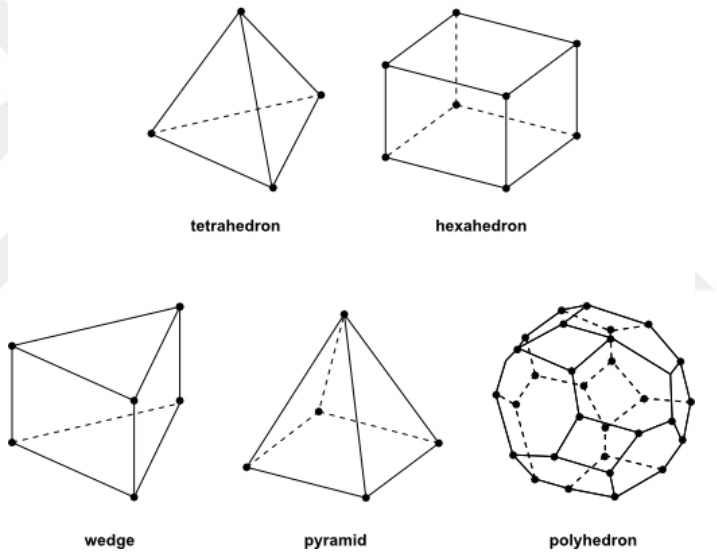

Figure 43: Mesh types[111]

Using a polyhedral mesh compared to a tetrahedral mesh will provide a lower cell count than the original mesh. Although the mesh becomes coarser with this mesh type, convergence will generally be achieved earlier.

As a summary, Ansys Meshing Guide suggests[114];

- Quadrilateral/hexahedral meshes are better for simple geometries.
- Unstructured quadrilateral/hexahedral meshes are better for semi-complex geometries
- Triangular/tetrahedral meshes are the preference for complex geometries.

Due to the narrow flow passages and complex geometries inside the VADs, tetrahedral meshing is the preference for CFD simulations.

3.2.6 γ^+ Value

The flow around the viscous sublayer which is adjacent to the surface is essentially laminar due to the no-slip condition. Therefore, the molecular viscosity controls the momentum close to the surface. SThe second region is usually named the buffer zone where a transition between laminar and turbulent flow is observed. The most external layer becomes fully turbulent at high Reynolds numbers. the length scale of these layers is defined by a distance factor y^+[111].

$$\frac{y}{y^+} = \frac{\mu}{\sqrt{\sigma_{ss}\rho}} \qquad 3.30$$

γ^+ is the distance between surface and boundary, μ is the fluid viscosity, ρ is the density and σ_{ss} is the local wall-shear stress.

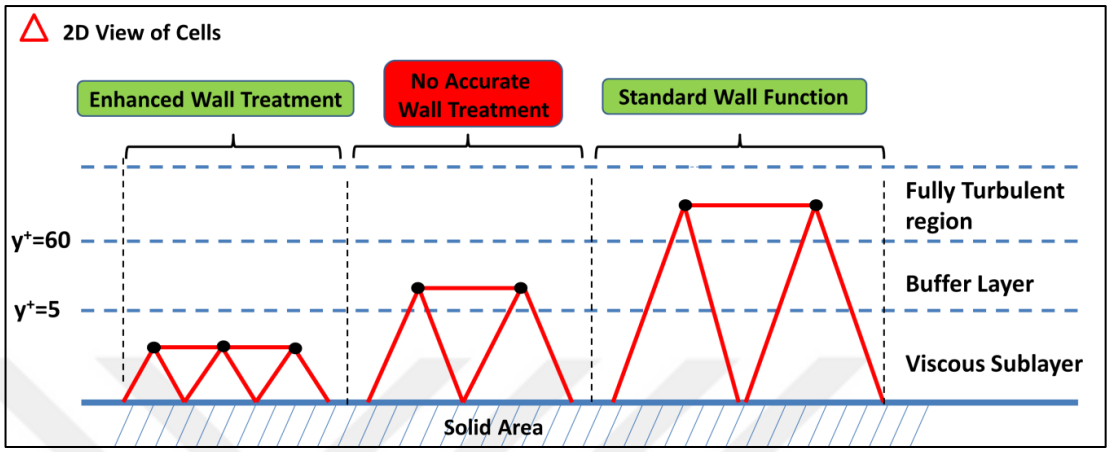

Figure 44: Mesh structure bound the are for turbulence model selection[115].

Enhanced Wall Treatment is to be used for viscous sublayer for flow modeling, and Standard Wall Function is utilized for the fully turbulent layer. However, There is no accurate way of modeling the flow regime inside the buffer zone. Therefore, first node neighboring to the surface should be located inside the viscous sublayer (with enhanced wall treatment) or the fully turbulent region (for standard k-epsilon). Wall treatment technique must be decided considering the first node or in other words considering the surface element size of the mesh.

3.2.7 Hemolysis Estimation

Prediction of the hemolytic competence of a blood contacting device is crucial for reducing the number of prototyping and number of required blood tests during the optimization process. There have been numerous hemolysis estimation models however the most renown one is the power law presented by Giersiepen et al. in 1990 [116]. The power law is used to predict the blood hemolysis for rotary blood

pumps which is helpful for design improvements. According to the power law model, shear stress induced hemolysis is also related to exposure time along with the shear stress as [116];

$$HI = C\tau^{a}t^{\beta} \qquad 3.31$$

Where τ is shear stress, t is exposure time and C, α and β are empirical constants.

Power law equation is applicable in both Eulerian and Lagrangian flow simulations. Garon and Farinas created the Eulerian approach which is a stress-based model in 2004 [117]. In this method, the computation of blood damage is calculated with a volume integration of a damage function over the total flow domain. This method removes the need of residence time calculation and use of tracer particles which reduces the computation time and particle related convergence problems. Likewise, Arora et al. proposed a strain-based model for estimation of blood damage[118,119]. In their model, a morphology tensor S is used for estimating the shape of deformed RBCs. The study suggested an excellent concordance between the in-vitro and in-silico results for hemolysis. This method is called Lagrangian due to the use of tracing particles to compute the hemolysis index. Pauli et al. applied the same strain-based method in a Eulerian transient simulation[120].

In this research, stress based models are applied to both Eulerian and Lagrangian simulations. Computational NIH levels were obtained and compared

with the in-vitro blood test results. The numerical NIH level in both cases was calculated using[121]:

$$NIH[g/100L] = 100 \times HI \times (1 - H_{ct}) \times H_b \qquad 3.32$$

Where H_{ct} is hematocrit and H_b is the hemoglobin content.

3.2.8 Lagrangian model

The Lagrangian technique is another widely used hemolysis estimation approach [122]. The shear stress occurs on the RBC was simulated with the particle tracking technique by using the Euler forward integration method[112,113]. Exposure time information and shear stress at a given instance were calculated by discharging massless particles from the inlet each CFD model. Blood damage index (D) was calculated cell by cell where the particle resides, as an integral of total time frame until the particle is released from the outlet.

$$D = \int_{inlet}^{outlet} 1.8 \times 10^{-6} \tau^{1.991} t^{0.765} \qquad 3.33$$

$$\mathrm{D} = \sum_{inlet}^{outlet} 1.8 \times 10^{-6} \tau^{1.991} \Delta T^{0.765} \qquad 3.34$$

The number of complete particles must be kept as high as possible for a realistic simulation.

3.2.9 Stress-based model

In the stress-based method, equivalent shear stress is used. This method integrated both the principle and shear stresses acting on the fluid and shown as[125]:

$$\tau = \sqrt{\left[\frac{1}{6}\left(\tau_{ii} - \tau_{jj}\right)^{2} + (\tau_{ij})^{2}\right]} \qquad 3.35$$

Where, τ_{ij} is the shear stress and τ_{ii}, τ_{jj} are principle stresses.

3.2.10 Tensor-based (strain) model

The tensor-based method utilizes a morphology tensor for describing the shape of deformed RBCs. The effective shear stress acting on the blood cells are calculated as [107, 108]:

$$\tau_{eff} = \mu_{blood} G_{eff} \qquad 3.36$$

G_{eff} is the intensity, which is correlated to the instantaneous shape distortion(D_{ef}) of given blood cell. Resembling an ellipsoid, (which mimics the biconcave shape of a RBC) distorted blood cell is described with length 'L' of the major axis and length 'B' of the minor axis. The instantaneous shape distortion is found with the equation;

$$D_{ef} = \frac{L-B}{L+B} = \left[\frac{\sqrt{f_1^2 + f_2^2 G_f} - f_1}{f_2 G_f}\right] \qquad 3.37$$

G_f is the intensity of flow, the value of f_1 and f_2 are given 5.0 s^{-1} and 4.2298x10^{-4} respectively. [120]. Then, the effective shear stress is calculated as;

$$G_{eff} = \frac{2f_1 D_{ef}}{(1 - D_{ef}^2) f_2} \qquad 3.38$$

Hemolysis index is found from the substitution as;

$$HI = C\left(\mu_{blood} \times G_{eff}\right)^{\alpha} t^{\beta} \qquad 3.39$$

ISTANBUL HEART VAD: DESIGN

This chapter explains the design of a novel centrifugal flow LVAD, namely the Istanbul Heart VAD (iHeart VAD). The design methodology and CFD methodology described before is applied in the design. The pump geometry is the central element which alters the flow field and therefore defines the hydraulic and hemolytic performance of an LVAD.

In this chapter, the hydraulic performance and hemolytic threshold requirements are explained in detail. Later, the geometric design of the pump was introduced. Impeller and volute structures were revealed as a result of an optimization study. Results of the final geometry are discussed in Chapter 5 detailly.

This section investigates the structural design of the iHeart VAD. Design steps involve hydraulic performance, blade angles, impeller design and volute design.

4.1.1 Conceptual Model

The outer surface of the pump, the shroud consists of two parts as the top and the bottom shroud. Permanent magnets embedded inside the impeller, which actuates it with magnetic coupling to the external electric motor placed under the bottom shroud. Naturally, in LVADs, an embedded motor design is required where the impeller acts as the rotor, and the shroud acts as the stator. The impeller gives kinetic energy to the blood, and the volute converts it to the static pressure.

Design of the current prototype iHeart is initiated based on a preceding design, namely, the Heart Turcica Centrifugal (HTC). The design was a second-generation centrifugal pump with eight straight blades and volute[22]. iHeart includes the same size impeller. However, blade angles and volute design is optimized with a numerical study.

4.1.2 Impeller Design and Blade Angles

The impeller is one of the most vital parts of blood pumps as it outlines flow field. Parametric design of the blade design is essential since that these parameters control the resident velocity which has a significant influence on streamlines of the flow field and transfer of the kinetic energy to the fluid.

As the first step in impeller design, velocity triangle method was used for estimating the hydraulic performance of the pump. In order to estimate blade angles, the mean velocity in the aorta of a person is required. Assuming the physiologic flow rate of 5 lt/min, mean aortic velocity becomes 1.061 m/s considering the 10mm inlet diameter of the iHeart. A physiologic pressure need of 100 mmHg must be provided with the design. The critical components of the turbomachinery approach are the diameter and the rotation speed of the impeller. iHeart is desired to be a low rpm blood pump to operate around 2000 rpm. Therefore, a relatively large impeller diameter is needed. An impeller of 45 mm diameter and a blade height of 4 mm satisfy our design criteria using the turbomachinery calculations. However, changing the attack and trail angles alters the performance. The head

pressure varies from 95 to 105 mmHg depending on the blade angles. In this study, our research group was aimed to find the blade design where both hydraulic and hemolytic performance is satisfactory for human physiologic needs.

The wrap angle was presented in this study as the control parameter to increase hydraulic performance, avoid recirculating zones, and excessive shear stress in the flow field. The influence of blade wrap angle on hemolytic and hydraulic performance was studied in our research group in collaborative work with Çağlar Öztürk[21].

Enhancing the impeller blades by altering the wrap angle (and therefore the blade inlet and outlet angles) could provide a higher efficiency (more hydraulic power with fewer mechanical energy), and fewer recirculating zones compared to the radial blades. Blade wrap angle is a description of blade angle through the meridional profile. Usually, blade angle is described as a function of the radius from the impeller eye through the trailing edge of the impeller. However, for our impeller optimization study, a constant blade angle and therefore the task of defining a blade flow angle distribution. Therefore, blade inlet and outlet angles were equal and represented as the blade angle. Blades are 90° twisted between the eye and outlet of the impeller.

Table 2: Wrap angle and corresponding blade angles

	Model **I**	Model **II**	Model **III**	Model **IV**	Model **V**
Wrap Angle (°)	0	60	120	180	240
Blade Angle (°)	90	56	36.5	26.3	20.3

Five different wrap angles were chosen for tests. The wrap angles of blades (θ°) between 0° to 240° were implemented on impellers for models I-V. Table 2 demonstrates the physical configurations for the five impellers. For all designs, blade height was 4 mm, and blade thickness was 1.25 mm. All impellers have 8 blades and were intended to function at 2000 rpm and 5 L/min flow rate and almost at 100 mmHg pressure head. The outer diameter was 45 mm, and the height was 18 mm. The relative position of the remaining components was fixed. The pump geometry was designed using the Siemens NX software

Table 3: Number of blades

	Num. of Main Blades	**Num. of Splitter**
Model III	8	0
Model VI	4	4
Model VII	10	0
Model VIII	***5***	***5***
Model IX	6	0
Model X	3	3

In addition to the wrap angle study, the outcome of the number of blades was also studied. The wrap angle of 120° was decided to be the reference due to its capable hemolytic and hydraulic performance. Six, eight and ten bladed designs

were tested. Splitters were also included to examine the splitter effect on pump performance. Table 3 discloses the blade-splitter numbers of tested models.

Table 4: Geometric features of the final design

Inlet and Outlet Pipe Diameter	10 mm
Inducer blade Angle	0^0
Twist Angle	90^0
Impeller Blade Wrap Angle	120^0
Impeller Leading Edge Angle	36.5^0
Impeller Trailing Edge Angle	36.5^0
Specific Speed (N_s)	2.1

Specific speed of iHeart is 2.1 (Ns) at the design point which makes it an appropriate decision to use a radial machine for such relatively low specific speed conditions.

4.1.3 Volute Design

Effects of volute tongue geometry on hydraulic and hemolytic performance were studied with five different volute tongues. The volute tongue is defined with the tongue angle (θ°) (Figure 45). Constant mean velocity technique was implemented to design the volute geometry by Stepanoff design rule as explained in Chapter 3.1.6 [98]. The volute tongue angle characterizes the volute tongue location.

In this study, volute tongue angles (θ°) ranging from 10° to 50° were evaluated. All of the other geometric parameters were kept constant. Cross section of the volute was circular for all models. The pump geometry was created using the Siemens NX software (NX 10.0, TX, USA).

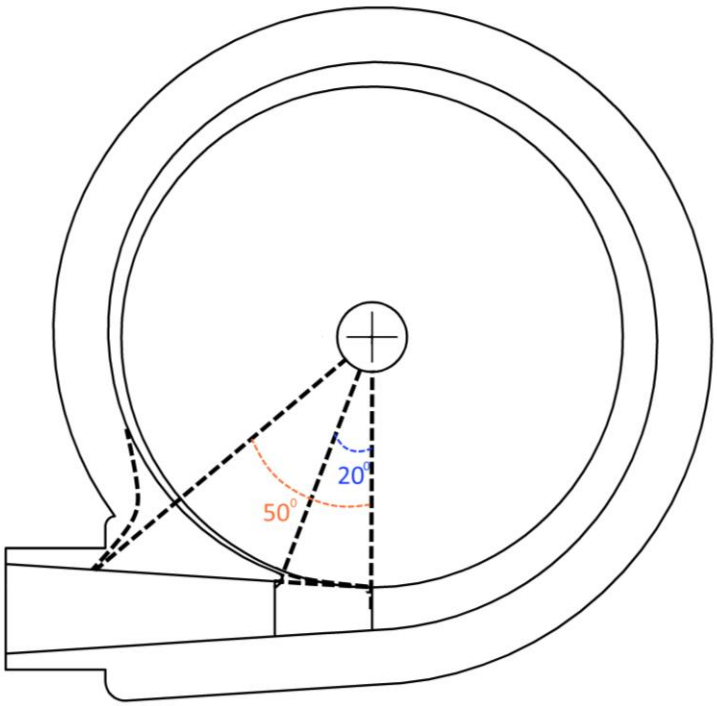

Figure 45: Volute tongue angle of 20° is the best performing model. 5 Models tested from 10° to 50°.

4.1.4 Final Design of iHeart VAD

Final design parameters of the iHeart are shown in Table 5. Design optimization studies include in-silico, in-vitro and in-vivo tests which are discussed in the next chapter.

Table 5: iHeart Geometric Parameters

Inlet and Outlet Pipe Diameter	10 mm
Nominal Speed	2000 rpm
İmpeller Diameter	45 mm
Inducer blade Angle	0^0
Twist Angle	90^0
Impeller Blade Wrap Angle	120^0
Impeller Leading Edge Angle	36.5^0
Impeller Trailing Edge Angle	36.5^0
Specific Speed N_s	2.1
Volute Cross Section	Round
Volute Angle (°)	20
Radial Gap (δ%)	5
Diffuser End Cross Section	Circle
Diffuser End Diameter (mm)	9

ISTANBUL HEART VAD: ANALYSIS EXPERIMENTATION AND DISCUSSION

This chapter presents the results, analyses, and discussion of iHeart VAD. The primary focus of the study was to optimize the flow path for assuring a well guided steady flow and lessen the shear-induced hemolysis. Along with the CFD analysis, hydraulic tests were performed for the validation. Moreover, an in-vitro blood test was performed for validating the in-silico hemolytic performance estimations. In CFD analysis both "stress-based" and "strain-based" models were implemented. Lastly, results of the in-vitro and in-vivo studies are also presented.

5.1 CFD Preprocessing

The Flow pattern inside the pump was studied with the Commercial CFD software Fluent (ANSYS 17.0, PA, USA). During the impeller optimization study, finite volume method with frozen rotor technique or namely the multiple reference frame (MRF) method was applied. Moreover, Sliding mesh technique is used for volute tongue optimization study which provides an accurate simulation result at unsteady flow conditions due to the blade motion on the tongue region[101].

5.1.1 Boundary Conditions

The frozen rotor interface connected mesh domains at the contact zone of the impeller and the volute tongue region. Blood was modeled as a Newtonian fluid

with 1050 Kg/m3 density and 0.0035 Pas dynamic viscosity. The convergence accuracy was 10^{-4} for the scaled residuals. Double precision and second-order upwind solution methods were used for achieving a higher simulation accuracy. Inlet and outlet tubing were designed 75 mm longer to a certain length to avoid boundary condition effects on the convergence. Boundary conditions of the inlet were given as 5 L/min flow rate, and the outlet pressure was zero. Impeller rotation speed was 2000 rpm. The absolute pressure difference between the inlet and outlet was found.

5.1.2 Mesh and Grid Independence

The inducer, impeller, and volute models were created separately. Interfaces were defined between the contact zones. Inlet and outlet tubes were elongated for eliminating the boundary effects (Figure 46).

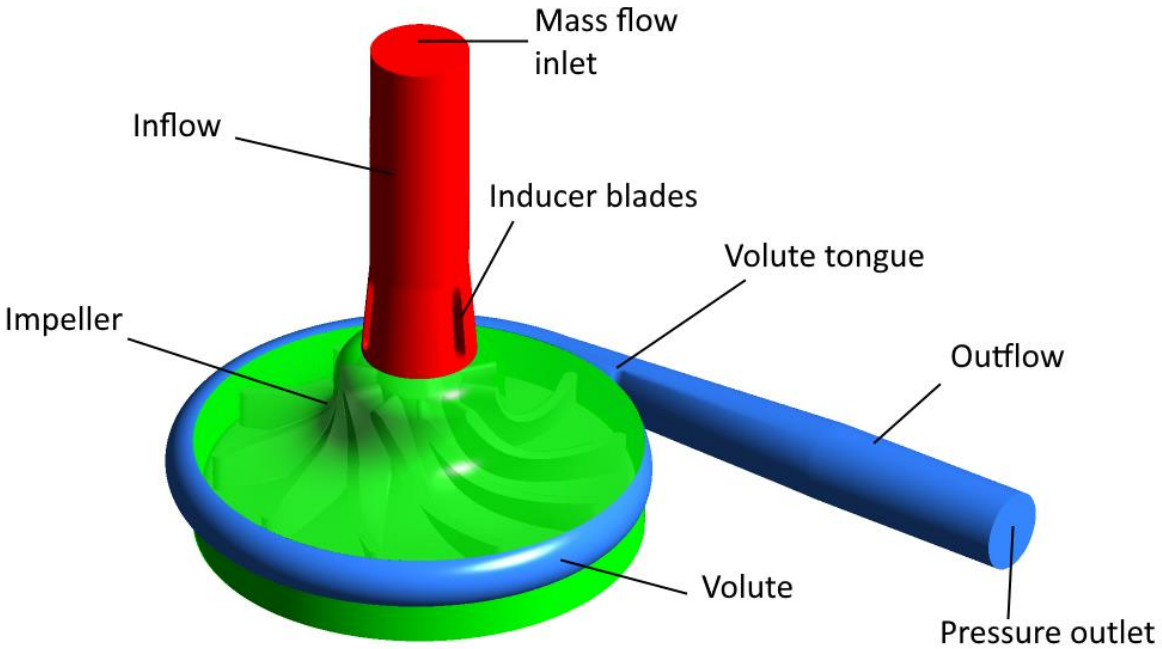

Figure 46: A Computational model for CFD analysis.

Mesh convergence was investigated using varying element sizes of 0.3 mm, 0.2 mm and 0.1 mm with tetrahedron elements. Boundary layer elements were generated with a size of 30 microns on the walls of the inducer, impeller, and volute. Wall y+ was below 5 (Figure 48). Therefore, enhanced wall treatment was used with k-e turbulence equation. A total of 12 to 15 million mesh elements were generated using an element size of 2^{-4} m on the body and 1^{-4} m on the inducer and impeller blades.

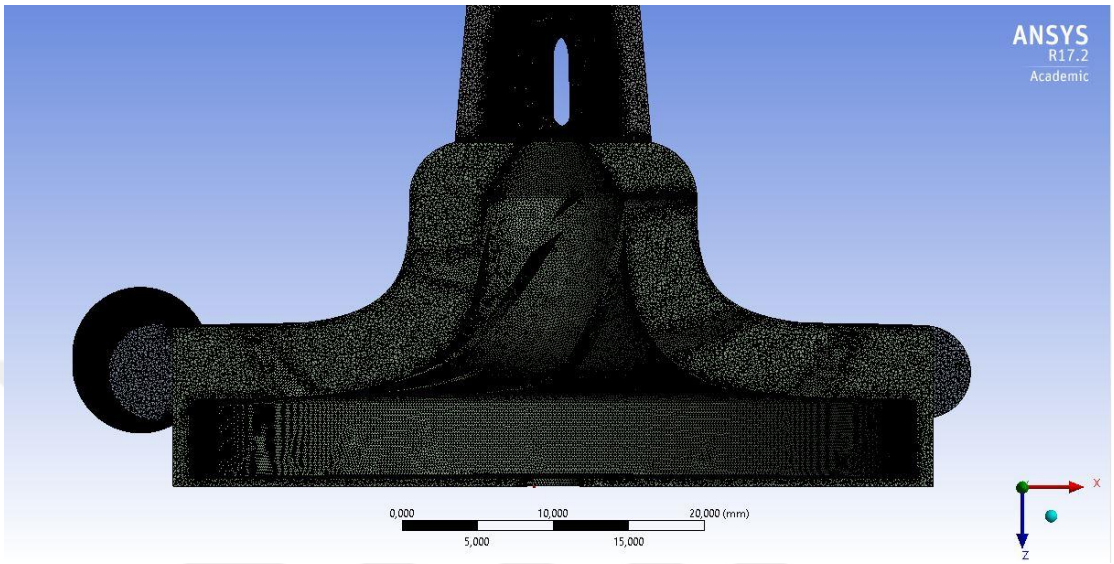

Figure 47: Meshing of iHeart.

The convergence criteria were set to be 10^{-4} residual. It took approximately 24 hours for the solution to converge on an HP Z840 workstation with 24 cores 2.4 GHz. Figure 47 shows the mesh generated for the domains of the inducer, the impeller, and the volute taken from the axial cross-section.

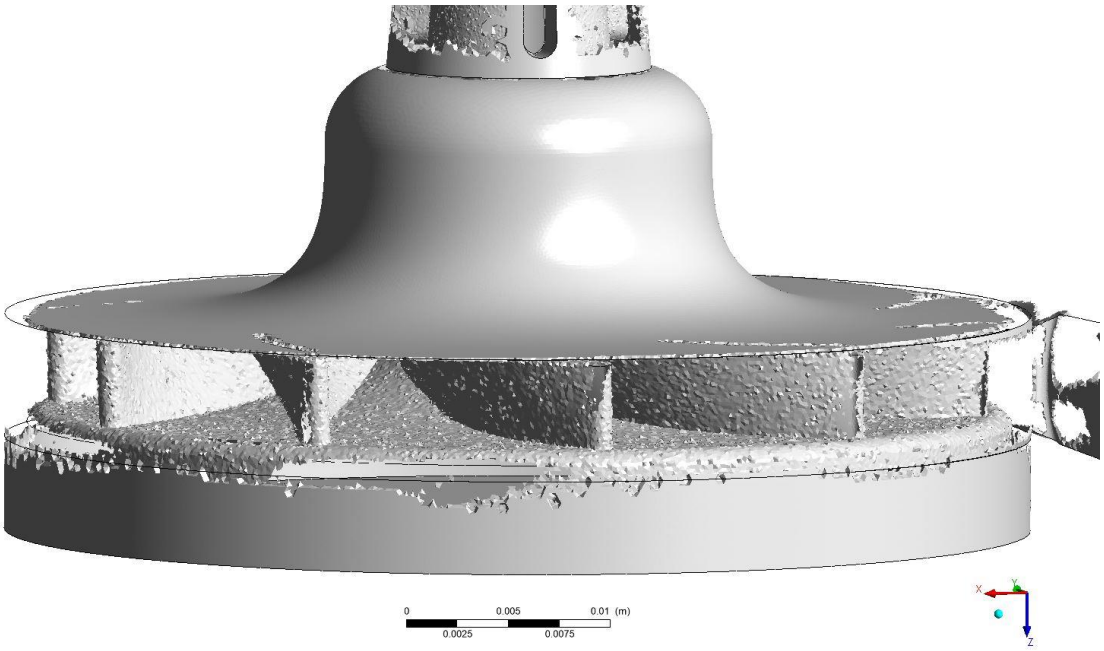

Figure 48: Regions where y+<3.

5.2 Impeller Optimization

In blood pump design, there are numerous features which control the blood damage and hydraulic performance. The impeller design is the most critical aspect of the blood pump. Blood damage index was calculated with two previously described hemolysis estimation models to discover the best performing wrap angle. Five models were simulated at 2000 rpm and 5 L/min flow rate. Hydraulic and hemolytic performance results are given in Table 6. The hydraulic performance of Model I, II, III and IV were almost the same. However, Model V with a wrap angle of 240° showed the worst hydraulic performance with a hydraulic efficiency of 46.9% and head pressure of 83.8 mmHg.

Table 6: Effect of the wrap angle on hydraulic and hemolysis Performance.

	Model I	**Model II**	**Model III**	**Model IV**	**Model V**
Wrap Angle [°]	0	60	***120***	180	240
Pressure Head [mmHg]	101	105.2	***104.1***	101.4	83.8
Hydraulic Efficiency [%]	52.1	54.3	***53.5***	54	46.9
Damage Index (Lagrangian)	1.37E-02	1.14E-02	***9.84E-03***	7.31E-03	1.85E-02
Damage Index (Eulerian)	1.26E-03	1.10E-03	***9.47E-04***	8.94E-04	1.40E-03

The difference in hydraulic performance of Model I to IV was less than 4%. Though, hemolysis indices declined as the wrap angle varied from 0° to 180, as much as 46.6% (Lagrangian) and 29.1% (Eulerian). This enhancement trend in hemolytic performance was not seen in Model V due to the large hemolysis index and deprived hydraulic performance.

Figure 49 (A) demonstrates the scalar shear stress (SSS) on the midplane of the volute. Figure 49 (B) shows maximum and average scalar shear stresses induced in all five designs 362.8, 319.8, 258, 241.5 and 416.6 Pa, respectively for Model I to V. The average shear stress values were ranged between 22 to 32 Pa. Worst average stresses were observed where the wrap angle is least and the most.

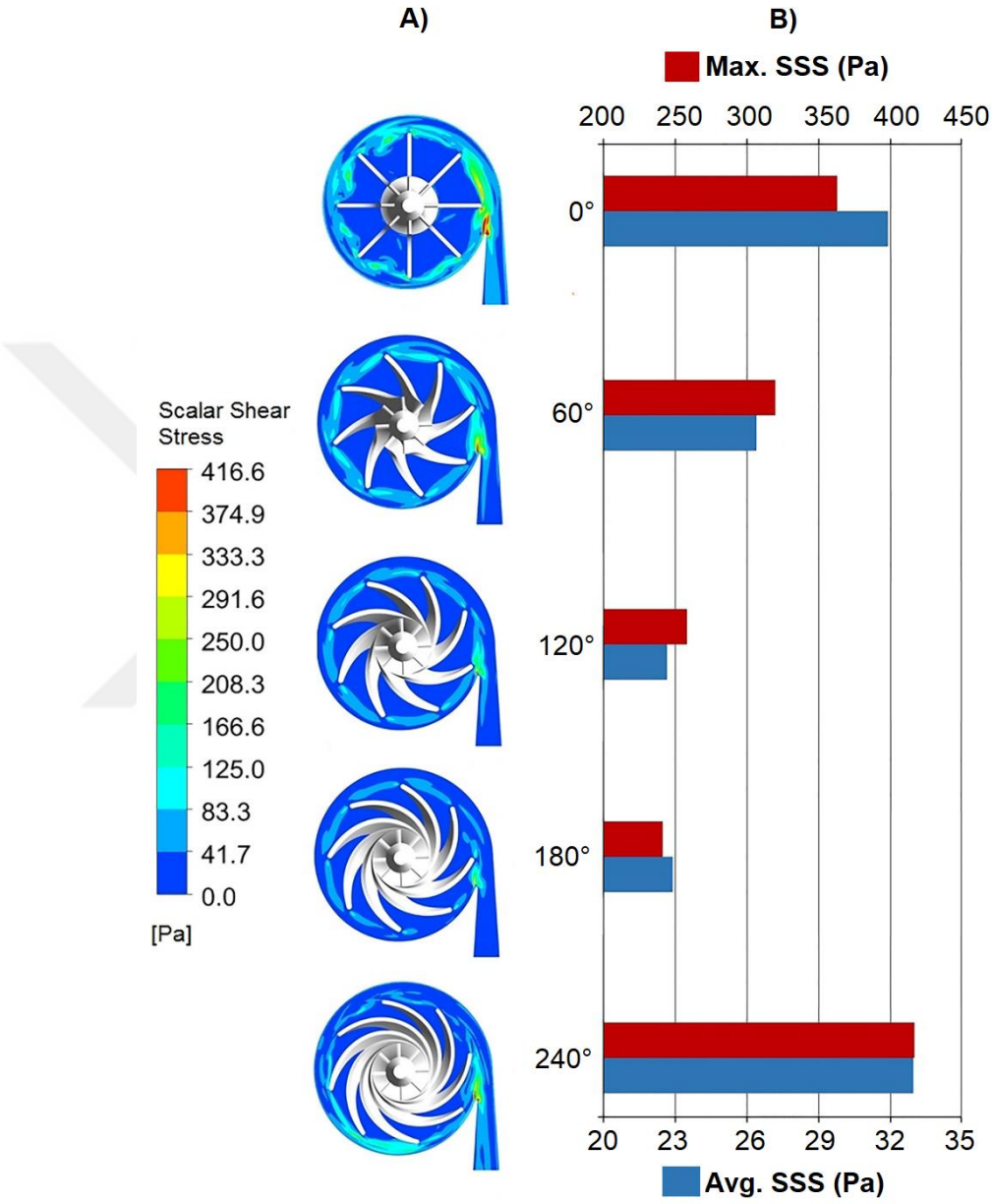

Figure 49: (A) SSS distribution at various wrap angles. (B) The average and maximum SSS values at various wrap angles[23].

Furthermore, the number of blades and splitters were investigated at the best performing wrap angle, 120°. Results shown in Table 7 indicate that an increase in blade number leads to a higher blood damage index so that RBCs are more likely to have hemolysis.

Table 7: Effect of the number of blades on hydraulic and hemolysis Performance.

	Model III	**Model VI**	**Model VII**	**Model VIII**	**Model IX**	**Model X**
Num. of Blades	8	4	10	***5***	6	3
Num. of Splitter	0	4	0	***5***	0	3
Pressure Head [mmHg]	104.1	103.1	104	***99.6***	96.8	94.9
DI (Lagrangian)	9.84E-3	1.20E-2	1.08E-2	***8.41E-3***	1.94E-2	9.44E-3
DI (Eulerian)	9.47E-4	1.32E-3	1.09E-3	***9.39E-4***	1.68E-3	7.56E-4

Along with the effect of blade number, splitter blades were introduced in Models III, VII, and IX. Table 8 shows lower blood damage indices after the addition of splitters, compared to the design without splitters. Adding splitters to the impeller geometry indicates a decay in hemolysis index. The Model VIII (five splitters, five blades) performed the best hemolytic results.

5.3 Volute Tongue Optimization

The volute geometry was also investigated with CFD simulations. The hydraulic and hemolytic characteristics of five volute tongue geometries were investigated. Table 8 demonstrates the simulation conditions and results. The tongue angle altered from 10° to 50° by 10° increments. It is observed that the tongue angle is inversely proportional to the pressure head and hydraulic efficiency. The

worst hydraulic results were seen in Model V with a hydraulic efficiency of 44.4% and head pressure of 94.8 mmHg. Hemolysis index was lowest in the volute angle of 20°.

Table 8: Effect of the volute tongue on hydraulic and hemolysis performance.

	Model I	Model II	Model III	Model IV	Model V
Volute Angle (°)	10	***20***	30	40	50
Pressure Head (mmHg)	103.4	***102.1***	99.6	96.8	94.8
Hydraulic Efficiency (%)	53.3	***51.9***	50	48.3	44.4
Net Radial Force (N)	0.29	***0.26***	0.23	0.21	0.18
Damage Index (Lagrangian)	1.20E-02	***1.18E-02***	1.35E-02	1.58E-02	1.56E-02
Damage Index (Eulerian)	3.26E-03	***2.84E-03***	4.14E-03	8.39E-03	1.24E-02

Pressure distribution was unchanging around the impeller when the tongue angle was set to 50°. The effect of increasing tongue angle also reduced the net radial force on the impeller surface. Also, the lower tongue angles resulted with well-guided flow paths due to the more circular shape of it. Whirls and flow separation was observed at higher tongue angles.

The SSS distribution of volute tongue models was illustrated in Figure 50 (A). High shear stress regions were observed near the trailing edges and the volute tongue edge. The maximum and averaged SSS were shown in Figure 50 (B). The highest damage index was found at the tongue angle of 50°, where the maximum SSS was 394.2 Pa, and the average SSS was 15.6 Pa.

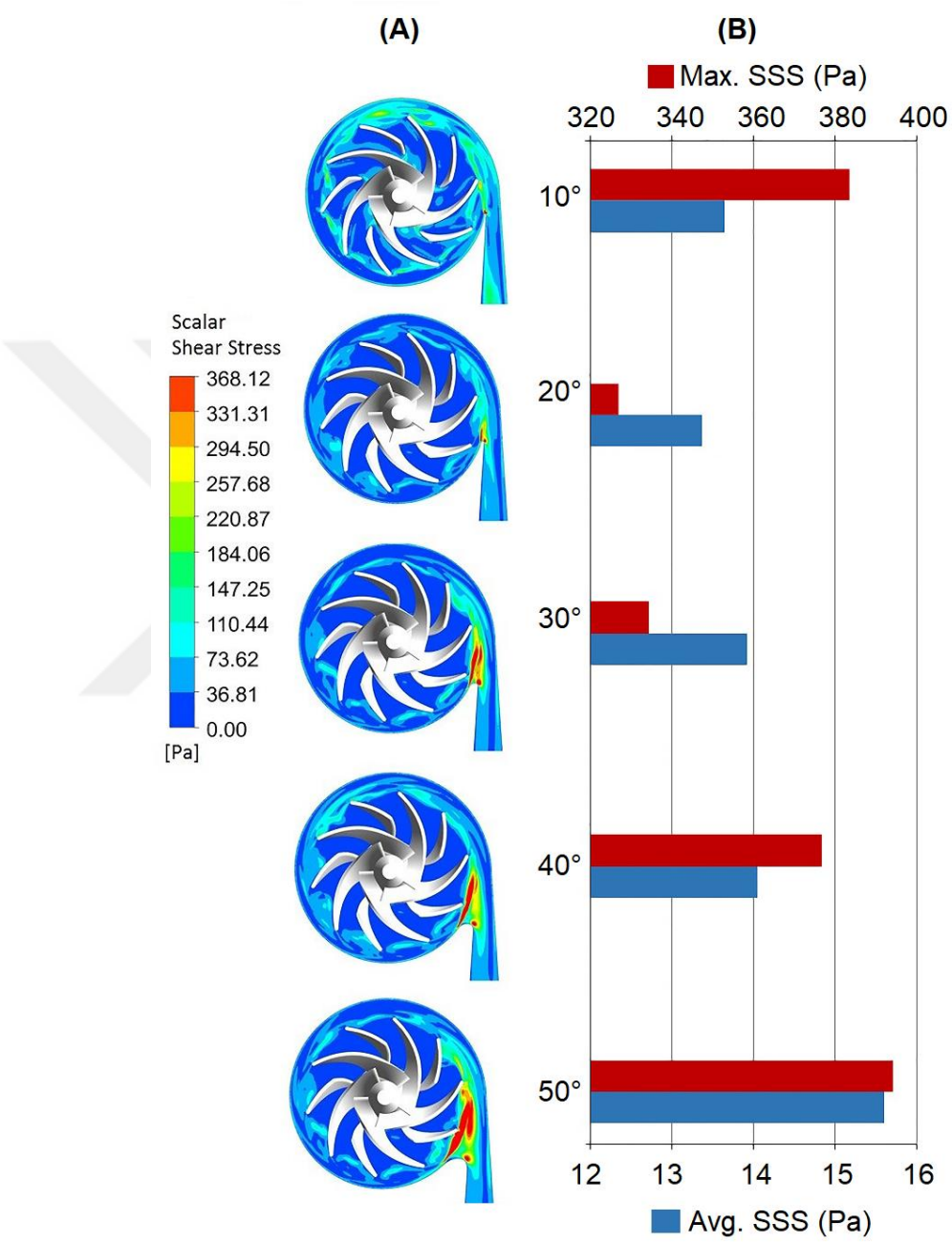

Figure 50: (A) SSS distribution at various volute tongue angles. (B) The average and maximum SSS at various volute tongue angles [23].

5.4 Flow Field

One of the critical aspects of designing a pump is its streamlined structure. The flow recirculation and separation region are undesired for the better hemodynamic performance of the pump. The velocity vector and streamlines are used to check these areas. The velocity vector shows that at low flow rate the is a flow separation occurring at the exit of the diffuser, but as that flow rate increases, this separation of flow disappears. The same improvement was observed with the introduction of splitter blades. Splitter blades guide the flow and eliminate recirculation zones (Figure 51). These findings agree with the hemolytic results.

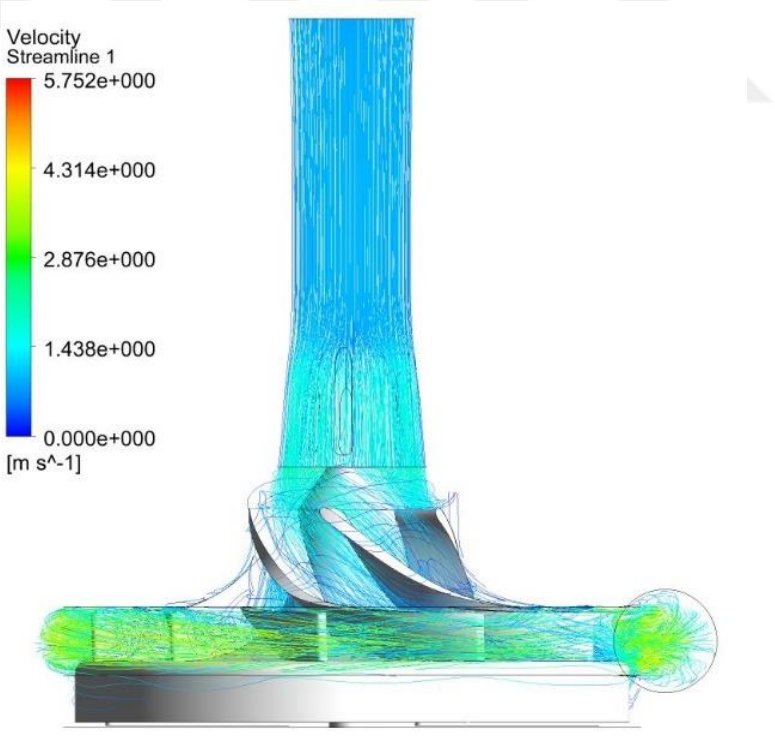

Figure 51: Streamlines of iHeart.

5.5 Hemolysis

Both the Lagrangian and Eulerian Hemolysis estimation methods described in Chapter 3.2.7 was applied to the presented models. Figure 52 depicts the Eulerian hemolysis results of iHeart VAD where the hemolysis risk is above 0.01% or more. Detailed damage index estimations are shown in Tables Table 6, 7 and 8.

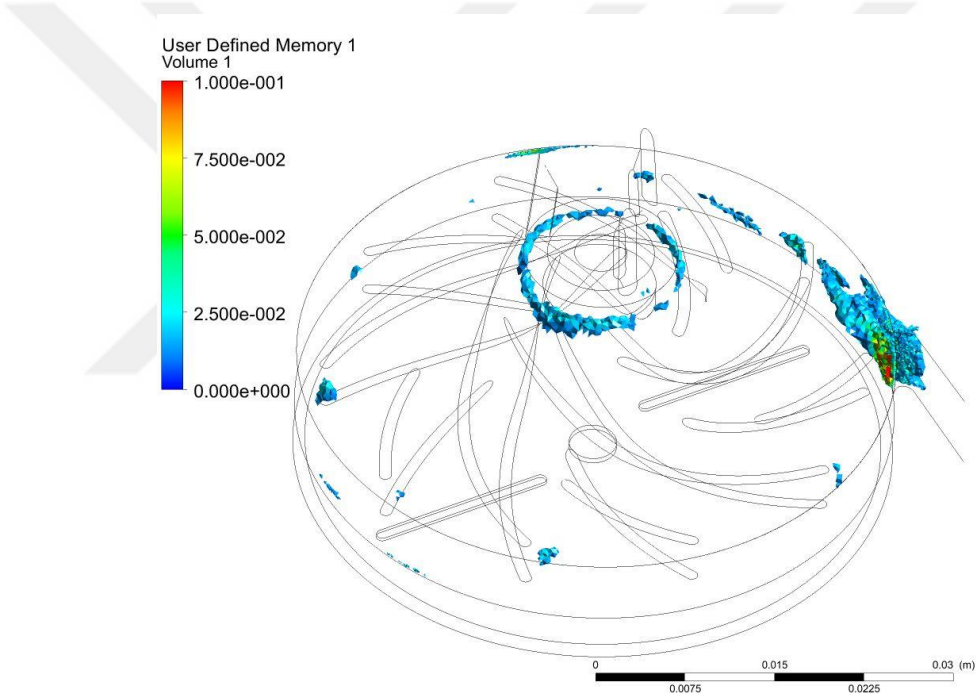

Figure 52: Eulerian damage index where the possibility of hemolysis is 0.01% or more.

A Higher blood damage index was typically detected at the blade tips and about the volute tongue region. Maximum hemolysis index is usually observed on the volute tongue edge.

In Lagrangian hemolysis estimation study, massless particles released from the inlet of the pump were observed until they are completed at the outlet. The number of released particles was between 2280 and 2338 dependent on the number of the mesh faces placed at the inlet. The residence time of the released particles fluctuated between 0.14s to 3.24s. Lagrangian blood damage indices varied between nearly 0 to 0.48. Almost 75% of the particles traced in the wrap angle 180° were in the very low blood damage possibility region between 0-0.005. Nevertheless, the wrap angle of 0° and 240° had the worst damage results (agreeing with the Eulerian findings) as 27.4% and 28.6%, respectively. So, almost 30% of the particles were at the range of 0.015-0.48 in models with the wrap angle of 0° and 240°.

5.6 Summary of CFD Results of iHeart VAD

The optimized geometry was decided with a numerical optimization study. Results of this computational study revealed that the parameters like the wrap angle, blade number, volute tongue angle, have an essential impact on hydraulic and hemolytic performances of a radial flow blood pump. The two hemolysis estimation techniques have allowed us to inspect the hemolytic performance of centrifugal pump geometries numerically, which are further investigated with physical blood tests and in-vivo experiments.

The concluded geometry comprises impeller blades with a wrap angle of 120°, five blade-five splitters carrying impeller and a volute tongue angle of 20°.

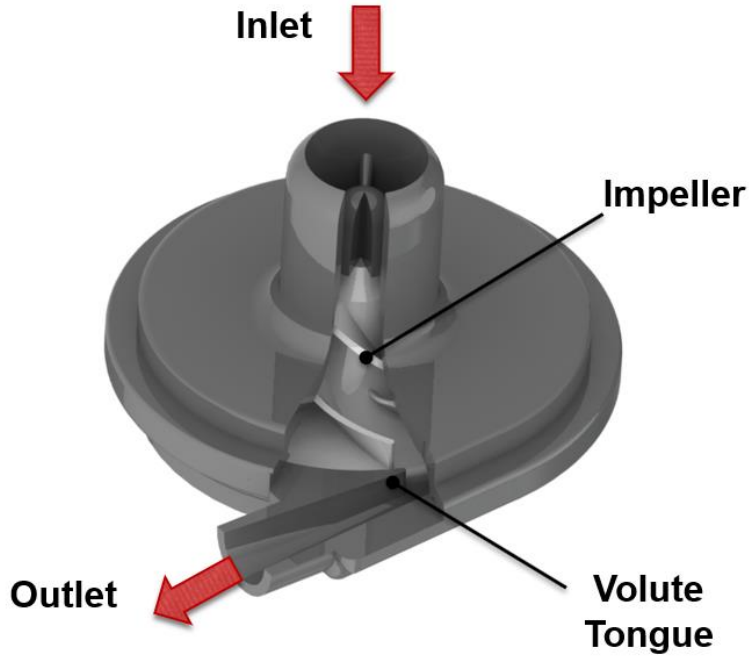

Figure 53: Final Prototype of Istanbul Heart VAD (iHeart VAD)[23].

5.7 Experimental Validation

Physical validation experiments include hydraulic tests with 3D printed pump prototypes for the wrap angle and volute tongue study. Moreover, 5 axes machined Ti6Al4V models were also manufactured and tested with blood analog fluid and human blood. Moreover, the final prototype namely the İstanbul Heart VAD was tested on an acute porcine model with 3 animals up to 6 hours. A detailed explanation of these tests and manufacturing processes were covered in the dissertation of Çağlar Öztürk [23]. In this chapter, the results of these tests were explained for the validation of the design.

5.7.1 Hydraulic Tests

With the aim of evaluating the hydraulic capacity of the final prototype, Istanbul Heart VAD (iHeart VAD), a flow testing setup was constructed . The hydraulic test loop comprises the pump prototype, a flow meter, two pressure transducers, a controller box, a LabVIEW DAQ card (National Instruments, TX, USA), 2m silicone tubing (3/8 inch diameter) and a tank. Water (67%) glycerol (33%) mixture was prepared which mimics the viscosity of human blood at room temperature. An adjustable valve was placed at the outlet for regulating the resistance and, consequently varying the flow rate. The pressure-flow rate characteristics were tested between 1000-3200 rpm pump speed. An ultrasonic flowmeter was placed on the outlet tubing for flow rate measurements. Also, two piezo pressure transducers were placed near to the inlet and outlet ports for pressure measurements.

The manufactured pump is tested under various flow/pressure conditions considering physiological requirements. The performance data under varying motor speed and outlet resistance are shown in Figure 54.

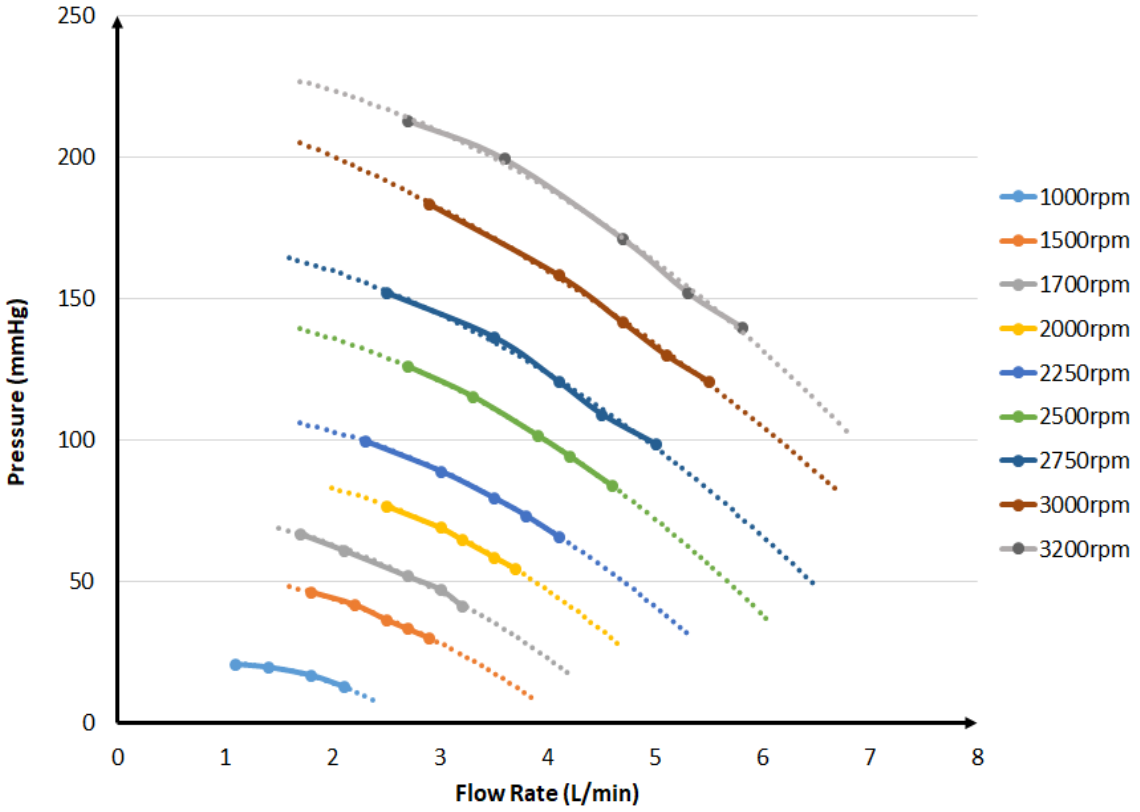

Figure 54: Performance Characteristic of the iHeart VAD[23].

Maximum pressure head of 218.9 mmHg was achieved at 3200 rpm. The design point was recorded at 2750 rpm where the pump provides a flow at 5 L/min and 100 mmHg.

5.7.2 Blood Tests

Donor selection, blood collecting and storing procedures were followed according to the ASTM F1841-97 [126]. Blood samples (90 ml) were taken from a healthy 27-year-old volunteer and anticoagulated with sodium heparin. The blood

count was measured by ABX Micros OT analyzer (ABX Inc, Montpellier, France). Red blood cells (RBC) were secluded with a centrifuge (1400xg, 5 min). PBS solution was used for the resuspension of the cells to achieve a hematocrit of 26%. The hematocrits were found with the microhematocrit method (10,000×g, 4 min).

The circuit was filled with 90 ml blood+ PBS solution (26% Ht), and any air was released from the flow loop before the test. 1 mL blood samples were taken from the loop at desired time intervals. Instant hematocrit rates were measured for each sample.

Figure 55 shows the measured plasma free hemoglobin levels (pHb). The horizontal axis shows the period, and the vertical axis shows the delta hemoglobin. All results were normalized regarding the initial sample. The changing trend was almost linear.

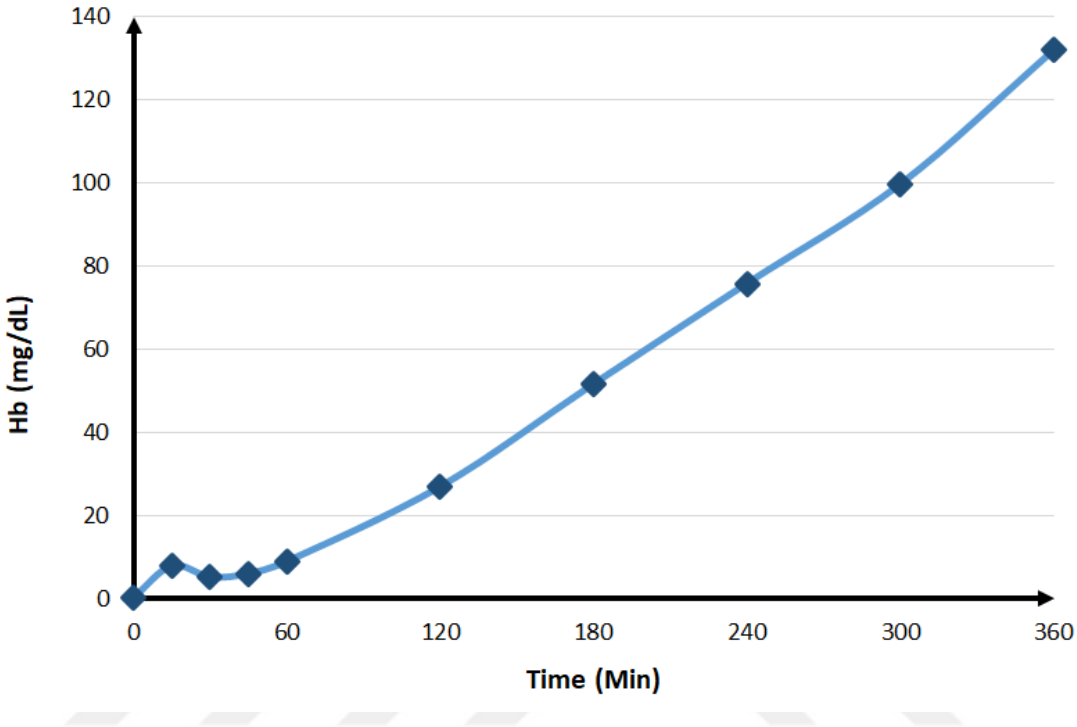

Figure 55: Plasma free hemoglobin level during the experiment. Data were normalized concerning the initial blood volume[23].

The rates of change of hemolysis summarized as NIH values in Figure 56. NIH values were considered for 6 hours duration by taking samples per 15 minutes in the first hour and per hour for the rest. Hematocrit was almost constant through the test, and NIH values were between 0.00053 and 0.00159 g/100L. The mean value of NIH was 0.00098 g/100L.

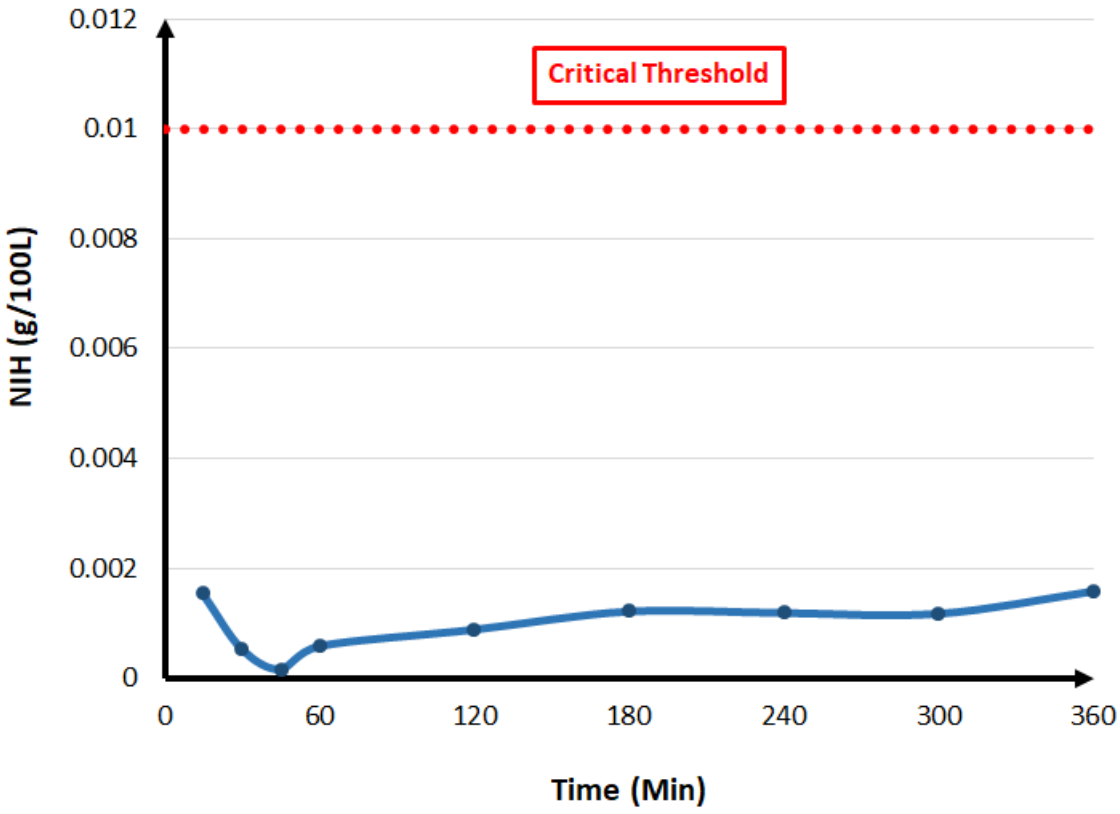

Figure 56: NIH Results during the in vitro blood test[23].

No device malfunction was observed during the experiment. Besides, thrombosis was not observed during the inspections after the experiment.

5.7.3 Acute In-Vivo Tests

Acute trials are the preliminary in-vivo test to be performed initially to evaluate the anatomic fit of the device and short-term hemocompatibility. Chronic tests follow the acute tests for evaluating the mid to long duration performance of a blood pump.

Complete Istanbul Heart VAD (iHeart VAD) device consists of 170x120x55mm control unit, the pump, two lithium-ion batteries each providing 17 hours operation at nominal conditions (Figure 57).

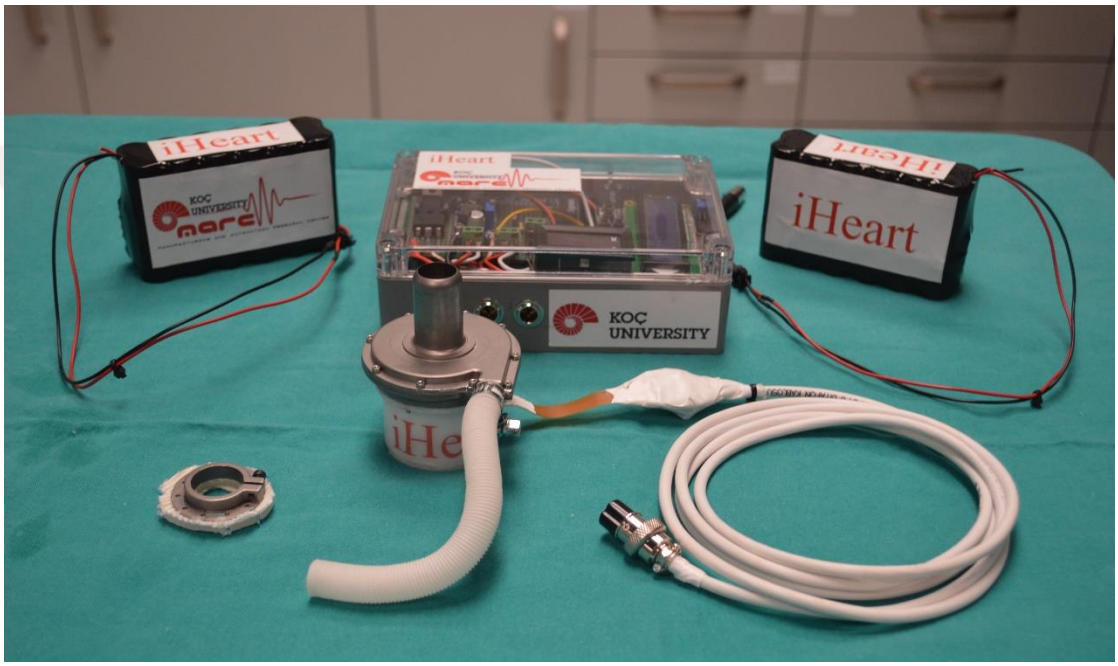

Figure 57: Implantable Istanbul Heart VAD (iHeart VAD) system.

The in vivo study includes the development of a porcine model for the LVAD implementation and the application of a standard surgical technique for LVAD implantation. This chapter explains our preliminary acute in vivo test which was completed with the collaboration of Center of Advanced Simulation and Education (CASE), Acibadem University, Istanbul, Turkey.

Three acute animal tests were conducted in porcine models to investigate the in-vivo performance of the iHeart VAD. The “Guide for Care and Use of Laboratory

Animals" was followed during the experiments for providing a human care for animals [127]. The study was approved by the Ethics Committee of the Acibadem University.

Three pigs weighed 77–92 kg, were implemented with iHeart VAD system. The pigs were obtained from a private farm associated with Acibadem University. Pigs were transported to the CASE laboratory two days prior to the surgery.

For each experiment, the pig was intubated and anesthetized. Proper ventilation was provided during the experiment. Intravenous heparin (4 mg/kg) was given to avoid coagulation. The ventilation and gas content was kept at the physiologic pH and carbon dioxide (pCO2) limits. The pump was tested for 5 minutes with saline for the final check. The chest was opened via median-sternotomy. A PTFE outflow graft was anastomosed to the descending aorta in an end-to-side fashion.

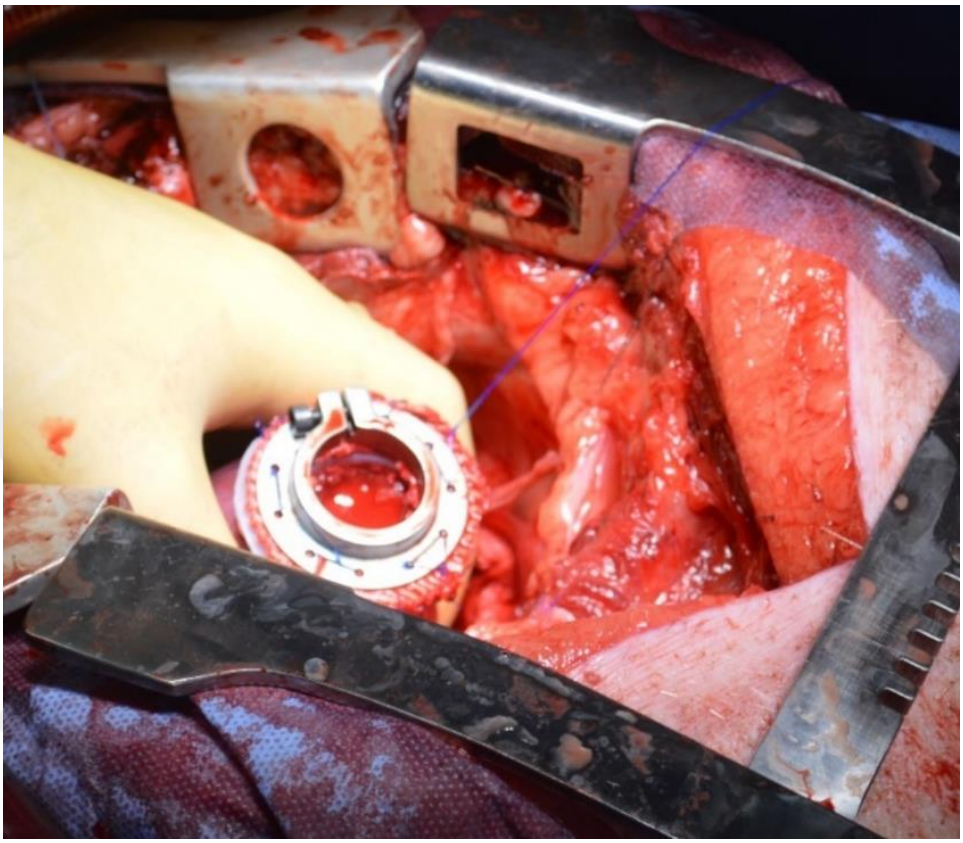

Figure 58: The process of suturing the sewing ring.

The left ventricular (LV) apex was elevated by placing lap sponges underneath the heart. The sewing ring was fixed to the LV apex with 10 pledged sutures (Figure 58). A circular incision was made on the beating heart. The pump was inserted into the LV cavity and secured with the screw on the sewing ring. Air was removed from the system. Figure 59 depicts the pump implantation during the second in vivo experiment.

The controller box and batteries were placed close to the surgery table. A flow probe was located at the outflow graft to measure the flow rate. The pump flow was initiated with 1250 rpm prior to the removal of the occlusion clamp from the outflow graft and then slowly increased to 2000 rpm. The pump was expected to provide a blood flow of 3 L/min to attain maximum unloading of the ventricle. Circulating blood volume was maintained by continuous administration of isotonic saline.

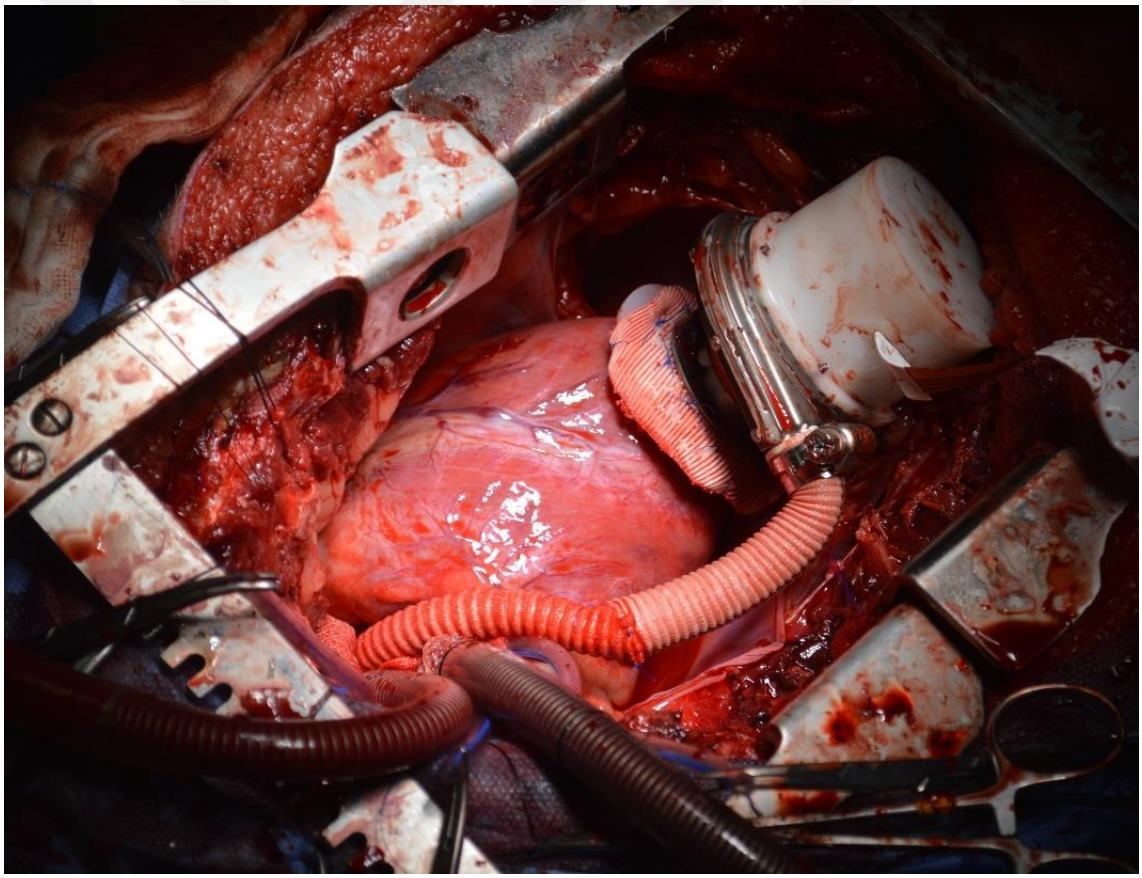

Figure 59: Implantation of the pump in the second in vivo experiment.

Every half an hour, blood samples were collected to measure the blood gases (pO2, pCO2, etc.), hematocrit and hemoglobin levels. The heart was regularly monitored with a GE Vivid T8 ultrasound electrocardiogram system (General Electric Healthcare, WI, USA). The left ventricular ejection fraction was measured and calculated with this system.

No device associated complications happened throughout the experiments. The experiment duration was between 3 to 5 hours. Mean flow rate was 2.5 ± 0.4 L/min and the mean power consumption was 8.4 ± 3.1 watts. The impeller speed was changed between 1250 rpm and 3000 rpm according to the ventricular volume. The physiological data like heart rate, O_2 saturation, respiratory rate, and body temperature were in the physiologic limits through the experiments.

Each pig was sacrificed at the end of test duration, prior to the inspection of end-organs. The decreases of the red blood cell count and hematocrit ratio were detected in all animals. The hematocrit level was measured under the physiologic range. The plasma free hemoglobin (pHb) levels showed differences through the experiment (Figure 60).

After the conclusion of each experiment, the LVAD was removed and inspected to examine the anatomical fit of the inflow cannula in the apex (Figure 61).

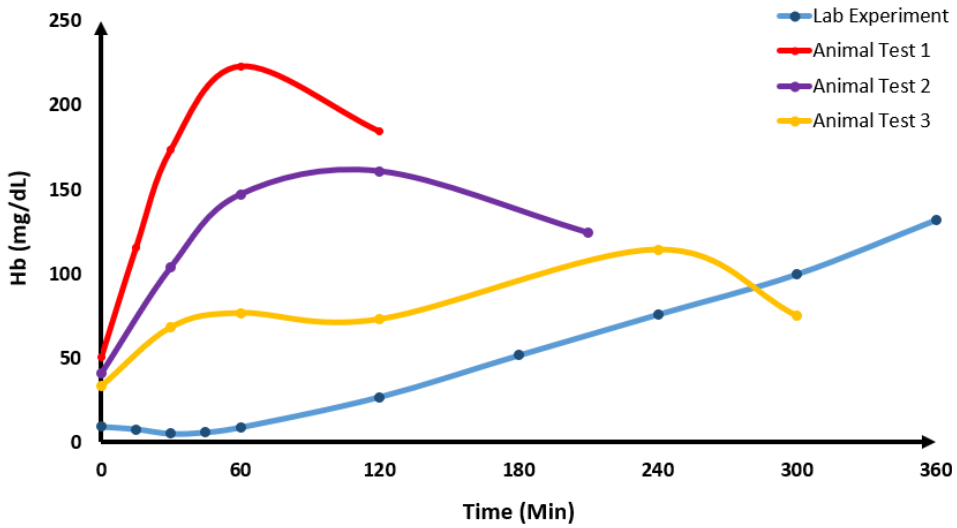

Figure 60:Plasma free hemoglobin level of in vitro and in vivo experiments

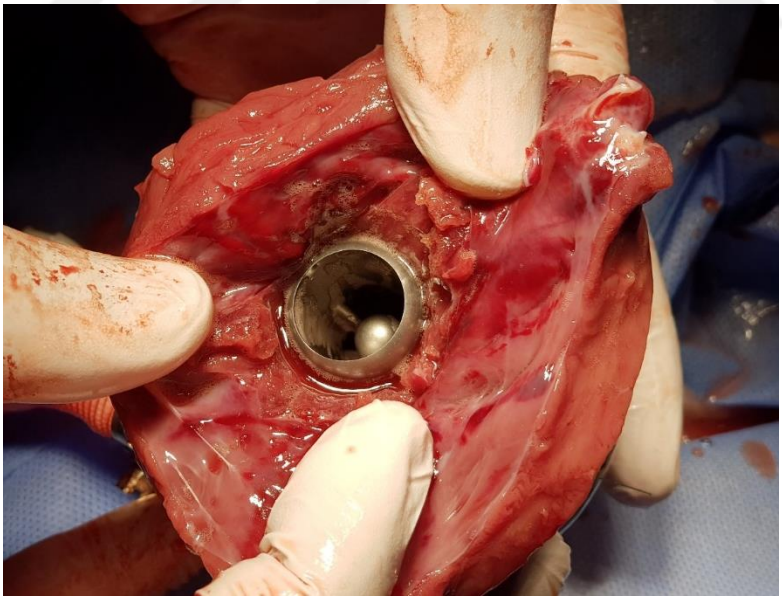

Figure 61: Examination of inflow cannula position at the apex.

The inflow cannula was seen to be well-located into the LV. Furthermore, the inspection of the internal structure of the LVAD showed no indication of thrombus formation on the blood contacting surface and bearings (Figure 62).

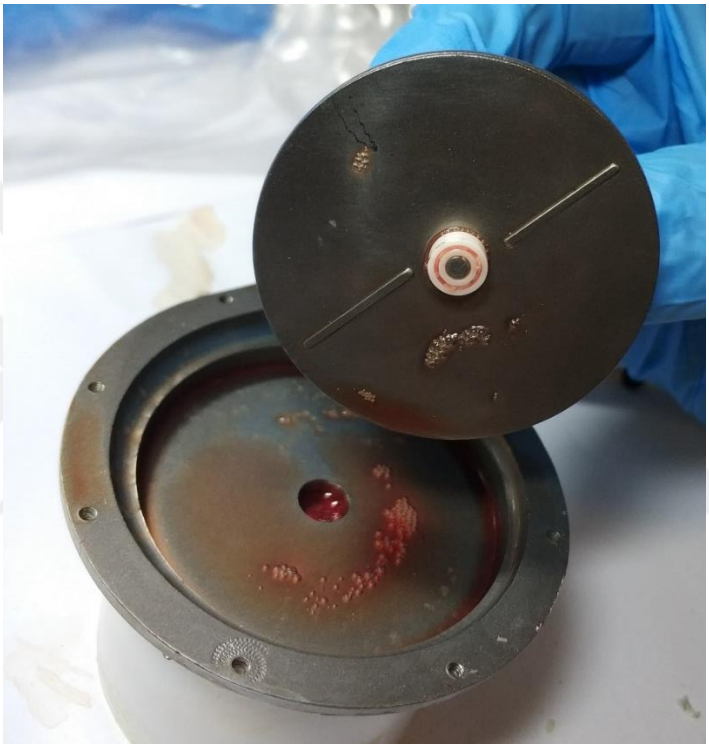

Figure 62: Internal view of the pump after the experiment.

Nevertheless, small pieces of myocardia were detected after the second in vivo test, which is apparently the residuals of the removing process.

5.8 Discussion

Results of the hydraulic, hemolytic and in-vivo tests are discussed in separate sub-chapters.

5.8.1 Optimization Study

According to the CFD findings, the flow structure of radial bladed models caused flow separation at the trailing edge of the blades where vorticies occurred. Likewise, the relatively large flow path inside this model caused recirculating regions and higher SSS calculations. Therefore, introducing some wrap angle creates a thinner flow passage, consequently decreases the flow separation and assures superior guidance to the fluid. Though, an extreme wrap angle elongates the blade contact, decreases the priming volume which undesirably increases SSS and therefore providing a poor performance as observed in the model having a wrap angle of 240°.

Regarding the volute tongue study, increasing volute tongue angle endorses the reduction of the net radial force acting on the impeller. However, hydraulic performance was shortened as tongue angle increases. Hydraulic tests also agree with the pressure and flow rate findings of the CFD study. CFD studies showed that the SSS generation and tongue angle are directly proportional. The tongue angle of 20° provides a superior hemolytic performance by 5.7% (Eulerian) and 12.9% (Lagrangian). On the other hand, lower tongue angles are disadvantageous on the net radial force acting on the impeller. Blood damage risk is usually higher on the tongue edge, around the volute tongue region and the trailing edge of blades. A well-matching impeller and volute tongue minimizes the vortex formation, flow separation, the imbalanced radial force acting on the impeller and, to conclude, lower hemolysis.

Two hemolysis estimation models showed the same trend through the optimization study. However, orders of magnitude of these models were different. The difference between these blood estimations is due to the fact that both are based on different numerical methods. None of the shear-induced blood damage estimation methods are valid as of today [101,122]. However, these models are valid to be used as a comparative tool for estimating the relative hemolysis for optimization studies.

Contrary to encouraging outputs of this numerical study, there are some limitations. The frozen rotor method used accounts only the steady-state effects. In fact, each blade passage around the volute tongue alters the flow field as centrifugal pump volute is non-axisymmetric. Furthermore, the experimental study has several limitations. Manufacturing tolerances of the 3D printed parts were about 100μ, and hand polishing was applied for removal of the support material and assuring a good surface finish. Nonetheless, results of the hydraulic tests were in a good agreement with the numerical simulations.

5.8.2 Blood Tests

In this hemolytic performance analysis, 100 mmHg of pressure head was the target based on the ASTM F1841–97 [126]. However, the amount of blood (100 mL) used in this experiment was less than the suggested blood volume for ASTM F1841–97 standard due to the restriction of the approved ethical protocol. Nevertheless,

running blood tests with a smaller volume is challenging considering each cell is subjected to the high shear stress zones of the blood pump more frequently.

Though numerical and experimental hemolysis findings provided different orders of magnitude; they presented the same trend as the wrap angle varies. Also, the rate of the difference of damage indices agreed with other studies in the literature [101,122]. The shear-induced hemolysis estimation methods have still not accurate, yet they are reliable for having a relative hemolysis amount for optimization studies [101].

5.8.3 Acute In-Vivo Tests

The preliminary acute in-vivo tests of iHeart VAD have been completed to assess the hydraulic performance, hemocompatibility and, anatomical fitting. The VAD confirmed proper hemocompatibility in the acute porcine model. The level of hemolysis was measured in an acceptable range.

The porcine models used had healthy heart function. As these devices are designed for end-stage heart failure patients, testing a VAD with normal functional heart is a limitation. Therefore, hemodynamic performance of the VAD should also be tested with a heart failure model.

The clean cutting process must be performed while opening the cavity on the left ventricle, considering that small myocardial tissues were found inside the device post-operatively for the second test. Additionally, the tension of the outflow cannula has a substantial influence on the performance of the pump which is altered by the

pump placement. Any error in the placement of the pump would cause unnecessary workload on the heart due to the bending of the outflow graft which affects the pressure and flow rates eventually. This phenomenon increases power consumption.

Isotonic saline was used to preserve the circulating volume of blood during the experiments. However, due to the internal bleeding caused by heparinization, the hematocrit levels of the animals reduced significantly while the constant saline administration was applied. In future studies, some blood of the animal will be drawn days before the operation for the usage in the surgery instead of saline while compensating the blood loss.

In general, Istanbul Heart VAD indicated sufficient performance. However, a size reduction of the pump is required for the future studies. Explicitly, the motor casing and the external motor which is positioned under the pump must be replaced with a smaller and embedded custom-made motor design where the impeller acts as the rotor of the motor. An internal motor design will reduce the overall size of the pump and assure a better fit for the patients.

IATVA: DESIGN

Single ventricle defects are treated with a series of palliative open-heart surgeries where a single-ventricle or namely, the Fontan circulation is created. This paradoxical circulation progressively fails as the patient ages, due to increased venous pressure levels. Additional subpulmonic energy would reverse this paradox. Circulatory assist devices can deliver this extra energy. This work aimed to evaluate the hemodynamic performance of an implantable integrated aortic turbine venous-assist (iATVA) device. The iATVA system does not need an external power source and maintains low venous pressure for the Fontan circulation.

The co-rotating turbine and pump impellers were designed following the turbomachinery theory, 3 prototypes for various flow conditions were manufactured. iATVA device was evaluated for hemodynamic performance under pediatric and adult physiologic flow conditions with a pulsatile mock-loop. The iATVA system was also investigated in clinical off-design flow scenarios.

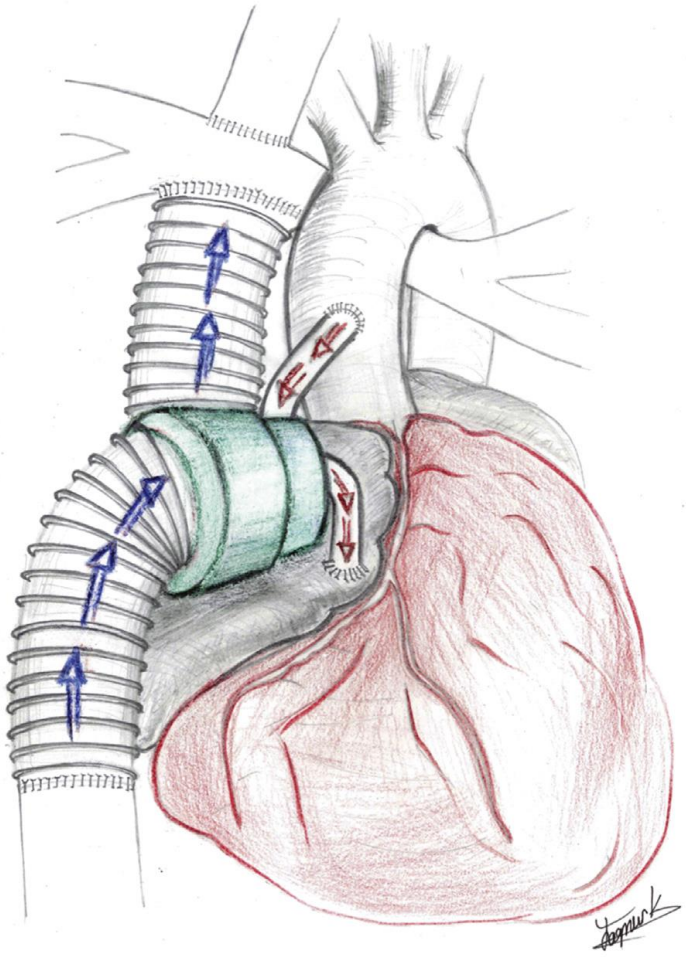

Figure 63: A sketch of iATVA implanted in the heart[6].

Turbine and pump impellers of the iATVA device connected through a shared shaft. Aortic turbine steals a slight amount of aortic flow to transfer this available energy to the venous pump where it is most needed in Fontan circulation (Figure 63). The iATVA device is able to remedy the Fontan paradox by reversing its gradual vascular problems passively. This chapter covers the investigation of the feasibility of the first-generation iATVA prototypes using a bench-top single-

ventricle circulation mock-up circuit. The complete mechanical design and planned animal experiments will be conducted shortly.

Even though the causes for complications of Fontan circulation are multifactorial, persistently high systemic venous pressure (SVP) is the main problematic factor known in the literature that results in regular surgical remodeling in the venous vascular system as described before in Chapter 2.1.2.

The requirement of an external power to operate an FVAD is a main technological challenge. This requirement meaningfully limits the patient mobility and independent long-term use of FVADs. To overcome the need for an external power source, our research group proposed a novel implantable Fontan assist system that passively resolves the Fontan paradox by utilizing the indigenous circulatory power. The device draws a slight amount of high pressured aortic flow and uses this available energy to drive an aortic turbine (Figure 63). In sequence, the blood turbine drives a centrifugal mechanical circulatory assist device, which provides the needed high-flow and low-pressure venous flow through the IVC and SVC.

6.1 Pump Design

Parametric design of the iATVA system was prepared considering the physiologic flow conditions exists in Fontan circulation to discovery possible and ideal operating ranges and capabilities. The design parameters were framed

according to the 2 baseline physiologic conditions, corresponding to the 3 liters per minute 60%IVC flow ratio (post-operative pediatric) and 5 liters per minute 80%IVC flow ratio (adult Fontan patients). The turbomachinery design of 3 iATVA prototypes was completed with respect to these physiologic conditions.

Both the turbine and the pump sides of iATVA are low specific speed centrifugal machines. However, in very low specific speed range (Ns<0.25), the hydraulic efficiency of a traditional centrifugal pump becomes meaningfully low. Therefore, for the industrial application of such flow conditions, pulsatile pumps have been widely used [128]. However, the pulsatile pumps remain problematic due to membrane material fatigue, noise and vibration and therefore, their current use for heart assist devices has been reduced significantly after the approval of rotary pumps[68].

As the main design approach, first, the turbine diameter is determined based on the physiologic flow characteristics and turbomachinery equations given in Chapter 3.1. The impeller velocity U is obtained from the substitution of Euler's pump equation and flow rate equation assuming a radial outlet profile;

$$\rho . U^2 - \rho . \cot\beta . \mathrm{V_r} . U - \Delta P_{turbine} = 0 \qquad 6.1$$

Where ρ is the blood density, β is the turbine blade attack angle, and $\mathrm{V_r}$ is the radial velocity component (the tangential component $\mathrm{V}_\theta = \Delta P_{turbine}/\rho U$) respectively. Resulting turbine rpm and torque T are calculated as;

$$N = 2\frac{U}{D_{\text{impeller}}}\ T = \rho Q_{turbine}(r.\mathrm{V}_{\theta}) \qquad 6.2$$

Relaying the rotational power to the pump side results in a venous pressure rise for the required venous flow Q_{pump} as;

$$\Delta P_{pump} = \eta N.T/Q_{pump} \qquad 6.3$$

For both impellers, a circular cross-sectioned logarithmic spiral shaped single volute has designed. The volute widths are equal to the impeller widths, which is required because of their low flow capacity and low specific speeds. A sharp volute tongue, having a more circular perimeter around the impeller is designed to reduce the non-axisymmetric radial forces acting on the impellers. Consequently, the extensive hydrodynamic designs and CAD drawings of 3 iATVA prototypes are generated using NX 10.0 software (Siemens Inc, TX, USA).

Ideal Device Characteristics

According to our literature survey, this is the first research to investigate the turbomachinery design of a blood turbine in cardiovascular device literature[6]. The low aortic steal obligation of the iATVA system means a low turbine specific speed calculated as 0.22 (N_s). A low specific speed causes a design challenge for radial impellers, even causing impulse turbine configuration if higher efficiency is required. For the venous assist side, a mixed-impeller is found to be optimal to

assist the Fontan circulation, with the nondimensional specific speed of 2.25 (N_s). The rotational speed of iATVA differs between 800 to 1800 revolutions per minute (rpm), providing a venous pressure head (ΔP) of 3 to 12 mmHg through the pump (observed as an SVP decrease or pulmonary artery pressure increase).

The ideal operating range of the iATVA device is calculated from the turbomachinery theory and plotted in Figure 64. It is observed that for both adult and pediatric physiology the iATVA system can deliver adequate venous pressure increase at the pump side that pumps the IVC flow even with a conservative hydromechanical efficiency (50%). Up to 5 mmHg venous pressure support is conceivable with less than 5% of aortic steal. As the top row of power generation chart in Figure 64 displays that larger turbine diameter and blade trail angle provides a higher power generation.

To attain a relatively unchanging operating point and smaller turbine size for easy implantation on infants, the design points are chosen at the relatively flat region which leads to a turbine diameter of 38 mm (see Figure 64 top left). For the selected turbine operating point, the matching venous pump hydraulic performance range is summarized in Figure 64 (top right). Finally, an impeller with 10 mm blade height and 32 mm pump diameter was chosen at a blade trail angle of 60°. For adult Fontan circulation (CO 5 lt/m and IVC flow rate 4 lt/m) pump pressure is 7.8 mmHg corresponding to an aortic steal of 10% at 90 mmHg aortic pressure. For the pediatric flow requirements (CO 3 lt/m and IVC flow 1.8

lt/m) pump head is 15 mmHg, with an aortic flow steal of 10% and 90 mmHg aortic pressure (Figure 64).

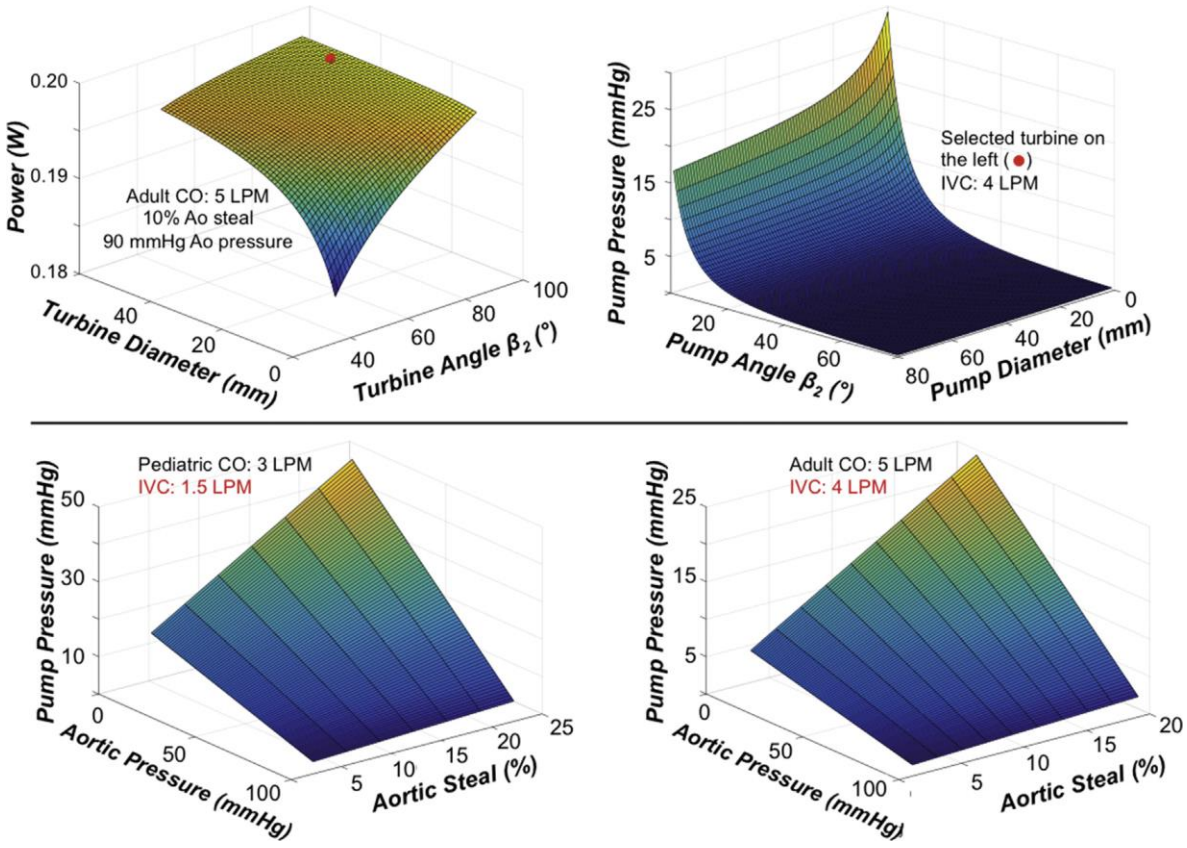

Figure 64: The ideal power characteristics of the iATVA system[6].

3 different locations were considered for the drainage of the turbine outlet; the single atrium, axillary artery, and distal pulmonary artery (PA), which results with varying available power for each (see Figure 64). Through this research, the turbine was placed between the aorta and the single (common) atrium

(Configuration 1), where the maximum obtainable pressure is almost 90 mmHg between the turbine inlet and outlet.

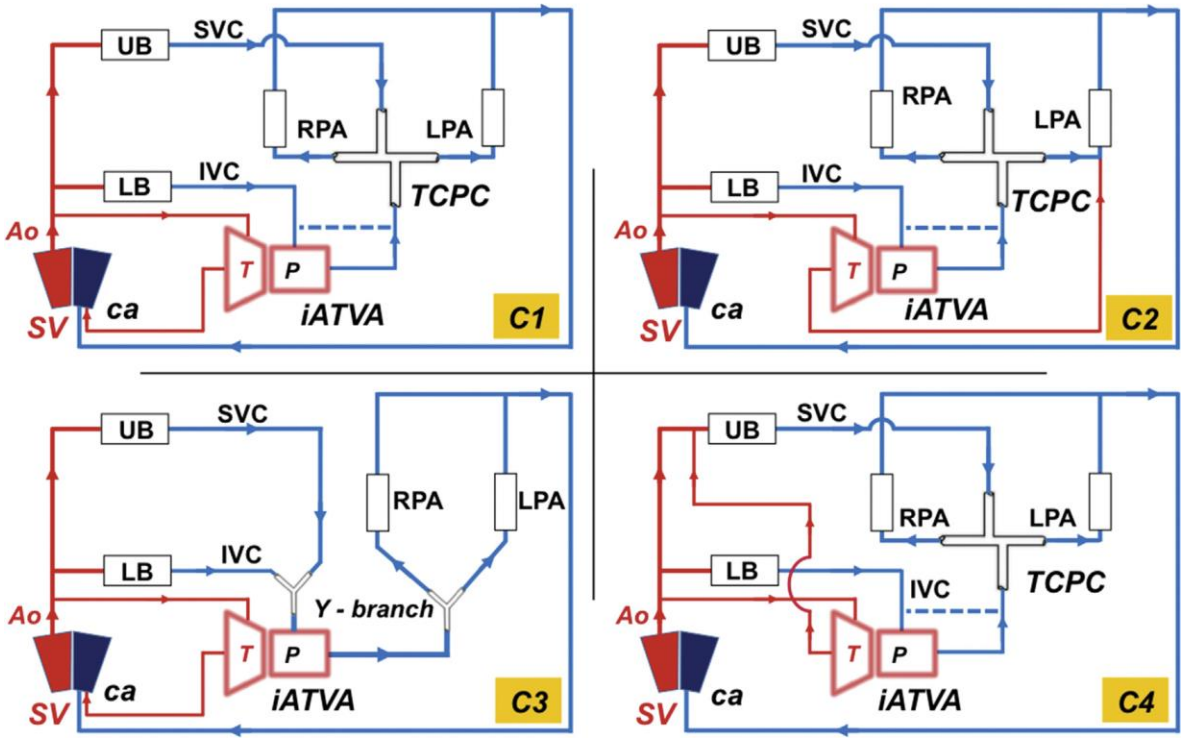

Figure 65: Different configurations for the turbine outlet of iATVA[6].

(UB, Upper body systemic bed; SVC, superior vena cava; RPA, right pulmonary artery; LPA, left pulmonary artery; LB, lower body systemic bed; IVC, inferior vena cava; Ao, aorta.)

All configurations were implanted in the mock-loop set to single ventricle (SV) circulation. Configurations 1, 2, and 4 diverge in turbine outlet placement. This study explored configuration 1 (C1) whereby the common atrium (ca) was the turbine outlet drainage. Configuration 2 (C2) drains the turbine outlet to the distal

PA. Configuration 4 (C4) drain the outlet into the axillary artery. Configuration 3 (C3) exemplifies a double-inlet double-outlet venous pump placement deprived of a total cavopulmonary connection (TCPC).

Table 9: Main design parameters of iATVA prototypes (P1, P2, and P3) are summarized[6].

	Turbine	Pump
Flow rate, lt/m	0.5	3.0 (P1), 1.8 (P2), 3 (P3)
Blade height, mm	5	9 (P1), 4.5 (P2), 9 (P3)
Impeller diameter, mm	38	32
Blade angle, b2	75°	60°
Number of blades	6 (P1), 6 (P2), 12 (P3)	5
Shroud volume, cm3	1.1 (P1), 1.1 (P2), 0.5 (P2)	12.6 (P1), 11.5 (P2), 11.5 (P2)
Volute volume, cm3	1.16	3.1 (P1), 2 (P2), 2 (P2)

The variations between iATVA versions are the turbine blade numbers and pump volute size. The turbine body was constant for all 3 designs to steal lower flow from the aortic current (0.5 lt/m) as a design point. Physiologic IVC flow rates corresponding to pediatric and adult hemodynamics are assumed (Table 9).

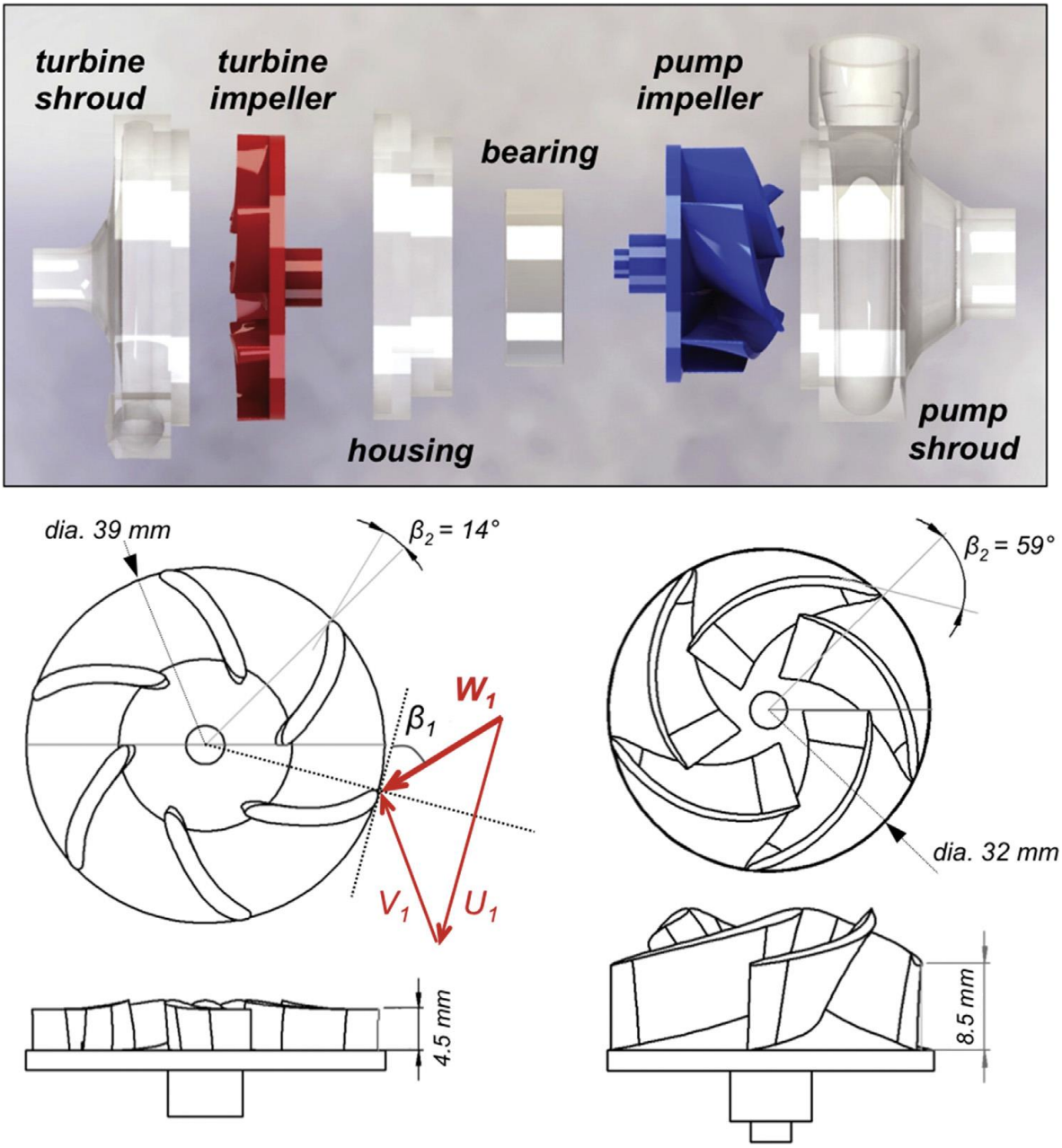

Figure 66: Blade angles and dimensions of iATVA (P1)[6].

6.2 Manufacturing and Assembly

All parts were rapid prototyped by +90 Rapid Prototyping (Istanbul, Turkey), using a Stratasys Connex500 3-D printer (Stratasys, Eden Prairie, Minn), excluding the bearing. The transparent shrouds and opaque impellers were manufactured from Polyjet Veroclear and Verowhite resins (Stratasys), correspondingly. A standard steel bearing (MOS, Istanbul, Turkey), with 5x14x5 mm dimensions, were utilized. Manual assembly of parts was achieved with tight-fitting tolerances and fine polishing. Six added blades are produced separately with a Projet 1200 high-accuracy 3-D micro stereolithography printer (3D Systems, Rock Hill, SC) using VisiJet FTX resin (3D Systems). These added blades were attached to the prototype 1 impeller. A total of 3 iATVA prototypes are evaluated in static as well as dynamic mock-loop conditions.

Figure 67: A close view of the turbine impeller and shroud of the iATVA prototype 3.

IATVA: ANALYSIS EXPERIMENTATION AND DISCUSSION

The rapid prototyped iATVA models were evaluated at the bench-top first using a steady turbine inlet flow setup and then using a pulsatile mock circulatory loop. Beforehand, both setups were validated for testing pediatric ventricle assist devices in Fontan circulation, and the experimental approach was explained thoroughly [129].

7.1 Steady State Performance

The iATVA prototypes were evaluated under various steady turbine flow rates (which mimics the aortic steal) and the resulting net venous pressure decrease (ΔP), on the pump side at IVC was logged. Steady flow test setup is shown in Figure 68.

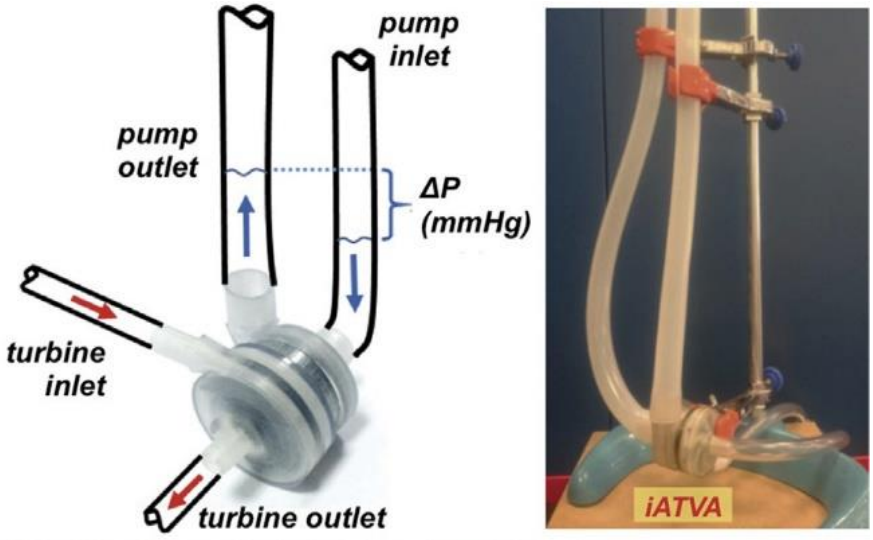

Figure 68: Steady flow experiments of iATVA[6].

For prototypes P2 and P3, a pressure difference of 5 mmHg was achieved at 1 lt/m turbine inflow. With a slight increase of flow rate (additional 0.2 lt/m) results with doubling of the pressure generation. Observed rotation speeds were lower than the predicted speeds (see Figure 69). The generated pressure head was steadied above 400 rpm powered by a turbine flow of 0.95 lt/m, for P1. Impeller speed of 700 rpm was recorded at a flow rate of 1.3 lt/m. For P2 and P3, higher impeller speeds were reached due to the torque rise provided by a bigger volute design. P2 and P3 indicated a similar performance trend between 0.85 and 1.3 lt/m turbine flow. However, the torque rise in P3 permits a very low aortic steal, reaching 0.6 lt/m and assuring roughly a 1 mmHg venous pressure rise.

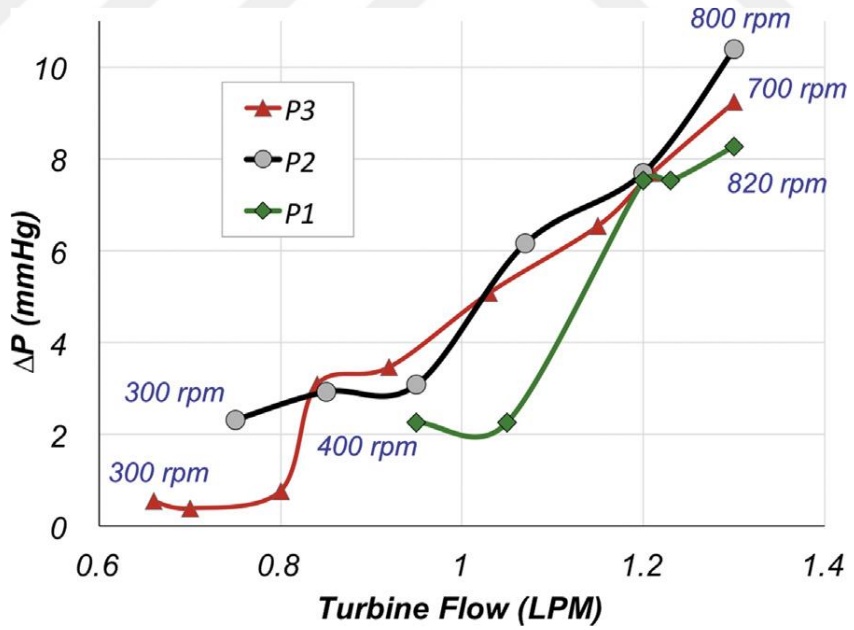

Figure 69: Steady-state performance chart of iATVA[6].

7.2 In Vitro Mock-Loop Experiments

The iATVA device was placed, parallel to the IVC along a bypass line, using Y-connectors, which permitted the rapid introduction and removal of the device in the single-ventricle circulation without interrupting the flow inside the beating circuit. The total cavopulmonary connection (TCPC) state was first set following the Fontan physiology, and all variations in hemodynamic parameters after the iATVA was introduced were measured.

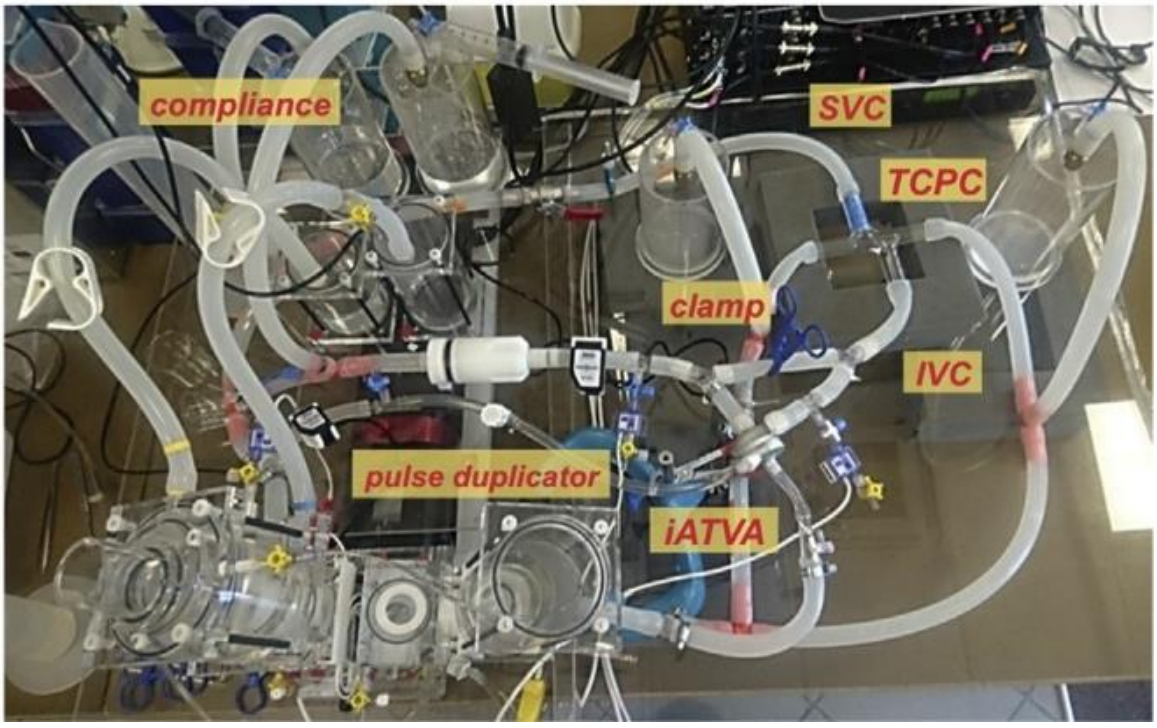

Figure 70: Pulsatile in-vitro performance test setup of iATVA[6].

In summary, the single-ventricle mock-loop comprises a 12.62-mm flow diameter TCPC replica which is fixed to 4 custom-made compliance chambers

(IVC, SVC, right and left pulmonary veins) as shown in Figure 70. The Y-connection created a parallel bypass line, which permitted convenient switching between the single- ventricle circulation with and without iATVA devices. In this study, enhanced single-ventricle waveforms were achieved with the computer-controlled Vivitro pump (Vivitro Labs, British Columbia, Canada). Anticipated pressures were achieved by altering the IVC and SVC resistances. Turbine rotational speeds were measured in a contactless fashion with a laser tachometer DT-2234C (Sanpo Instrument Co Ltd, Guangdong, China). Pulsatile flow rates were recorded with PXL-10 ultrasonic flowmeters (Transonic, Ithaca, NY). Dynamic flow measurements were obtained from the vena cavae and inlets-outlets of iATVA. Pressure measurements were recorded with Deltran pressure transducers (Utah Medical Products Inc, County Westmeath, Ireland). Dynamic pressure measurements were obtained from the aortic outlet and the iATVA pump/turbine inlets and outlets. Data acquisition was conducted using the Lab-chart data acquisition unit (AD Instruments, Colorado Springs, USA).

Distilled water was used in the experiments. An alternative dual-inlet and dual outlet (for supporting both vena cavae) configuration were also considered. However, it was chosen to use a simpler TCPC model to evaluate and report results that are compatible with the existing literature that mostly inspects single-IVC support. Single IVC support also permits an experimental simplicity in the single-ventricle mock-loop. A dual-inflow/outflow configuration would require a

more complex bypass circuit (to change between TCPC and the TCPC+Pump configurations), This would also increase the hydraulic resistance where demonstrating the benefits supplied iATVA would be difficult. Moreover, IVC only support is more beneficial for some patient groups since this requires a more straightforward modification on the existing TCPC connection.

The single-ventricle (Fontan) circulation was initially created in the mock-up circuit with 86.1, and 96.2 mmHg mean aortic pressure for pediatric and adult circulation, respectively. The resulting mean IVC flow rate was logged as 2.2 lt/m (pediatric) and 3.2 lt/m (adult), and the sample measurements are shown in Figure 71. Turbine impeller rotation was seen immediately after iATVA prototype 3 is introduced. A 1 lt/m aortic steal creates an immediate decrease in average systemic pressure levels up to 59.7 mmHg (for pediatric: 80.5 systolic, 46.3 diastolic) and 74.8 mmHg (for adult: 95.6 systolic, 64.2 diastolic), which were adjusted back to their initial aortic pressure levels.

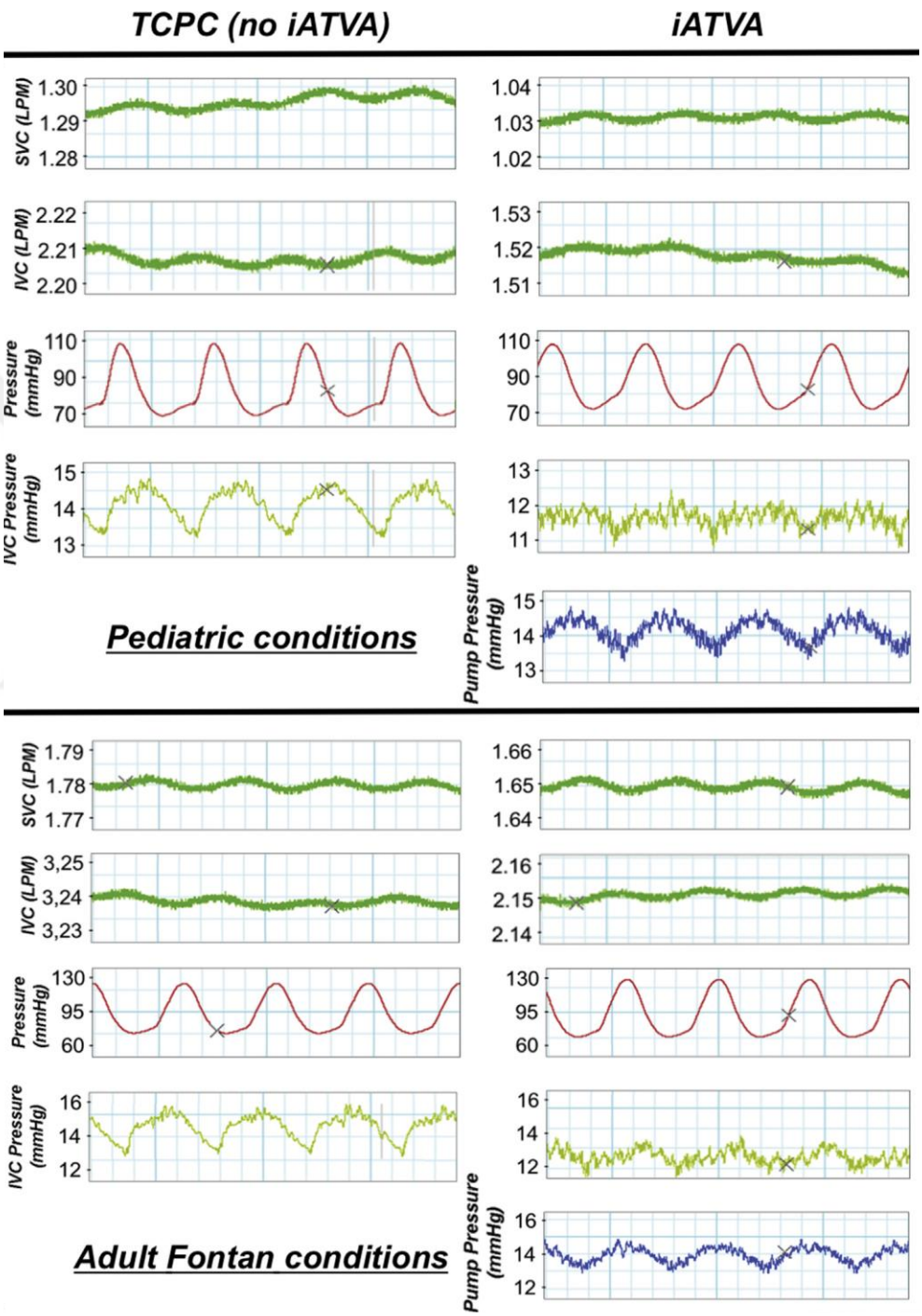

Figure 71: Sample pulsatile flow measurements of iATVA [6].

The IVC/SVC flow ratios are kept almost same, and a venous pressure level of 11.4 mmHg (pediatric) and 12.1 mmHg (adult) was logged at a net venous assist of 2 to 3 mmHg (Figure 71). Example per pulse measurements with and without iATVA are provided in Table 10. Pulsatile amplitudes are given in parenthesis.

Table 10: Sample hemodynamic measurements obtained during the pulsatile single-ventricle mock-loop tests of P3.

	TCPC state		TCPC + iATVA	
	Pediatric	Adult	Pediatric	Adult
SVC flow rate, lt/m	1.29 (0.005)	1.78 (0.002)	1.03 (0.0015)	1.65 (0.001)
IVC flow rate, lt/m	2.2 (0.005)	3.24 (0.0035)	1.52 (0.0075)	2.15 (0.0025)
Aortic pressure, mmHg	86.1 (18)	96.2 (28)	86.1 (17)	98.1 (31)
Venous pressure, mmHg	14.0 (0.5)	14.4 (1.1)	11.4 (0.3)	12.1 (0.4)
PA pressure—pump outlet, mmHg	–	–	14.1 (0.35)	14.2 (0.65)

Figure 72 depicts the venous pump flow and venous pressure head characteristics for iATVA prototype 2 (top chart) and prototype 3 (bottom chart) gotten from the pulsatile single-ventricle mock-loop tests. Mean values of pulsatile waveforms are shown for both pediatric (3.5 lt/m) and adult (5 lt/m) flow conditions after the iATVA is introduced into the single-ventricle circulation.

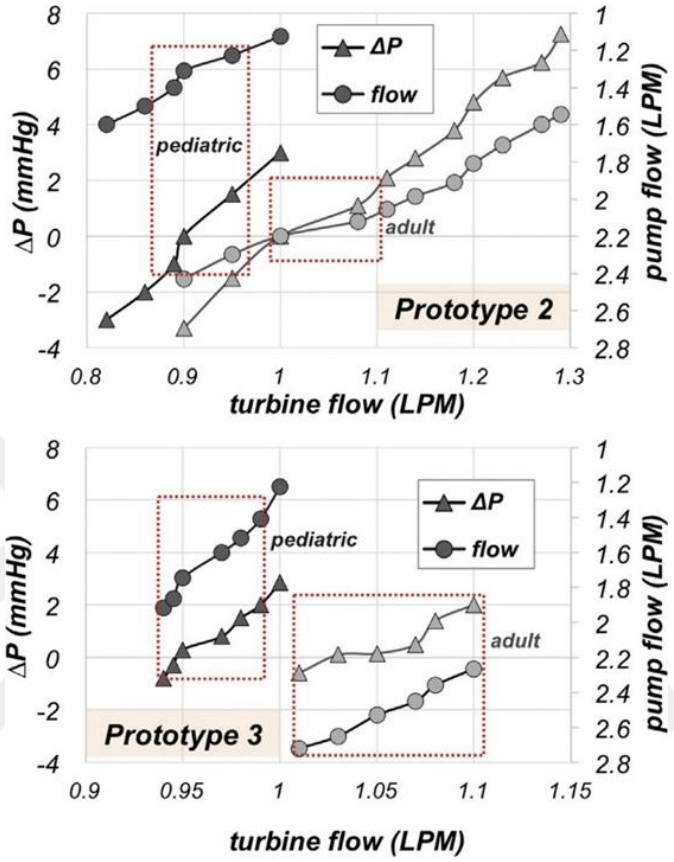

Figure 72: Pulsatile performance graph for iATVA (P2 and P3)[6].

The decrease in arterial pressure can also be regulated physiologically by increasing the cardiac output (rising the heart rate and stroke volume), which is also tested in our mock-up circuit. In this experiment, the iATVA was stopped using a thin wire to represent the TCPC state–shunt while the flow keeps passing through it. Removal of the wire allowed instantaneous switching TCPC + iATVA configuration without any alteration in aortic pressure since the turbine shunt is active nonetheless generating no power due to the wire catheter at the TCPC state–shunt. Initially, the TCPC state was created as in Table 10, and afterward the iATVA

device with the thin wire that halts the rotation was placed. The halt of the device decreased the systemic pressure, which was set back to the initial TCPC state by raising the stroke volume (instead of systemic resistance). Exclusion of the wire catheter caused the TCPC + iATVA hemodynamics without altering the stroke volume where the generated turbine power is now transferred to the pump side without restrictions, and venous pressure decline was recorded. This protocol was repeated with 3 different stroke volumes. These experiments indicate a better performance where the IVC pressure was reduced up to 8 mmHg as predicted (see Table 11). The table shows the results of prototype 3 at 70 bpm heart rate which mimics the pediatric physiological. Mean and pulsatile amplitudes (in parenthesis) are shown in Table 11.

Table 11: Summary of hemodynamic measurements obtained during the pulsatile mock-up single-ventricle flow loop experiments

	TCPC state–shunt		*TCPC + iATVA*		
Stroke column, mL	60	67	*60*	*67*	*51*
SVC flow rate, lt/m	1.1 (0.006)	1.1 (0.002)	*1.02 (0.001)*	*1.11 (0.01)*	*0.88 (0.002)*
IVC flow rate, lt/m	2.16 (0.001)	2.16 (0.002)	*2.17 (0.001)*	*2.27 (0.002)*	*1.7 (0.002)*
Aortic pressure, mmHg	94 (13)	114 (18)	*96 (15)*	*114 (19)*	*71 (13)*
Venous pressure, mmHg	18.6 (1.1)	16.6 (1.0)	*10.8 (0.8)*	*11.5 (0.8)*	*10.5 (0.8)*
PA pressure–pump outlet, mmHg	13.4 (0.9)	9.8 (0.7)	*12.2 (0.8)*	*12.9 (1.2)*	*12.0 (0.6)*

While altering the CO over stroke volume, a minor rise in venous pressure did not alter the amount of pressure decrease assisted by the iATVA system. Likewise, iATVA prototypes (P2 and P3) were tested at various turbine flow rates and the corresponding mean hemodynamic values are reported in Figure 72. A

higher venous pressure decrease at IVC (pump inlet) was achieved with an increased aortic steal for both adult and pediatric conditions. However, venous pressure rise is also achievable with a turbine flow of 0.9 lt/m for the evaluated prototypes.

Turbine and pump sides of iATVA are not separated entirely due to the leakage around and inside the bearing. The flow leakage from the turbine side (high pressure) to the pump side (low pressure) becomes substantial between 0.2 to 0.4 lt/m, which worsens the turbine efficiency dramatically. The highest head pressure generation at the design operating points (2 mmHg at 0.98 lt/m for pediatric - 2 mmHg at 1.1 lt/m for an adult) was achieved with the prototype P3 which has 12 turbine blades. This hydraulic performance is equal to the Fontan pumps presented in the literature (Table 12). Figure 73 compares all 3 iATVA prototypes over the impeller speed which proves the enhancement as the design is advanced.

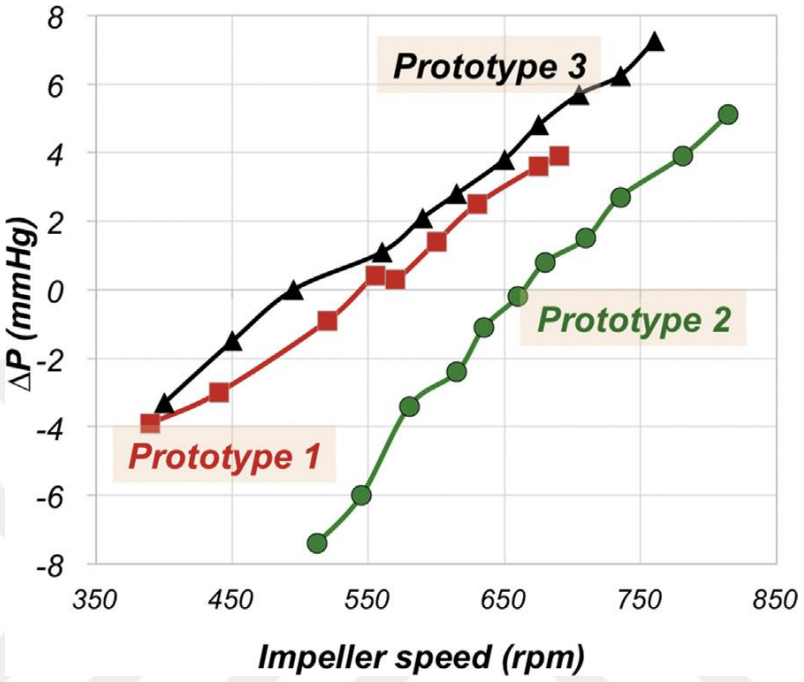

Figure 73: Comparison of All iATVA prototypes[6].

Effect of Rotational Speed

Thee impeller rpm was perceived to be a significant indication of system performance as observed in mock-loop tests. For the iATVA (prototype 3), an aortic steal range of 0.95 to 1.35 lt/m is in a good agreement with the adult hemodynamic conditions (see Figure 74). In this circumstance, the IVC flow rate differs between 2.4 and 1.5 lt/m and the SVC flow rate was between 1.6 and 2.6 lt/m. The impeller rpm was around 450 rpm at 1 lt/m turbine flow rate in 60%IVC and 40%SVC ratio for physiological values. Reduction of IVC flow leads to an increase in impeller speed at higher turbine inflow rates. A 10% rise in turbine flow rate leads to a 20% change in impeller speed. These results indicate that a dual

support pump configuration (IVC/SVC) is a more real-world option than IVC-only support, which is considered for future iATVA prototypes.

Figure 74 shows the adult Fontan hemodynamic conditions on mock-loop tests with iATVA along with the off-design operating conditions spanning 80 to 150 mmHg MAP. Only results of prototype 3 are shown as trends were comparable for all iATVA prototypes. Mean venous pressure rise, impeller speed, and turbine flow rates are shown.

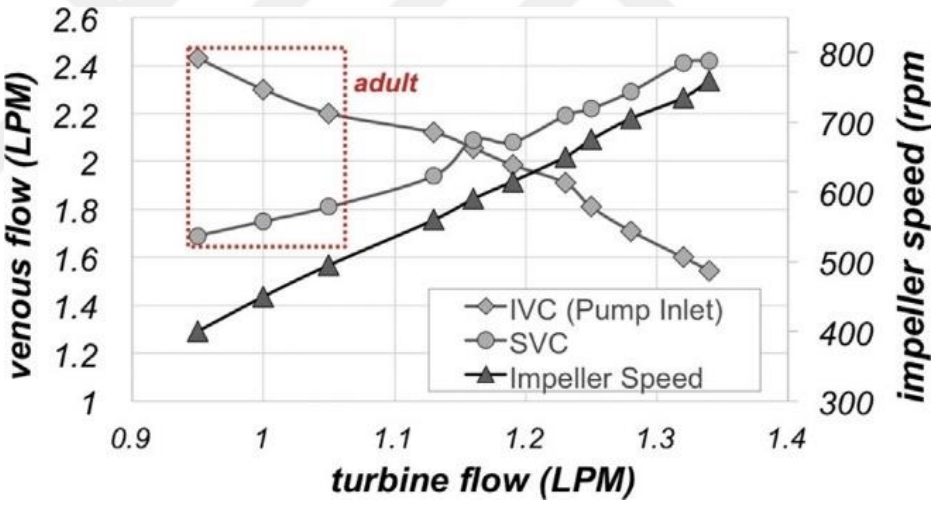

Figure 74: Hydraulic performance of iATVA P3[6].

Comparative Performance of iATVA Prototypes

Figure 73 compares all 3 iATVA prototypes. Compared with P1 (6 blades and 3-lt/m pump flow rate), P2 (6 blades and 1.8-lt/m pump flow rate) caused a meaningfully lower pressure generation due to this design enabling higher IVC flow rates. Similarly, the 12 bladed version P3 gave some enhancement. Overall, pressure rise of 1 mmHg is recorded between the prototypes P1 and P3 designs. Based on the in vitro experiments using the single ventricle pulsatile mock-loop, all 3 prototypes indicated a venous pressure decrease at a relatively low impeller rotation speeds of 500 (P3), 550 (P1), and 660 (P2). P1 and P3 deliver roughly a 4-mmHg pressure difference at 660 rpm, while the same differential pressure is found at a speed of 800 rpm for the prototype 2. These pressure differences agree with the steady-state performance gotten for almost a 1-lt/m turbine flow rate. The negative venous pressure effect was also detected when the iATVA turbine does not receive enough hydraulic power to generate sufficient torque.

7.3 Discussion

Transfer of the external power needed to run the mechanical circulatory assist devices is a difficult engineering challenge. Infections instigated by the percutaneous driveline are a significant complication of all totally implanted mechanical assist devices. The definitive solution is the transcutaneous energy transfer (TET) which energizes the device wirelessly [130]. However, this approach includes thermal tissue damage and unintended electromagnetic neural stimulation[131]. The projected iATVA device answers the need for external drive

power through a novel idea that principally suits single-ventricle patients because of its passively controlled nature. Based on our current investigations with iATVA, this system does not demand further turbine power to drive the venous pump for supporting a typical Fontan circulation. Depending on the physiology of the patient, aortic steal through these shunts can reach up to 50% of the CO[132]. So if required, iATVA can utilize higher aortic steals. Likewise, preload can increase up to 30% in Fontan fenestration patients. Besides, fenestration systems and shunts are causing an energy waste and oxygen desaturation without any hemodynamic benefits. Contrary to that, the aortic steal of iATVA is carried to the atrium without any oxygen desaturation which reduces the risk of stroke. Although stealing a portion of the aortic flow to energize the turbine can be considered as an additional load for the single ventricle, patients are living with an unoperated univentricular heart in which pulmonary flow is well endured up until 70 years of age[133].

Assuming the systemic-pulmonary shunts as the source of harvestable energy, new arterial-to-venous pathway intended to support the SVC flow at the Glenn stage can be considered[134]. In this scheme, high-pressure aortic flow increases the venous pressure levels however due to the lack of any turbine work, its performance significantly limited. The assisted Glenn shunt technique also steals a comparable amount of aortic blood ranging from 15% to 28%. Consequently, the iATVA system is a novel alternative to pediatric systemic

shunts by harvesting useful energy from the aortic and venous pressure difference, with no oxygen reduction.

This experimental study demonstrates the viability of the iATVA system. Nonetheless, significant design enhancements are probable for future prototypes. Possibly, the final version of implanted iATVA devices will be meaningfully different which will be used during future in-vivo tests. For instance, a double-inlet double-outlet configuration will be meaningful to support both IVC and SVC. This arrangement would advance performance as seen in Figure 65 (Configuration C3, approximating a 4-way TCPC). Assumed the passive operation of the iATVA system, utilizing this alternative arrangement, instead of the conventional TCPC, an ''iATVA assisted-TCPC'' can be implanted directly during the third stage completion surgery. Design of the iATVA device for Fontan circulation is restricted by the turbine design and turbine operating conditions which is a challenging turbomachinery problem. A more comprehensive volute design and volute-impeller interaction investigation are required for achieving a superior efficiency. Considering the lately developed centrifugal pumps are having higher in rotational speed and smaller size, there are expectations to advance a new centrifugal pump with superior performance even under very low specific speed conditions [128].

Moreover, the iATVA device is the only blood turbine seen in the literature to the best of our knowledge. Hemolytic performance of the system stands as an interesting research problem, which required to be compared with the conventional heart assist systems. It is predictable that the hemolytic performance of the turbine side would be meaningfully dissimilar than the pump side. The iATVA device might need a high dosage of anticoagulants considering it joins both the venous and aortic circulations. Theoretical and experimental performance is different due to the hydraulic and mechanical losses. Consequently, a new prototype that utilizes a magnetic coupling and low friction ceramic bearings were designed and developed in our laboratory which separates two sides and avoids the leakage from the turbine side to the pump side. The flat hydraulic performance estimations of the iATVA device (Figure 64) and its passive operation fashion prove it beneficial for off-design operation, compared with the conventional heart assist devices. For instance, the physical effort would cause a positive consequence on iATVA function due to the increase in CO and systemic pressure rise. One primary failure mode is predicted to be the obstruction of the blood pathway inside the aortic flow channel due to the low flow rate and narrow flow path. In such a case, the patient would need a high dosage anticoagulation administration. This failure mode was tested by fixing the turbine impeller where the pump impeller did not create a significant obstruction to the IVC flow as the TCPC state was observed. Future research will show if the long-term use of the iATVA system would substitute the traditional methods to reduce the workload on the single

ventricle and eliminate the need of venous remodeling. Thus, ideal iATVA implantation timing might not be the end stage of Fontan failure where the pulmonary vascular resistance is extraordinarily high, and CO required to operate the turbine is considerably low. In its place, iATVA implantation might be considered immediately after a raised SVP is identified. Because of its relatively larger size, the present device would fit in children more massive than 20 kg. Smaller-size devices are also hypothetically viable as presented in Figure 75 assuming a 50% hydraulic efficiency, 0.5 lt/m aortic steal and 3.5 lt/m IVC flow rate.

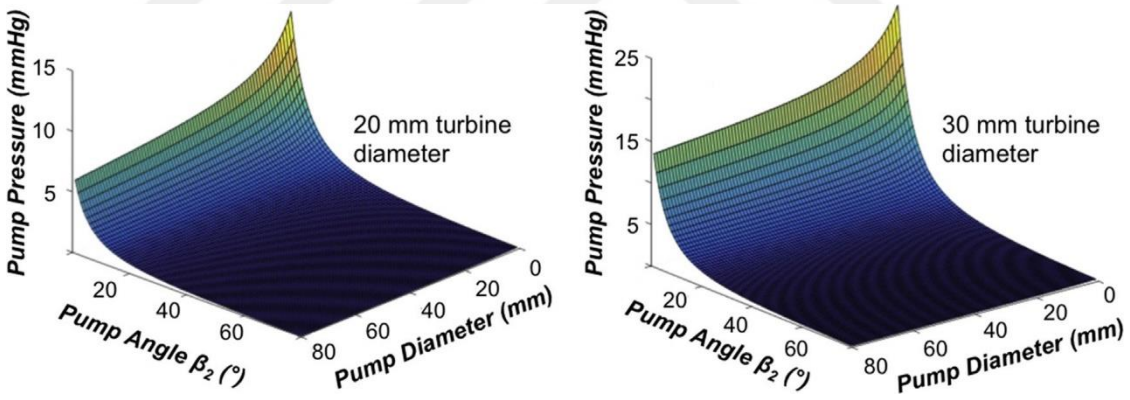

Figure 75: Performance characteristics of the iATVA system estimated for compact turbine impeller sizes of 20 and 30 mm[6].

Finally, it is proven that all parts of the iATVA system are producible with rapid prototyping, promising a cost-efficient and customizable device alternative for the individual patient. Experiments showed that a turbine impeller causes a slight venous pulsatility due to the cardiac cycle. Future designs might explicitly

target to advance pulsatile action by creating stiffer outlets, which mimics the natural circulation and might cause the healthy growth of pulmonary artery.

Table 12: Average operating points of existing cavopulmonary support devices are compared with the new iATVA prototype[20].

Pump design	Venous pressure drop, mmHg	Flow rate, lt/m	Rotation Speed, Rpm	Notes
Propeller[80]	5 to 50	0.5 to 3.5	5000 to 7000	Hydraulic in vitro
Axial[71]	5 to	2	1700 to 4500	Failing Fontan
Axial[78]	2.4	3.7	No information	
No impeller[75]	5 to 20	0 to 5	0 to 7000	Dual IVC/SVC support, Mock-up flow loop
Berlin heart[81]	No information	3.8	80 Strokes/min	Hypoplastic left heart
Centrifugal[82]	10	No information	No information	
Axial [83]	12	3.1 to 1.2	18,000 to 24,000	Piglet model
Axial [84]	7	4.6	10,000	Jarvik VAD
iATVA, present study	***5.7***	***5***	***705***	***IVC support***

CONCLUSION

8.1 Concluding Remarks – iHeart VAD

One of the two main aims of this thesis is to explain the development and validation procedures of a novel LVAD. The optimization study of the iHeart VAD was started with extensive CFD analysis on the impeller and volute geometries. Best performing models were subjected to hydraulic tests. The literature review of this work gives comprehensive information about state of the art VAD systems, development methodology and the design criteria of LVADs.

The VAD geometry has been investigated and characterized in-silico. Numerous impeller and volute formations were tested numerically and validated physically. The CFD models were utilized to estimate the hydraulic performance criteria like the pressure, flow rate, flow profile and the hydromechanical efficiency. The hemolytic performance was also analyzed for investigating and reducing the shear-induced hemolysis. Afterward, numerous impeller and volute couples were manufactured with 3D printing to achieve hydrodynamic experiments for the confirmation of in-silico findings. This optimization procedure gave relative information about the influence of varying VAD geometries on the performance. The analysis validated the final prototype, the Istanbul Heart VAD (iHeart VAD), which provided an excellent hydraulic performance while reducing the shear-induced hemolysis.

The final prototype of Istanbul Heart VAD (iHeart VAD) was tested with human blood for investigating the hemolytic performance. Ti-6Al-4V made prototype was manufactured and experimented according to ASTM F1841–97 standards. The in vitro tests showed adequate hemolytic performance similar to commercial VADs concerning the hemolysis index, plasma free hemoglobin amount and, hematocrit level.

Preliminary acute in-vivo experiments have also been performed in a porcine model proving the capacity to provide promising results in terms of high hydraulic performance and low hemolysis. The study also has a phenomenal status that a heart pump is tested on an animal for the first time in the history of Turkey. However, the in vivo study reported in this thesis is just an initial and acute evaluation of the performance of Istanbul Heart VAD (iHeart VAD). Further acute in vivo evaluations and chronical tests are required yet to prove the feasibility of the device. Longer duration acute tests are planned to be performed soon.

Mock circulatory loop mimics the dynamic flow conditions of the healthy and failing heart. Therefore, it decreases the number of in-vivo which are required for dynamic validation of the pump. iHeart VAD is required to be tested in a mock-loop for controller design, artificial pulse and dynamic characterization of the pump. The design also desired to be modified as a magnetically levitated ECMO device in future. The design of the final prototype must be modified to achieve more competitive miniature size by developing an embedded DC motor. For upcoming experiments, the improved pump prototype will be manufactured following the CE

standards while designing the electronics, motor, sealing, connectors for extensive animal and clinic experiments.

8.2 Concluding Remarks - iATVA

Another aim of this thesis was to propose a novel mechanical assist device for Fontan patients that do not need external drive power and therefore a percutaneous powerline. Feasibility of this concept is proven with turbomachinery approach and single-ventricle mock-loop tests conducted with evolving prototypes. Compared to the systemic shunts, the iATVA device needs a slight aortic steal and utilizes this power to provide the required venous pressure decrease. Further improvements are required for present prototypes for addressing the problems like leakage, off-design action, placement of the turbine drainage, and creating a pulsatile action. This study offered exciting research possibilities for the cardiovascular device community. Therefore, the iATVA device has the capacity to converse the harmful effects of Fontan circulation passively and is anticipated to lead to more innovations in the management of congenital heart diseases. The implantation timing of iATVA device is critical to reducing patient morbidity as well as mortality. Since the third-stage Fontan completion is characteristically achieved at roughly 2 to 3 years of age, the existing volume of the thoracic cavity for device insertion might yet be insufficient. Consequently, clinicians might study a new fourth-stage operation for implanting the iATVA.

Countless Fontan patients who had a modified Fontan operation eventually progress a low CO condition related to systemic venous congestion resilient to drug therapy. Problematic atriopulmonary connection configurations and flow path stenosis might then be treated via surgical or catheterized TCPC adaptation which provides nearly 1 to 3 mmHg enhancements in SVP which is comparable to the benefit that is provided by a conventional Fontan venous assist device or to the iATVA pump [135]. There is also a minor subclass of ''real'' failed Fontan patients with elevated PVR, for whom the only treatment possibility is heart transplantation. There is also the opportunity that the iATVA device might heal this patient group in advance before the terminal failed-state is reached, which needs further development and examination.

BIBLIOGRAPHY

[1] N. Farré *et al.*, "Real world heart failure epidemiology and outcome: A population-based analysis of 88,195 patients," *PLoS One*, vol. 12, no. 2, pp. 1–13, 2017.

[2] P. Ponikowski *et al.*, "2016 ESC Guidelines for the diagnosis and treatment of acute and chronic heart failure," *Eur. Heart J.*, vol. 37, no. 27, p. 2129–2200m, 2016.

[3] J. K. Kirklin and D. C. Naftel, "Mechanical circulatory support: registering a therapy in evolution.," *Circ. Heart Fail.*, vol. 1, no. 3, pp. 200–205, 2008.

[4] F. Fontan and E. Baudet, "Surgical repair of tricuspid atresia," pp. 240–248, 1971.

[5] K. N. Pundi *et al.*, "40-Year Follow-Up after the Fontan Operation Long-Term Outcomes of 1,052 Patients," *J. Am. Coll. Cardiol.*, vol. 66, no. 15, pp. 1700–1710, 2015.

[6] K. Pekkan *et al.*, "In vitro validation of a self-driving aortic-turbine venous-assist device for Fontan patients," *J. Thorac. Cardiovasc. Surg.*, vol. 156, no. 1, p. 292–301.e7, 2018.

[7] P. Ponikowski *et al.*, "Heart failure: Preventing disease and death worldwide," *Eur. Soc. Cardiol.*, vol. 373, no. 9667, pp. 941–955, 2014.

[8] E. J. Benjamin, M. J. Blaha, S. E. Chiuve, and M. Cushman, *Heart Disease and Stroke Statistics—2017 Update*, vol. 135, no. 10. 2017.

[9] A. Cassar, D. R. Holmes Jr, C. S. Rihal, and B. J. Gersh, "Chronic coronary artery disease: diagnosis and management," in *Mayo Clinic Proceedings*, 2009, vol. 84, no. 12, pp. 1130–1146.

[10] P. A. Heidenreich *et al.*, "Forecasting the future of cardiovascular disease in the United States a policy statement from the American heart association," *Circulation*, vol. 123, no. 8, pp. 933–944, 2011.

[11] E. Wilkins, L. Wilson, K. Wickramasinghe, P. Bhatnagar, M. Rayner, and N. Townsend, "European Cardiovascular Disease Statistics 2017 edition," *Eur. Hear. Netw.*, 2017.

[12] N. YARDIM and Y. ERKOÇ, "Türkiye'de Bulaşıcı Olmayan Hastalıklar ve Risk Faktörleri ile Mücadele Politikaları," *Bakanl. SAĞLIK MÜDÜRLÜĞÜ, TEMEL SAĞLIK HİZMETLERİ GENEL MÜDÜRLÜĞÜ*, no. 809, 2011.

[13] Health Consumer Powerhouse, *Euro Heart Index 2016*. 2016.

[14] M. Figueroa and J. Peters, "Congestive Heart Failure: Diagnosis, Pathophysiology, Therapy, and Implications for Respiratory Care," *Respir. Care*, pp. 403–412, 2006.

[15] C. Angelika Lindinger *et al.*, "Prevalence of Congenital Heart Defects in Newborns in Germany: Results of the First Registration Year of the PAN Study Pr ä valenz angeborener Herzfehler bei Neugeborenen in Deutschland: Ergebnisse des ersten Geburtsjahrganges (Juli 2006 bis Juni 2007)," *Klin Padiatr Klin Padiatr Preval. Congenit. Hear. Defects Newborns Ger. … Klin Padiatr*, vol. 222, no. 222, pp. 321–326, 2010.

[16] M. D. Reller, M. J. Strickland, T. Riehle-Colarusso, W. T. Mahle, and A. Correa, "Prevalence of Congenital Heart Defects in Metropolitan Atlanta, 1998-2005," *J. Pediatr.*, vol. 153, no. 6, pp. 807–813, 2008.

[17] J. I. E. Hoffman and S. Kaplan, "The incidence of congenital heart disease," *J. Am. Coll. Cardiol.*, vol. 39, no. 12, pp. 1890–1900, 2002.

[18] M. Jorgensen, E. Mcpherson, C. Zaleski, P. Shivaram, and C. Cold, "Stillbirth: The heart of the matter," *Am. J. Med. Genet. Part A*, vol. 164, no. 3, pp. 691–699, 2014.

[19] P. W. O'Leary, "Prevalence, clinical presentation and natural history of patients with single ventricle," *Prog. Pediatr. Cardiol.*, vol. 16, no. 1, pp. 31–38, 2002.

[20] K. Pekkan *et al.*, "In vitro validation of a self-driving aortic-turbine venous-assist device for Fontan patients," *J. Thorac. Cardiovasc. Surg.*, 2018.

[21] C. R. Broda, D. A. Taylor, and I. Adachi, "Progress in experimental and clinical subpulmonary assistance for Fontan circulation," *J. Thorac. Cardiovasc. Surg.*, no. Video 1, 2018.

[22] O. Demir, E. Biyikli, I. Lazoglu, and S. Kucukaksu, "Design of a centrifugal blood pump: Heart Turcica Centrifugal," *Artif. Organs*, vol. 35, no. 7, pp. 720–725, 2011.

[23] Ç. Öztürk, "Development of a Novel Centrifugal Left Ventricular Assist Device and the First In Vivo Study: Istanbul Heart VAD," Koç University, 2018.

[24] İ. B. Aka, "Design Of A Platform For Physical Performance Testing Of An Axial-Flow Left-Ventricular Assist Device," Bahçeşehir University, 2014.

[25] K. Toptop and K. A. Kadipasaoglu, "Design and Numeric Evaluation of a Novel Axial-Flow Left Ventricular Assist Device," *ASAIO J.*, vol. 59, no. 3, pp. 230–239, 2013.

[26] W. LM, G. MH, G. JH, and Jr., "Temporary arrest of the circulation to the central nervous system: Ii. pathologic effects," *Arch. Neurol. Psychiatry*, vol. 43, no. 5, pp. 961–986, May 1940.

[27] W. LM, G. MH, G. JH, and Jr., "Temporary arrest of the circulation to the central nervous system: I. physiologic effects," *Arch. Neurol. Psychiatry*, vol. 43, no. 4, pp. 615–634, Apr. 1940.

[28] D. J. Kozik and M. D. Plunkett, "Mechanical circulatory support," vol. 7, no. 1, pp. 50–63, 2011.

[29] D. N. Helman and E. A. Rose, "Progress in Cardiovascular Diseases," vol. 43, no. 1, pp. 1–4, 2000.

[30] A. Kantrowitz *et al.*, "Initial clinical experience with intraaortic balloon pumping in cardiogenic shock," *JAMA*, vol. 203, no. 2, pp. 113–118, Jan. 1968.

[31] D. Liotta, D. W. Wieting, C. W. Hall, J. J. Chidoni, and M. E. DeBakey, "In vitro and in vivo flow studies in blood pumps," *ASAIO J.*, vol. 13, no. 1, pp. 280–

287, 1967.

[32] K. Bourque *et al.*, "HeartMate III: pump design for a centrifugal LVAD with a magnetically levitated rotor," *Asaio J*, vol. 47, no. 4, pp. 401–405, 2001.

[33] M. E. DeBakey, "Left ventricular bypass pump for cardiac assistance. Clinical experience," *Am. J. Cardiol.*, vol. 27, no. 1, pp. 3–11, 1971.

[34] A. B. Weisse, "Cardiac Surgery," vol. 38, no. 5, 2011.

[35] J. E. Hall, *Guyton and Hall Textbook of Medical Physiology: Enhanced E-book*. Elsevier Health Sciences, 2010.

[36] T. J. Thom and W. B. Kannef, "Congestive Heart Failure Epidemiology and Cost of Illness," vol. 1, no. 2, pp. 75–83, 1997.

[37] J. McMurray, M. Komajda, S. Anker, and R. Gardner, "23 Heart Failure: Epidemiology, Pathophysiology and Diagnosis," 2006.

[38] M. Gewillig, "The Fontan circulation," *Heart*, vol. 91, no. 6, pp. 839–846, 2005.

[39] J. Rychik, "The Relentless Effects of the Fontan Paradox," *Semin. Thorac. Cardiovasc. Surg. Pediatr. Card. Surg. Annu.*, vol. 19, no. 1, pp. 37–43, 2016.

[40] A. Hauck, N. Porta, S. Lestrud, and S. Berger, "The Pulmonary Circulation in the Single Ventricle Patient," *Children*, vol. 4, no. 8, p. 71, 2017.

[41] W. W. L. Glenn, "Circulatory Bypass of the Right Side of the Heart," *N. Engl. J. Med.*, vol. 259, no. 3, pp. 117–120, 1958.

[42] A. K. Pridjian *et al.*, "Usefulness of the Bidirectional Glenn," pp. 959–962.

[43] Y. Kawashima, S. Kitamura, H. Matsuda, Y. Shimazaki, S. Nakano, and H. Hirose, "Total cavopulmonary shunt operation in complex cardiac anomalies. A new operation," *J. Thorac. Cardiovasc. Surg.*, vol. 87, no. 1, p. 74—81, Jan. 1984.

[44] S. N. Birewar, "Dual-Axial Blood Pump Mechanical Circulatory Support for Fontan Patients," 2016.

[45] The Children's Heart Clinic, "Modified Fontan Procedure," 2012. [Online].

Available: http://www.childrensheartclinic.org/ProcedureIllustrations/Fontan.pdf. [Accessed: 01-Jul-2018].

[46] D. H. Kafagy *et al.*, "Design of axial blood pumps for patients with dysfunctional fontan physiology: Computational studies and performance testing," *Artif. Organs*, vol. 39, no. 1, pp. 34–42, 2015.

[47] T. M. M. H. de By *et al.*, "The European Registry for Patients with Mechanical Circulatory Support (EUROMACS) of the European Association for Cardio-Thoracic Surgery (EACTS): Second report," *Eur. J. Cardio-thoracic Surg.*, vol. 53, no. 2, pp. 309–316, 2018.

[48] J. K. Kirklin *et al.*, "Seventh INTERMACS annual report: 15,000 patients and counting," *J. Hear. Lung Transplant.*, vol. 34, no. 12, pp. 1495–1504, 2015.

[49] J. K. Kirklin *et al.*, "Eighth annual INTERMACS report: Special focus on framing the impact of adverse events," *J. Hear. Lung Transplant.*, vol. 36, no. 10, pp. 1080–1086, 2017.

[50] R. C. Starling, "Advanced heart failure: Transplantation, LVADs, and beyond," *Cleve. Clin. J. Med.*, vol. 80, no. 1, pp. 33–40, 2013.

[51] N. Moazami *et al.*, "Lessons Learned From the First Fully Magnetically Levitated Centrifugal LVAD Trial in the United States: The DuraHeart Trial," *Ann. Thorac. Surg.*, vol. 98, no. 2, pp. 541–547, 2014.

[52] A. Prinzing, U. Herold, A. Berkefeld, M. Krane, R. Lange, and B. Voss, "Left ventricular assist devices-current state and perspectives," *J. Thorac. Dis.*, vol. 8, no. 8, pp. E660–E666, 2016.

[53] J. K. Kirklin *et al.*, "Fifth INTERMACS annual report: risk factor analysis from more than 6,000 mechanical circulatory support patients," *J. Hear. Lung Transplant.*, vol. 32, no. 2, pp. 141–156, 2013.

[54] S. A. S. Von Ruden, M. A. Murray, J. L. Grice, A. K. Proebstle, and K. J. Kopacek, "The pharmacotherapy implications of ventricular assist device in the patient with end-stage heart failure," *J. Pharm. Pract.*, vol. 25, no. 2, pp.

232–249, 2012.

[55] H. Hoshi, T. Shinshi, and S. Takatani, "Third-generation blood pumps with mechanical noncontact magnetic bearings," *Artif. Organs*, vol. 30, no. 5, pp. 324–338, 2006.

[56] H. G. Wood, A. L. Throckmorton, A. Untaroiu, and X. Song, "The medical physics of ventricular assist devices," *Reports Prog. Phys.*, vol. 68, no. 3, p. 545, 2005.

[57] J. R. Miller and P. Eghtesady, "Ventricular assist device use in congenital heart disease with a comparison to heart transplant," *J. Comp. Eff. Res.*, vol. 3, no. 5, pp. 533–546, 2014.

[58] L. E. Samuels, E. C. Holmes, P. Garwood, and F. Ferdinand, "Initial experience with the abiomed AB5000 ventricular assist device system," *Ann. Thorac. Surg.*, vol. 80, no. 1, pp. 309–312, 2005.

[59] M. S. Slaughter *et al.*, "Results of a multicenter clinical trial with the Thoratec Implantable Ventricular Assist Device**Thoratec Corporation, Pleasanton, Calif.," *J. Thorac. Cardiovasc. Surg.*, vol. 133, no. 6, 2007.

[60] K. Mizuguchi *et al.*, "Development of an axial flow ventricular assist device: In vitro and in vivo evaluation," *Artif. Organs*, vol. 19, no. 7, pp. 653–659, 1995.

[61] G. P. Noon and M. Loebe, "Current status of the MicroMed DeBakey Noon Ventricular Assist Device.," *Tex. Heart Inst. J.*, vol. 37, no. 6, pp. 652–653, 2010.

[62] B. P. Griffith *et al.*, "HeartMate II left ventricular assist system: from concept to first clinical use," *Ann. Thorac. Surg.*, vol. 71, no. 3, pp. S116–S120, 2001.

[63] M. P. Siegenthaler *et al.*, "Mechanical reliability of the Jarvik 2000 Heart," *Ann. Thorac. Surg.*, vol. 81, no. 5, pp. 1752–1759, 2006.

[64] S. Westaby *et al.*, "First permanent implant of the Jarvik 2000 Heart," *Lancet*, vol. 356, no. 9233, pp. 900–903, 2000.

[65] R. Hetzer *et al.*, "First experiences with a novel magnetically suspended axial flow left ventricular assist device," *Eur. J. Cardio-thoracic Surg.*, vol. 25, no. 6,

pp. 964–970, 2004.

[66] K. E. Griffith, E. Jenkins, and F. D. Pagani, "First American experience with the Terumo DuraHeart™ left ventricular assist system," *Perfusion*, vol. 24, no. 2, pp. 83–89, 2009.

[67] E. Tuzun *et al.*, "In vivo evaluation of the HeartWare centrifugal ventricular assist device," *Texas Hear. Inst. J.*, vol. 34, no. 4, pp. 406–411, 2007.

[68] D. J. Farrar, K. Bourque, C. P. Dague, C. J. Cotter, and V. L. Poirier, "Design features, developmental status, and experimental results with the Heartmate III centrifugal left ventricular assist system with a magnetically levitated rotor.," *ASAIO J.*, vol. 53, no. 3, pp. 310–315, 2007.

[69] R. K. Woods, N. S. Ghanayem, M. E. Mitchell, S. Kindel, and R. A. Niebler, "Mechanical Circulatory Support of the Fontan Patient," *Semin. Thorac. Cardiovasc. Surg. Pediatr. Card. Surg. Annu.*, vol. 20, pp. 20–27, 2017.

[70] M. R. De Leval, "The Fontan circulation: What have we learned? What to expect?," *Pediatr. Cardiol.*, vol. 19, no. 4, pp. 316–320, 1998.

[71] F. G. Lacour-Gayet *et al.*, "An Artificial Right Ventricle for Failing Fontan: In Vitro and Computational Study," *Ann. Thorac. Surg.*, vol. 88, no. 1, pp. 170–176, 2009.

[72] R. B. Medvitz, D. A. Boger, V. Izraelev, G. Rosenberg, and E. G. Paterson, "Computational fluid dynamics design and analysis of a passively suspended tesla pump left ventricular assist device," *Artif. Organs*, vol. 35, no. 5, pp. 522–533, 2011.

[73] D. Wang, M. Plunkett, J. Lynch, X. Zhou, C. Ballard-Croft, and J. B. Zwischenberger, "Wang-zwische double-lumen cannula leads to total cavopulmonary support in a failing fontan sheep model," *Ann. Thorac. Surg.*, vol. 91, no. 6, pp. 1956–1960, 2011.

[74] D. Wang *et al.*, "A paired membrane umbrella double-lumen cannula ensures consistent cavopulmonary assistance in a Fontan sheep model," *J. Thorac. Cardiovasc. Surg.*, vol. 148, no. 3, pp. 1041–1047, 2014.

[75] M. D. Rodefeld *et al.*, "Cavopulmonary assist for the univentricular Fontan circulation: Von Kármán viscous impeller pump," *J. Thorac. Cardiovasc. Surg.*, vol. 140, no. 3, pp. 529–535, 2010.

[76] G. M. Pantalos, S. C. Koenig, K. J. Gillars, G. A. Giridharan, and D. L. Ewert, "Characterization of an adult mock circulation for testing cardiac support devices," *ASAIO J.*, vol. 50, no. 1, pp. 37–46, 2004.

[77] R. Wang *et al.*, "Initial experience with the development and numerical and in vitro studies of a novel low-pressure artificial right ventricle for pediatric fontan patients," *ASAIO J.*, vol. 52, no. 6, pp. 682–692, 2006.

[78] M. D. Rodefeld *et al.*, "Cavopulmonary Assist: Circulatory Support for the Univentricular Fontan Circulation," *Ann. Thorac. Surg.*, vol. 76, no. 6, pp. 1911–1916, 2003.

[79] A. L. Throckmorton *et al.*, "Numerical, hydraulic, and hemolytic evaluation of an intravascular axial flow blood pump to mechanically support fontan patients," *Ann. Biomed. Eng.*, vol. 39, no. 1, pp. 324–336, 2011.

[80] A. L. Throckmorton, K. K. Ballman, C. D. Myers, S. H. Frankel, J. W. Brown, and M. D. Rodefeld, "Performance of a 3-Bladed Propeller Pump to Provide Cavopulmonary Assist in the Failing Fontan Circulation," *Ann. Thorac. Surg.*, vol. 86, no. 4, pp. 1343–1347, 2008.

[81] M. W. A. Chu *et al.*, "Berlin Heart Ventricular Assist Device in a Child With Hypoplastic Left Heart Syndrome," *Ann. Thorac. Surg.*, vol. 83, no. 3, pp. 1179–1181, 2007.

[82] C. D. Myers *et al.*, "Twenty-four hour cardiopulmonary stability in a model of assisted newborn Fontan circulation," *Ann. Thorac. Surg.*, vol. 81, no. 1, pp. 264–271, 2006.

[83] X. Wei *et al.*, "Mechanical Circulatory Support of a Univentricular Fontan Circulation with a Continuous Axial-Flow Pump in a Piglet Model," *ASAIO J.*, vol. 61, no. 2, pp. 196–201, 2015.

[84] G. Derk *et al.*, "Novel techniques of mechanical circulatory support for the

right heart and Fontan circulation," *Int. J. Cardiol.*, vol. 176, no. 3, pp. 828–832, 2014.

[85] R. S. R. Gorla and A. A. Khan, *Turbomachinery: Design and Theory*. CRC Press, 2003.

[86] S. A. Korpela, *Principles of Turbomachinery*. Wiley, 2012.

[87] C. E. Brennen, *Hydrodynamics of Pumps*. Cambridge University Press, 2011.

[88] J. ŠKORPÍK, "Classification of the turbomachines by the stream direction in relation to the axis of the shaft," *Turbomachine*, 2009. .

[89] J. González, J. Fernández, E. Blanco, and C. Santolaria, "Numerical Simulation of the Dynamic Effects Due to Impeller-Volute Interaction in a Centrifugal Pump," *J. Fluids Eng.*, vol. 124, no. 2, p. 348, 2002.

[90] L. E. Harris, "Some Factors in the Early Development of the Centrifugal Pump 1689 to 1851," *Trans. Newcom. Soc.*, vol. 28, no. 1, pp. 187–202, 1951.

[91] E. Humphrys, "On Surface Condensation in Marine Engines," *Proc. Inst. Mech. Eng.*, vol. 13, no. 1, pp. 99–124, 1862.

[92] A. A. Williams, "Pumps as turbines for low cost micro hydro power," *Renew. Energy*, vol. 9, no. 1–4, pp. 1227–1234, 1996.

[93] H.-P. Dickmann, T. Secall Wimmel, J. Szwedowicz, D. Filsinger, and C. H. Roduner, "Unsteady Flow in a Turbocharger Centrifugal Compressor: Three-Dimensional Computational Fluid Dynamics Simulation and Numerical and Experimental Analysis of Impeller Blade Vibration," *J. Turbomach.*, vol. 128, no. 3, p. 455, 2006.

[94] J. Galindo, P. Fajardo, R. Navarro, and L. M. García-Cuevas, "Characterization of a radial turbocharger turbine in pulsating flow by means of CFD and its application to engine modeling," *Appl. Energy*, vol. 103, pp. 116–127, 2013.

[95] C. Scheit, B. Karic, and S. Becker, "Effect of blade wrap angle on efficiency and noise of small radial fan impellers—a computational and experimental study," *J. Sound Vib.*, vol. 331, no. 5, pp. 996–1010, 2012.

[96] Y. W. Wong, W. K. Chan, and W. Hu, "Effects of tongue position and base circle diameter on the performance of a centrifugal blood pump," *Artif. Organs*, vol. 31, no. 8, pp. 639–645, 2007.

[97] H. Alemi, S. A. Nourbakhsh, M. Raisee, and A. F. Najafi, "Effect of the volute tongue profile on the performance of a low specific speed centrifugal pump," *Proc. Inst. Mech. Eng. Part A J. Power Energy*, vol. 229, no. 2, pp. 210–220, 2015.

[98] A. J. Stepanoff, *Centrifugal and axial flow pumps: theory, design, and application*. Wiley New York, 1957.

[99] M. Behbahani *et al.*, "A review of computational fluid dynamics analysis of blood pumps," *Eur. J. Appl. Math.*, vol. 20, no. 04, p. 363, 2009.

[100] A. Date, *Introduction to computational fluid dynamics*. 2005.

[101] K. H. Fraser, M. E. Taskin, B. P. Griffith, and Z. J. Wu, "The use of computational fluid dynamics in the development of ventricular assist devices.," *Med. Eng. Phys.*, vol. 33, no. 3, pp. 263–280, 2011.

[102] J. Tu, G. H. Yeoh, and C. Liu, *Computational Fluid Dynamics: A Practical Approach*. Elsevier Science, 2018.

[103] X. Song, A. L. Throckmorton, H. G. Wood, P. E. Allaire, and D. B. Olsen, "Transient and quasi-steady computational fluid dynamics study of a left ventricular assist device," *ASAIO J.*, vol. 50, no. 5, pp. 410–417, 2004.

[104] R. Biggs and G. Macfarlane, *Human blood coagulation and its disorders*. Blackwell Scientific Publications, 1962.

[105] P. B. Canham, "The minimum energy of bending as a possible explanation of the biconcave shape of the human red blood cell," *J. Theor. Biol.*, vol. 26, no. 1, pp. 61–81, 1970.

[106] M. Behbahani *et al.*, "A review of computational fluid dynamics analysis of blood pumps," *Eur. J. Appl. Math.*, vol. 20, no. 04, pp. 363–397, 2009.

[107] P. Constantin and C. Foias, *Navier-stokes equations*. University of Chicago Press, 1988.

[108] R. Temam, *Navier-Stokes equations: theory and numerical analysis*, vol. 343. American Mathematical Soc., 2001.

[109] L. Davidson, "An Introduction to Turbulence Models b Y," no. November, 2003.

[110] F. G. Schmitt, "About Boussinesq's turbulent viscosity hypothesis: historical remarks and a direct evaluation of its validity," *Comptes Rendus Mécanique*, vol. 335, no. 9–10, pp. 617–627, 2007.

[111] F. U. Guide, "Version 15, ANSYS," *Inc., April*, 2014.

[112] D. Wilcox, "C.(1998): Turbulence modeling for CFD." DCW Industries. 540pp, 1998.

[113] J. Bumrungpetch, "MECHANISM DESIGN OF VENTRICULAR ASSIST DEVICE," 2000.

[114] I. Ansys, "ANSYS Meshing User's Guide," *vol*, vol. 15317, pp. 724–746, 2010.

[115] K. Toptop, "Computational Fluid Dynamic Analysis Of Axial-Flow Left-Ventricular Assist Device," *Bahcesehir Univ.*, 2013.

[116] M. Giersiepen, L. J. Wurzinger, R. Opitz, and H. Reul, "Estimation of shear stress-related blood damage in heart valve prostheses--in vitro comparison of 25 aortic valves.," *Int. J. Artif. Organs*, vol. 13, no. 5, pp. 300–306, 1990.

[117] A. Garon and M. I. Farinas, "Fast three-dimensional numerical hemolysis approximation," *Artif. Organs*, vol. 28, no. 11, pp. 1016–1025, 2004.

[118] D. Arora, M. Behr, and M. Pasquali, "A tensor-based measure for estimating blood damage," *Artif. Organs*, vol. 28, no. 11, pp. 1002–1015, 2004.

[119] D. Arora, M. Behr, O. Coronado-Matutti, and M. Pasquali, "Estimation of hemolysis in centrifugal blood pumps using morphology tensor approach," *Comput. Fluid Solid Mech.*, no. 713, pp. 578–582, 2005.

[120] L. Gesenhues, L. Pauli, and M. Behr, "Strain-based blood damage estimation for computational design of ventricular assist devices," *Int. J. Artif. Organs*, vol. 39, no. 4, pp. 166–170, 2016.

[121] J. Zhang *et al.*, "Computational and experimental evaluation of the fluid dynamics and hemocompatibility of the centrimag blood pump," *Artif. Organs*, vol. 30, no. 3, pp. 168–177, 2006.

[122] M. E. Taskin, K. H. Fraser, T. Zhang, C. Wu, B. P. Griffith, and Z. J. Wu, "Evaluation of Eulerian and Lagrangian Models for Hemolysis Estimation," *ASAIO J.*, vol. 58, no. 4, pp. 363–372, 2012.

[123] J. Apel, R. Paul, S. Klaus, T. Siess, and H. Reul, "Assessment of hemolysis related quantities in a microaxial blood pump by computational fluid dynamics," *Artif. Organs*, vol. 25, no. 5, pp. 341–347, 2001.

[124] X. Song, A. L. Throckmorton, H. G. Wood, J. F. Antaki, and D. B. Olsen, "Computational fluid dynamics prediction of blood damage in a centrifugal pump," *Artif. Organs*, vol. 27, no. 10, pp. 938–941, 2003.

[125] X. Song, A. L. Throckmorton, H. G. Wood, J. F. Antaki, and D. B. Olsen, "Computational Fluid Dynamics Prediction of Blood Damage in a Centrifugal Pump," *Artif. Organs*, vol. 27, no. 10, pp. 938–941, 2003.

[126] ASTM, "ASTM F1841-97: Standard Practice for Assessment of Hemolysis in Continuous Flow Blood Pumps," 2005.

[127] N. R. Council and others, *Guide for the care and use of laboratory animals*. National Academies Press, 2010.

[128] Y.-D. Choi, J. Kurokawa, and J. Matsui, "Performance and Internal Flow Characteristics of a Very Low Specific Speed Centrifugal Pump," *J. Fluids Eng.*, vol. 128, no. 2, p. 341, 2006.

[129] O. Dur *et al.*, "Pulsatile in vitro simulation of the pediatric univentricular circulation for evaluation of cardiopulmonary assist scenarios," *Artif. Organs*, vol. 33, no. 11, pp. 967–976, 2009.

[130] Y. Kassif, M. Zilbershlag, M. Levi, A. Plotkin, and S. Schueler, "A new universal wireless transcutaneous energy transfer (TET) system for implantable LVADs--Preliminary in vitro and in vivo results," *J. Hear. Lung Transplant.*, vol. 32, no. 4, pp. S140--S141, 2013.

[131] L. Lucke and V. Bluvshtein, "Safety considerations for wireless delivery of continuous power to implanted medical devices," in *Engineering in Medicine and Biology Society (EMBC), 2014 36th Annual International Conference of the IEEE*, 2014, pp. 286–289.

[132] S. Piskin, H. F. Altin, O. Yildiz, I. Bakir, and K. Pekkan, "Hemodynamics of patient-specific aorta-pulmonary shunt configurations," *J. Biomech.*, vol. 50, pp. 166–171, 2017.

[133] V. Gesuete, M. Fabi, and M. Bonvicini, "A 74-year-old unoperated univentricular heart: The oldest reported survival," *Cardiol. Young*, vol. 26, no. 4, pp. 805–807, 2016.

[134] M. Esmaily-Moghadam, T. Y. Hsia, and A. L. Marsden, "The assisted bidirectional Glenn: A novel surgical approach for first-stage single-ventricle heart palliation," *J. Thorac. Cardiovasc. Surg.*, vol. 149, no. 3, pp. 699–705, 2015.

[135] H. Hong, O. Dur, H. Zhang, Z. Zhu, K. Pekkan, and J. Liu, "Fontan conversion templates: Patient-specific hemodynamic performance of the lateral tunnel versus the intraatrial conduit with fenestration," *Pediatr. Cardiol.*, vol. 34, no. 6, pp. 1447–1454, 2013.